FRICTION PRESSURE DROP MEASUREMENTS AND FLOW DISTRIBUTION ANALYSIS FOR LEU CONVERSION STUDY OF MIT RESEARCH REACTOR

by

SUSANNA YUEN-TING WONG

Submitted to the Department of Nuclear Science and Engineering in Partial Fulfillment of the Requirements for the Degrees of

Bachelor of Science in Nuclear Science and Engineering
and
Master of Science in Nuclear Science and Engineering

at the
Massachusetts Institute of Technology
September
August 2008

Signature of Author: _____
Department of Nuclear Science and Engineering
August 25, 2008

Certified by: _____
Dr. Lin-wen Hu, Thesis Supervisor
Nuclear Reactor Laboratory

_____
Professor Mujid S. Kazimi, Thesis Co-supervisor
Department of Nuclear Science and Engineering

Accepted by: _____
Professor Jacquelyn C. Yanch
Chairman, Department Committee on Graduate Students

FRICTION PRESSURE DROP MEASUREMENTS AND FLOW DISTRIBUTION ANALYSIS FOR LEU CONVERSION STUDY OF MIT RESEARCH REACTOR

by

SUSANNA YUEN-TING WONG

Submitted to the Department of Nuclear Science and Engineering on August 25th, 2008 in Partial Fulfillment of the Requirements for the Degrees of

Bachelor of Science in Nuclear Science and Engineering
and
Master of Science in Nuclear Science and Engineering

Abstract

The MIT Nuclear Research Reactor (MITR) is the only research reactor in the United States that utilizes plate-type fuel elements with longitudinal fins to augment heat transfer. Recent studies on the conversion to low-enriched uranium (LEU) fuel at the MITR, together with the supporting thermal hydraulic analyses, propose different fuel element designs for optimization of thermal hydraulic performance of the LEU core. Since proposed fuel design has a smaller coolant channel height than the existing HEU fuel, the friction pressure drop is required to be verified experimentally.

The objectives of this study are to measure the friction coefficient in both laminar and turbulent flow regions, and to develop empirical correlations for the finned rectangular coolant channels for the safety analysis of the MITR. A friction pressure drop experiment is set-up at the MIT Nuclear Reactor Laboratory, where static differential pressure is measured for both flat and finned coolant channels of various channel heights. Experiment data show that the Darcy friction factors for laminar flow in finned rectangular channels are in good agreement with the existing correlation if a pseudo-smooth equivalent hydraulic diameter is considered; whereas a new friction factor correlation is proposed for the friction factors for turbulent flow. Additionally, a model is developed to calculate the primary flow distribution in the reactor core for transitional core configuration with various combinations of HEU and LEU fuel elements.

Thesis Supervisor: Lin-wen Hu
Title: Associate Director of MIT Nuclear Reactor Laboratory

Thesis Co-supervisor: Mujid S. Kazimi
Title: Professor of Nuclear Science and Engineering

Acknowledgements

I would like to express my sincere gratitude to my thesis advisors, Dr. Lin-wen Hu and Professor Mujid Kazimi, for their tremendous amounts of guidance, patience and their endless ideas throughout the course of this study. I am also grateful to Dr. Thomas Newton for the unparallel opportunity to be part of the low enrichment uranium conversion efforts for the MIT Reactor. This thesis work would not be made possible without their support in many ways.

I owe a debt of gratitude to many experts and individuals whom I interacted with at the MIT Nuclear Reactor Laboratory, in particular, Gordon Kohse, Edward Pilat and Tom McKrell for their invaluable input on the experiment loop design; Adam Grein for his enormous support and knowledge on the experiment fabrication; Paul Menedier and Edward Block for their expertise on the instrumentation; Edward Lau for the dramatic transformation of laboratory space; Bao Truong, Joshua Whitman, Matt Denman and Harvey Tang for their calm and inspiration; and last but not least, Rachel Morton for the miraculous retrieval of a massive amount of experiment data from a broken hard disk in a hot summer.

Additionally, I would like to thank my undergraduate academic advisor, Professor Andrew Kadak, as well as the administrative staff members of the Massachusetts Institute of Technology, who have been supportive of my academic and extra-curricular experience at MIT.

Finally, I would like to thank RERTR for the financial support of this thesis work. I also would like to thank my parents and little sister, Kitty, for taking care of me, and many colleagues who have showed kindness and made a difference in my experience in Massachusetts. I am grateful for the friendship that I certainly do and will treasure.

Table of Contents

List of Figures

List of Tables

1. Introduction

1.1. Overview of MIT Reactor

The MIT Reactor (MITR-II), which began operations in 1975, is a light water cooled and moderated, heavy water reflected reactor that is designed to operate at up to 5 MW. The reactor utilizes flat, plate-type fuel elements with 93% high enrichment uranium (HEU), and produces a high quality thermal neutron flux for interdisciplinary research in the areas of advanced fuel and material for nuclear energy system, neutron science, nuclear medicine, and radiation science and technology. It provides useful experimental facilities and serves as tremendous resource for users from both inside and outside the MIT community.

The original MIT Reactor (MITR-I) was a heavy water cooled and moderated reactor with an open array of plate-type fuel elements. It first attained criticality in 1958 and operated at up to 5 MW until 1973. The reactor core of the MITR-I was later modified to use light water to cool and moderate a close array of plate-type fuel elements, surrounded by a heavy water reflector. The modified reactor core of the MITR-II is designed to maximize the thermal neutron flux in the reflector region where the experimental beam ports are located.

1.1.1. Core configuration

The hexagonal core of the MITR-II contains 27 fuel element positions in three designated rings shown in Figure 1. The inner-most ring, or the A-ring, contains 3 positions; the B-ring contains 9 positions and finally the C-ring, the outer-most ring, contains 15 positions.

The 27 fuel element positions are normally filled with 24 fuel elements, leaving 3 positions available for solid aluminium dummy elements and/or in-core irradiation facilities. Owing to power peaking concerns, two solid aluminium dummy elements are often located in the central A-ring where the fast neutron flux is highest [1].

1.1.2. Fuel elements

A fuel element cross section is shown in Figure 2. The overall length of the fuel element, including the end nozzles, is 26.25". Each fuel element consists of fifteen 23" long fuel plates assembled between two 0.188" thick side plates (Figure 3).

Held by the side plates, each fuel element consists of 14 full flow channels and 2 half-channels. According to the engineering drawing of the side plate as shown in Figure 3, the base-to-base channel height, here defined as the distance between the fin bases of two opposing finned rectangular fuel plates, is 0.098" in the full flow channel and 0.131" in two neighboring half-channels[1].

1.1.3. Fuel plates

The fuel plates are 0.080" thick with 110 continuous longitudinal rectangular fins on both sides. The fin spacing is 0.010" high, 0.010" wide and 0.010" apart from one another as shown in Figure 4.

Currently, each finned rectangular fuel plate contains 33.7 grams of 93% high enrichment uranium in the form of an aluminide (UAl_x) cermet matrix. In each finned rectangular fuel plate, the thickness of high enrichment uranium (HEU) fuel meat is 0.030", and the minimum thickness of aluminium alloy cladding is 0.015".

1.1.4. Primary flow and heat removal

To remove heat generated in the reactor core, light water as the primary coolant enters the reactor core tank through the inlet plenum. It flows through the annular region between the core tank and the core shroud, followed by the six flow channels around the hexagonal core support housing assembly as shown in Figure 1.

---

[1] See Section 4.

The primary coolant is then directed upward through the coolant channels in the fuel elements, the flow guide, and the core support housing assembly, the outlet plenum, and finally to three coolant pipes exiting the core tank. Heat is removed from the primary coolant to the secondary coolant through heat exchangers. A small fraction of the heat generated is also removed by the heavy water reflector and the light water shield cooling systems.

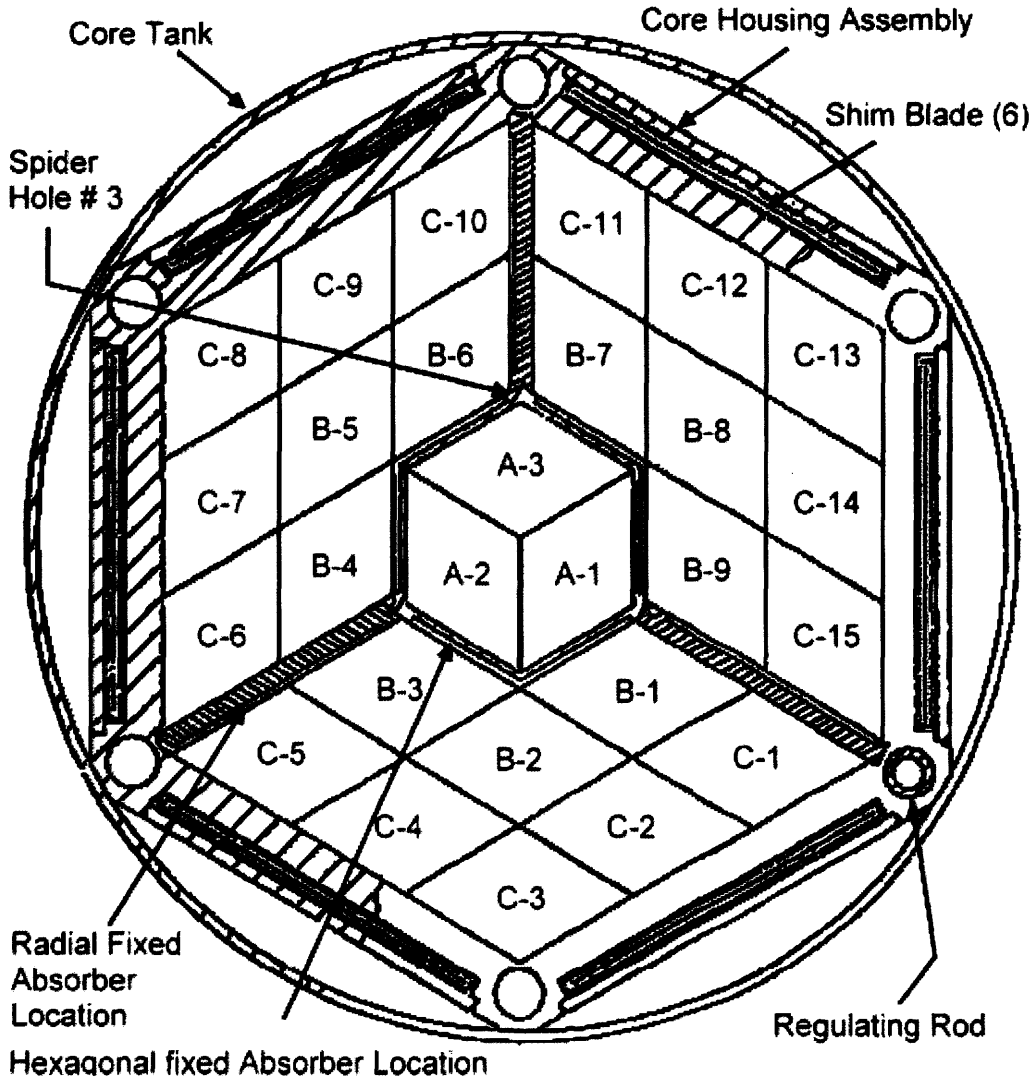

Figure 1: Core configuration of the MITR-II as adopted from Ref.[2].

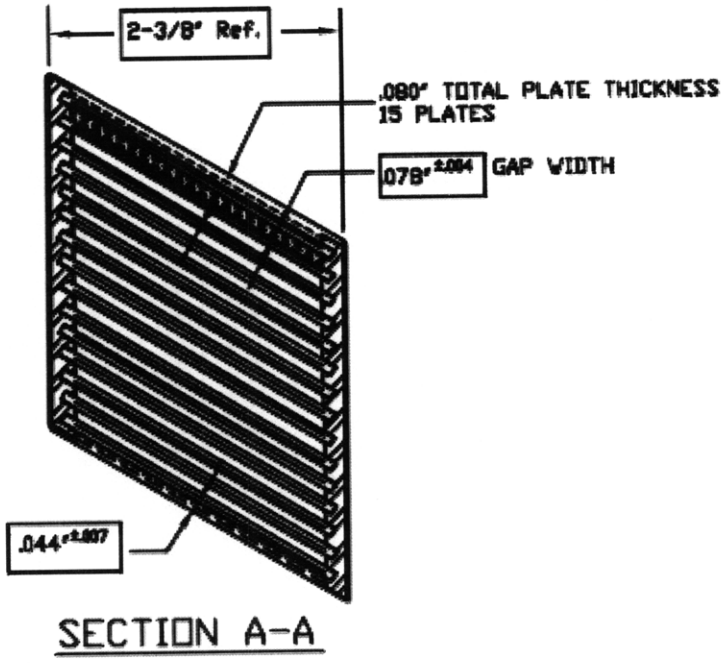

Figure 2: Cross section of the MITR-II fuel element.

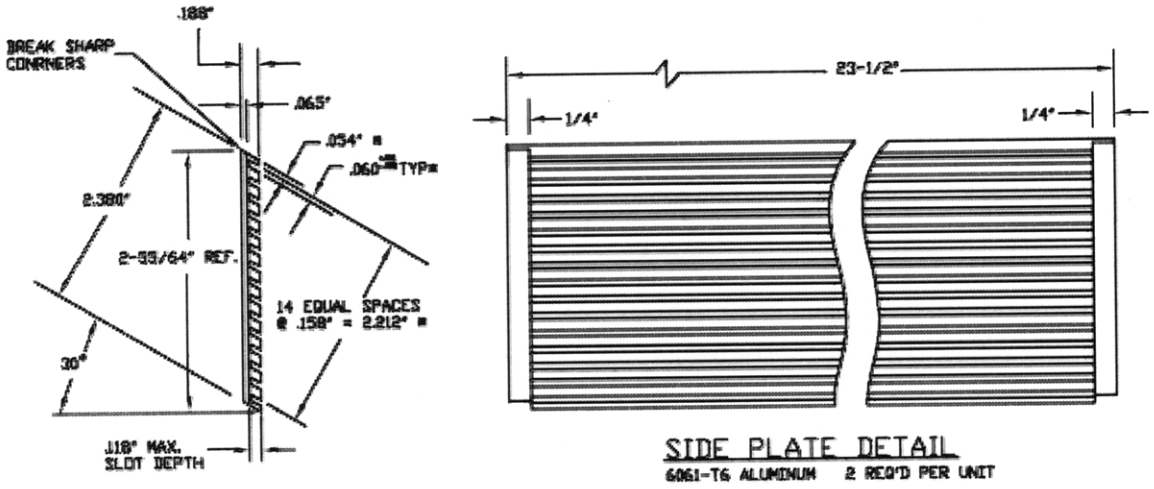

Figure 3: Top and side views of the side plate as part of the MITR-II fuel element.

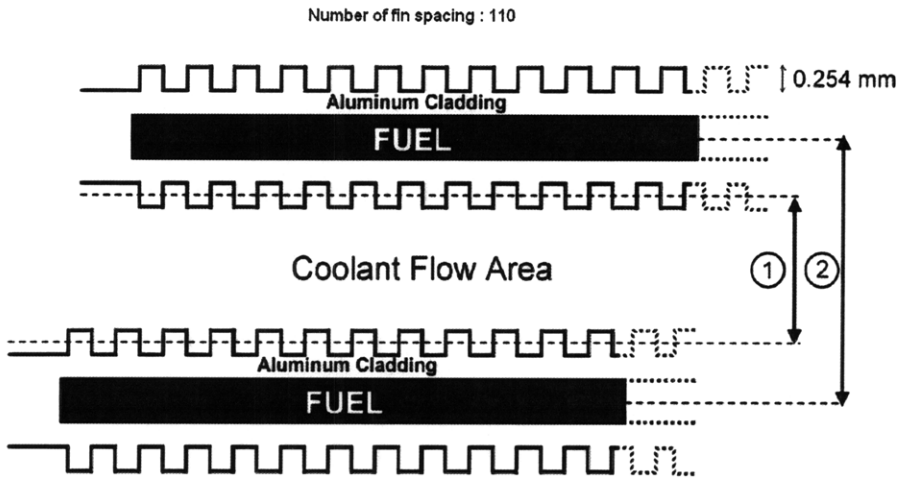

Figure 4: Cross sectional view of a flow channel between two finned fuel plates. (1) and (2) indicate the mean and base-to-base channel heights respectively. Figure adopted from Ref.[2].

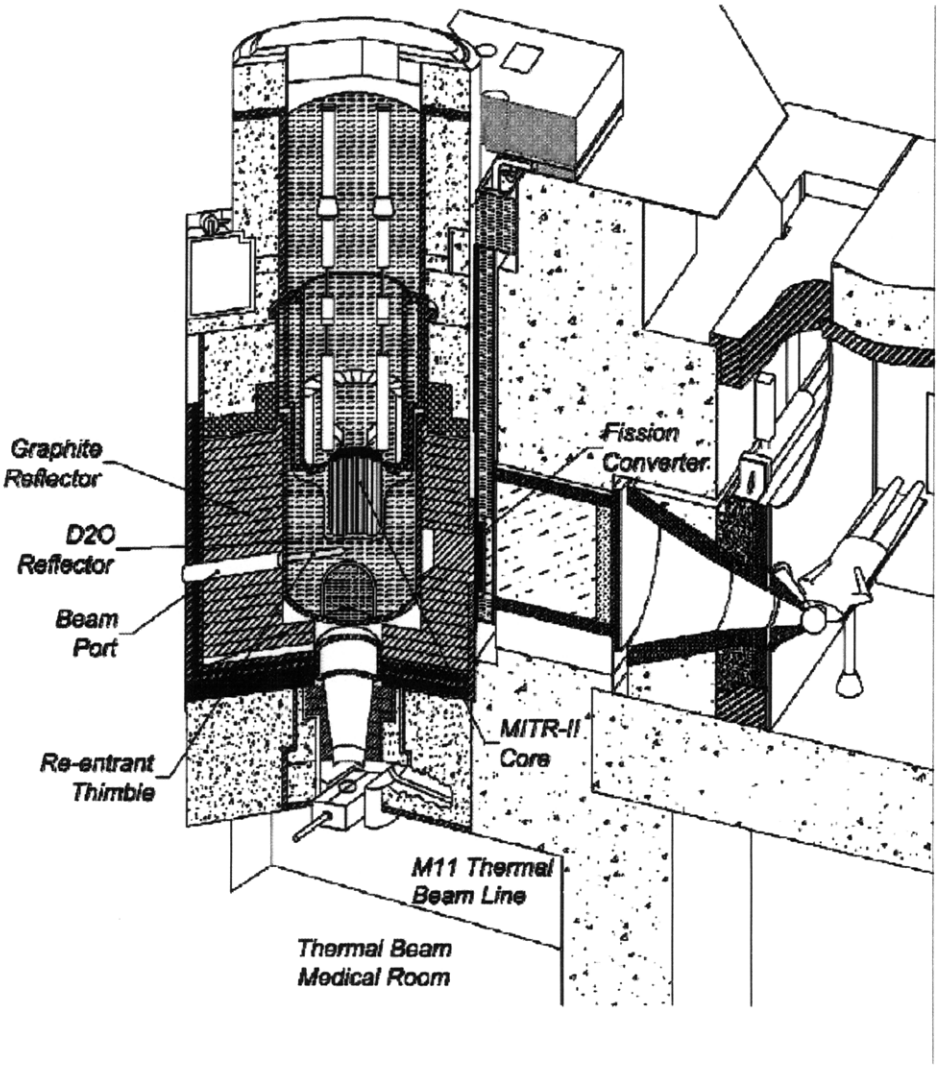

Figure 5: Isometric view of the MITR-II adopted from Ref[2].

1.2. Reduced Enrichment for Research and Test Reactors (RERTR)

The Reduced Enrichment for Research and Test Reactors (RERTR) program was initiated by the Department of Energy in 1978 to develop the technology necessary to reduce the use of high enriched uranium (HEU) fuel in research reactors by converting them to low enriched uranium (LEU) fuel [1, 3, 4]. It is the goal of the RERTR program to reduce and ultimately eliminate the international commerce in weapon-grade uranium.

1.2.1. Major technology components

Low enriched uranium is defined as one having less than 20% enrichment of uranium-235. Preliminary studies show that the use of LEU fuel can create significant drawbacks, such as, possible loss of useful neutron flux and increased production of actinides in the spent fuel from Ref.[1]. It is therefore part of the continuing efforts of the RERTR program to overcome these technological difficulties and maintain or improve the performance of research reactors that are to be converted to LEU core.

Some of the major technology components of the RERTR program include the development of advanced LEU fuels, the design and safety analysis for research reactor conversion, and the development of LEU targets and processes for the production of the medical isotope Molybdenum-99.

1.2.2. Progress on RERTR program

Today, a total of 129 research reactors worldwide are included in the RERTR program as given in Ref.[5]. As a consequence of the regulations from the U.S. Nuclear Regulatory Commission that require research reactors to convert to LEU fuel should suitable fuel be available [1, 6], eleven research reactors in the United States were converted to the use of low enrichment uranium (LEU) fuel by the end of 1986. Eight U.S. reactors were

scheduled to be converted using currently developed LEU fuels. In addition, five HEU-fueled U.S. reactors, including MITR, are unable to use currently qualified LEU fuels because of their compact core design and high power density. These reactors require the development of high-density LEU fuel for conversion.

Previous design studies on the material for the LEU fuel show that the monolithic uranium-molybdenum (U-Mo) fuel has sufficient density and is a viable option to be used as the LEU fuel at the MIT Reactor [1]. It is proposed that U-Mo fuel with 10% molybdenum content, with uranium density of $17.5 g/cm^3$, can be used as the LEU fuel; moreover, U-Mo fuel with additional 1-2% molybdenum content can also be considered.

1.2.3. MITR-II LEU conversion efforts

Studies on the utilization of LEU fuel at the MIT Reactor are performed by Newton [1] and Gehret [7]. In particular, it is suggested in [1] that should high density LEU fuel of which $\rho > 17.5 g/cm^3$ become available, the MITR-II can be converted from HEU fuel to LEU fuel while maintaining an equivalent or higher neutron flux for experiments. It is also suggested that the refueling interval of the reactor core with LEU fuel can be twice longer than that with HEU fuel at the current reactor thermal power of 5 MWt.

Thermal hydraulic analyses in support of the LEU fuel design are also performed by Ko, Hu and Kazimi [2, 8, 9], in which the in-house multi channel thermal hydraulics code (MULCH-II) is utilized. The results of the steady state and loss of primary flow analyses from the MULCH-II code are compared with the results from PLTEMP/ANL and RELAP5-3D codes. It is suggested in [2, 9] that the steady state analysis using MULCH-II is in agreement with PLTEMP and RELAP5, while RELAP5 seems to give more conservative predictions than MULCH-II in the loss of flow analysis [10].

1.3. Objectives

The MIT Reactor is the only research reactor in the United States that utilizes finned, plate-type fuel elements. The flow channels in the reactor core are rectangular ducts with continuous, longitudinal, rectangular fins as shown in Figure 4. These fins enhance heat transfer between the fuel plate and the primary coolant by increasing the total heat transfer area by roughly a factor of 2 [11, 12]. The continuous, longitudinal, rectangular fins are made from a good conducting material and are, thus, efficient in the heat transfer from the base surface to the centre of coolant channel, but the reduced equivalent hydraulic diameter also affects the friction pressure drop characteristics in the flow channels.

Common friction factor correlations for fully developed laminar and turbulent flows, such as, Kays, Karman-Nikuradse, Blasius and McAdams equations [13], are applicable for flows in plane rectangular and circular conduits. More friction factor correlations for flows in different flow channel geometries are summarized in Section 2; however, little information is available for flows in rectangular ducts with continuous, longitudinal, rectangular fins to describe the friction pressure drop characteristics at the MIT Reactor.

1.3.1. Experimental study for friction factor correlation

The primary objective of this thesis work is to develop the friction factor correlations for fully developed laminar and turbulent flows in rectangular channels with continuous longitudinal rectangular fins that cover range of channel gap widths of interest for the LEU core design efforts. These correlations will be applied in the analysis of the friction pressure drop and flow disparity in the homogenous and transitional reactor cores during the conversion from HEU to LEU fuels.

In the experimental study of the friction factor correlation, data are collected from a flow loop that is set-up at the MIT Nuclear Reactor

Laboratory. The experiment loop includes a test section that consists of two aluminium plates with continuous longitudinal rectangular fins, and aluminium spacers that held the gap between the finned plates. Water is pumped through the experiment loop, and static differential pressure is measured from the side of the test section.

1.3.2. Flow distribution analysis

This study also aims to perform homogenous and transitional core analyses of the friction pressure drop and flow disparity characteristics of primary coolant in the reactor core during the conversion from HEU to LEU fuels at the MIT Reactor. Because of the different equivalent hydraulic diameters of the flow channels in the HEU and LEU fuels, the flow velocities of are likely to change depending on combination of HEU/LEU elements, causing a disparity of flow of the primary coolant in the reactor core. The transitional core analysis ensures that transition from HEU to LEU fuels can be performed safely without interrupting the normal operations of the MIT Reactor.

2. Literature Review

2.1. Overview

The friction pressure drop for fluids in different flow regimes and channel geometries is often characterized by Darcy or Fanning friction factor in the following equations,

$$-\frac{dP}{dz} = \frac{f_d}{D_e}\frac{\rho v^2}{2} \tag{1}$$

$$-\frac{dP}{dz} = \frac{2f_f \rho v^2}{D_e} \tag{2}$$

where f_d is Darcy friction factor,

$f_f = \frac{f_d}{4}$ is Fanning friction factor,

ρ is the fluid density,

v is the average velocity of the fluid,

L is the axial length of the channel, and

D_e is the equivalent hydraulic diameter.

Equations (1) and (2) show that differential friction pressure drop $-\frac{dP}{dz}$ depends on three well-defined variables (fluid density, average velocity of flow and equivalent hydraulic diameter of flow channel), as well as a dimensionless parameter in the form of the friction factor. In order to yield a good prediction of the friction pressure drop, the friction factor ought to be determined for fluids in different flow regimes and channel geometries.

2.1.1. Equivalent hydraulic diameter

In general, the equivalent hydraulic diameters D_e for circular and non-circular conduits are defined below:

$D_e = d$, for circular conduits, and (3)

$$D_e = \frac{4A_c}{P_w}, \text{ for non-circular conduits.} \quad (4)$$

where d is the diameter of the circular channel,

A_c is the cross-sectional area, and

P_w is the wetted perimeter of the channel.

The equivalent hydraulic diameter of plate-fin surfaces is defined by Manglic and Bergles in 1990, as it is summarized in [14]:

$$d_h = \frac{4A_c}{A_s} \quad (5)$$

In the case of rectangular ducts with continuous longitudinal rectangular fins, which is of interest to the finned plate-type fuel elements at the MIT Reactor, the expression in [14] can be rewritten as:

$$d_h = \frac{4A_c}{A_s} = \frac{4A_c}{P_w} \quad (6)$$

which is the same as the more general expression of the equivalent hydraulic diameter D_e.

2.2. Laminar and turbulent flow in tube

2.2.1. Background

At low flow rates, the fluid within the hydrodynamic boundary layer travels along streamlines, and is referred to as laminar flow. Laminar flow generally occurs when viscous force is dominant. It is characterized by a smooth, constant motion in the flow.

As the flow rate increases, disturbances in the flow begin to take place. Random eddies, vortices and other flow fluctuations in direction and magnitude are generated and destroy the laminar flow lines. This type of flow is referred to as turbulent flow. Near the wall of the channel, however, a laminar flow region, or a sub layer where the velocity flow is low, can often appears as suggested in [13].

2.2.2. Laminar flow

Fully developed laminar flow in circular tube has been solved analytically in [13] using the continuity equation and the momentum equation. For fluids of constant density, the solution is as follows:

$$v_m = \frac{R^2}{8\mu}\left(-\frac{dP}{dz}\right) \tag{7}$$

where v_m is the mean fluid velocity,

μ is the fluid viscosity, and

R is the tube radius.

Todreas and Kazimi [13] note the definition of friction factor f for fully developed laminar flow, which relates the pressure gradient to the kinetic head based on the average velocity and the pipe diameter. It leads to a special condition that is often applied to developed laminar flow, that the product of laminar friction factor and Reynolds number $(f\,\mathrm{Re})$ is a constant that depends on the geometry of the channel, as proposed in [15], where

$$f = \frac{64}{\mathrm{Re}}, \text{ for circular ducts, and} \tag{8}$$

$$f = \frac{96}{\mathrm{Re}}, \text{ for infinite parallel plate channels.} \tag{9}$$

where $Re = \dfrac{\rho V D_e}{\mu}$

For friction pressure drop for developed laminar flow in rectangular channels with non-zero aspect ratio, the friction factor correlation is summarized in [16, 17] as follows:

$$f = \frac{96}{\mathrm{Re}}\left[1 - 1.3553\beta + 1.9467\beta^2 - 1.7012\beta^3 + 0.9564\beta^4 - 0.2537\beta^5\right] \tag{10}$$

where β is the aspect ratio of the rectangular channel.

The above equations are used to describe the friction factors for laminar flows, often with $\mathrm{Re} \leq 2000$. The equations are independent of wall roughness [18]. Moody's chart [19] is also used extensively to determine the friction factors for turbulent and laminar flows in pipes of different surface roughness.

2.2.3. Turbulent flow

Turbulent flow generally occurs when inertial force is dominant. It generates random eddies, vortices and other flow fluctuations that destroy the laminar flow lines. Turbulent flow in smooth tubes occurs at high flow rates, at which Reynolds numbers are high. A commonly encountered expression for friction factor for turbulent flow in tubes is the Karman-Nikuradse equation [13], where the friction factor f is predicted as follows:

$$\frac{1}{\sqrt{f}} = -0.8 + 0.87 \ln\left(\mathrm{Re}\sqrt{f}\right) \tag{11}$$

Owing to the difficulty in using the Karman-Nikuradse equation in practice, simplified relations, such as the Blasius and the McAdams equations, are often applied to predict the friction factors for turbulent flows in smooth circular conduits.

The Blasius equation is used extensively, to predict the Darcy friction factor for turbulent flow, of which $\mathrm{Re} < 30{,}000$, in smooth tubes [13]:

$$f = 0.316 \cdot \mathrm{Re}^{-0.25} \tag{12}$$

The McAdams equation is used for far turbulent flow of higher Reynolds number, $30{,}000 < \mathrm{Re} < 10^6$, in smooth tubes [13]:

$$f = 0.184 \cdot \mathrm{Re}^{-0.2} \tag{13}$$

The friction factor correlation for flow in smooth circular tubes can similarly be derived for other geometries. It is, however, argued in [13] that the velocity gradient of turbulent flow is primarily near the wall of the channel, and geometries tend to have little influence on the friction factor.

2.2.4. Friction factor for fluid in rough tube

Roughness in tubes, characterized by the ratio of depth of surface protrusions to the channel diameter (λ/D_e), increases the effective friction factor. The Moody's chart is a graphic representation of the empirical Colebrook equation. It demonstrates the effect of roughness in the following expression:

$$\frac{1}{\sqrt{f}} = -2 \cdot \log_{10}\left[\frac{\lambda/D_e}{3.7} + \frac{2.51}{\mathrm{Re}\sqrt{f}}\right] \tag{14}$$

2.2.5. Friction factor for liquid in tube during heating and cooling

Heat transfer and pressure drop correlations for liquids in tubes during heating and cooling were proposed by Sieder and Tate in 1936 [20], to take into consideration the effects of radial temperature and viscosity gradients on the axial and radial components of velocity.

Sieder and Tate added the effects of viscosity gradient of liquids in tubes by means of dimensionless parameters $\frac{\mu_a}{\mu_w}$ for laminar and turbulent flows, and $\frac{\mu_a}{\mu_f}$ for transitional flow, where

μ_a is the viscosity of fluid at main stream temperature t_a,

μ_w is the viscosity of fluid at tube wall temperature $t_{f,lam}$ for laminar flow,

μ_f is the viscosity of fluid at tube wall temperature $t_{f,turb}$ for far turbulent flow,

$t_{f,lam} = t_a + \frac{1}{2}(t_w - t_a)$, and

$t_{f,turb} = t_a + \frac{1}{4}(t_w - t_a)$

Using data on fluid friction of Keevil [21], White [22], Clapp and Fitzsimmons [23], Sieder and Tate concluded the ratio of true friction factor to isothermal friction factor f/f_{iso} due to the effects of heating and cooling liquids in tubes is as follows:

$$\frac{f}{f_{iso}} = 1.1\left(\frac{\mu_a}{\mu_w}\right)^{0.25}, \text{ for laminar flow regime where } \mathrm{Re} < 2100, \text{ and} \quad (15)$$

$$\frac{f}{f_{iso}} = 1.02\left(\frac{\mu_a}{\mu_w}\right)^{0.14}, \text{ for turbulent flow where } \mathrm{Re} > 2100. \quad (16)$$

2.3. Double-pipe fin-tube heat exchanger

2.3.1. Background

The double-pipe heat exchanger is one of the most common apparatus for heat exchange between two fluids. It has the design of a tube inside another tube to separate the two fluid streams. The advantages of longitudinal fins were realized in the 1930s, to improve the heat transfer coefficients of gases and viscous liquids by increasing the area available for heat transfer.

2.3.2. Study by De Lorenzo and Anderson

Data on heat transfer and pressure drop of liquids in double-pipe heat exchangers are presented by De Lorenzo and Anderson in 1945 [24]. While the performance of plain-pipe heat exchangers can be predicted by correlations available for flow in circular conduits [25], the standard commercial double-pipe heat exchangers often have longitudinal fins attached to the outside of the inner pipe. A series of tests have been performed to evaluate the heat transfer and pressure drop on the fin side of standard double-pipe heat exchangers.

To include the effects of temperature and viscosity gradients during heating and cooling of liquids in double-pipe heat exchangers, De Lorenzo and Anderson modify the general isothermal Fanning friction factor correlation by adding the dimensionless parameters of viscosity ratio in Sieder and Tate [20]. Experimental data show good agreement with the isothermal friction factor correlation for $\mathrm{Re} < 400$, as well as $3{,}000 < \mathrm{Re} < 12{,}000$. It is also found that the transition between laminar and turbulent flow in the fin side of a standard double-pipe heat exchanger begins at $\mathrm{Re} > 400$, which is considerably lower than 2100.

2.3.3. Study by Braga and Saboya

Another study of turbulent flow in annular ducts with continuous longitudinal rectangular fins is made by Braga and Saboya in 1999 [26]. Experiments have been performed to determine the average heat transfer coefficients and friction factors using a double-pipe heat exchanger.

In order to measure the change in pressure along the annular ducts, 16 static pressure taps have been installed. To determine the value of friction factor from the experiments, the authors in [26] also define the following:

$$f = \frac{\Delta P}{L} \cdot \frac{2\rho D_h}{\dot{m} \Big/ \left[\left(\frac{\pi}{4}\right) \cdot \left(D_2^2 - D^2\right)\right]^2} \tag{17}$$

The friction factors, f and f_u, of finned annular duct and plain unfinned annulus respectively are given as follow:

$f = 2.8467\,\mathrm{Re}^{-0.2863}$, for air flow where $10^4 \le \mathrm{Re} \le 5.2 \times 10^4$, and (18)

$f_u = 0.5134\,\mathrm{Re}_u^{-0.2911}$, for air flow where $10^4 \le \mathrm{Re}_u \le 6 \times 10^4$. (19)

The friction factors for turbulent flow in plain unfinned annulus are found to be much smaller than that in annular duct with continuous longitudinal rectangular fins.

2.3.4. Early transition from laminar to turbulent flow

Experiments on continuous and non-continuous fins for liquids in the laminar flow regime, by Gunter an[27]d Shaw in 1942 [28], also show an early transition from laminar flow to turbulent flow for liquids in the longitudinal fin-tubes of double-pipe heat exchangers. In their investigation, the transitional flow begins somewhere near $\mathrm{Re} > 200$ for liquids with long longitudinal fins (in agreement with Davies and White [29]), and $\mathrm{Re} > 600$ for air with short longitudinal fins.

Similar observation is also found in the investigation of single-phase forced convection in small tubes with $D = 0.05 - 0.747\,mm$ [30-32], in which the transition from laminar flow to turbulent flow occurs in the range of $500 \le \mathrm{Re}_{D_h} \le 1500$.

2.4. Shrouded longitudinal rectangular fin array

2.4.1. Background

Friction pressure drop characteristics for shrouded longitudinal rectangular fin array have been studied extensively in Naik and Probert [33], as well as Thombre and Sukhatme [34]. Experimental data have been obtained, in Naik and Probert in 1988 [33], for liquids in rectangular ducts with or without shroud clearance.

2.4.2. Study by Naik and Probert

The authors thus proposed the turbulent flow friction factor correlations for two shroud clearance to fin height ratios C/H_f below:

$$f = 0.4158 \cdot \mathrm{Re}^{-0.273}, \text{ for } {}^{C}/_{H_f} = 0 \text{ and } 3{,}000 \le \mathrm{Re} \le 40{,}000, \tag{20}$$

$$f = 0.1643 \cdot \mathrm{Re}^{-0.1852}, \text{ for } {}^{C}/_{H_f} = 0.5 \text{ and } 3{,}000 \le \mathrm{Re} \le 40{,}000. \tag{21}$$

The authors also conclude that the empirical friction factor correlations yield lower values of friction factor than suggested by Prandtl-Karman when $\mathrm{Re} < 10^4$, and higher values of friction factor in the far turbulent flow, where $\mathrm{Re} > 3 \times 10^4$.

$$\frac{1}{\sqrt{f}} = 2\log_{10}(\mathrm{Re} \cdot f) - 0.8, \text{ for } 3 \times 10^3 \le \mathrm{Re} \le 3 \times 10^6 \tag{22}$$

The empirical friction factor correlations seem to be in good agreement with Prandtl-Karman for liquids in the turbulent flow, where $10^4 \le \mathrm{Re} \le 3 \times 10^4$. The discrepancy in friction factors merely suggests that Prandtl-Karman is inadequate in describing the friction pressure loss characteristics for shrouded fin arrays when ${}^{C}/_{H_f} > 0$.

2.4.3. Shrouded duct with longitudinal rectangular fins by Thombre and Sukhatme

Another set of empirical friction factor correlations for shrouded rectangular channel with longitudinal rectangular fins are found in Thombre and Sukhatme in 1995 [34], in which the shroud clearance to fin height ratios ${}^{C}/_{H_f}$ is embedded as part of the correlation as follows:

$$f = 0.040\left[2.058 - \left({}^{C}/_{H_f}\right)^{0.313}\right] \cdot \mathrm{Re}^{-0.075\left[3.40 - \left({}^{C}/_{H_f}\right)^{0.711}\right]}, \text{ for } 3{,}000 < \mathrm{Re} < 15{,}000, \tag{23}$$

$$f = 0.033\left[1.394 - \left({}^{C}/_{H_f}\right)^{0.408}\right] \cdot \mathrm{Re}^{-0.138\left[1.435 - \left({}^{C}/_{H_f}\right)^{0.773}\right]}, \text{ for } \mathrm{Re} \ge 15{,}000. \tag{24}$$

Experimental data in Thombre and Sukhatme [34] seem to agree with Naik and Probert [33], in particular, friction factors for liquids in

shrouded longitudinal rectangular fin arrays are found to be lower than the Prandtl-Karman equation at low values of Re, where $3{,}000 < \mathrm{Re} < 6{,}000$; but higher than the Prandtl-Karman equation in the far turbulent region, where $\mathrm{Re} \geq 15{,}000$.

2.5. Fluid in duct with other geometric properties

2.5.1. Study by Yang and Webb

Experiment on adiabatic, single-phase liquids in rectangular channels with hydraulic diameters of 2.64 mm and 1.56 mm, in Yang and Webb in 1996 [35], shows that single-phase friction factors for smooth and micro-finned channels are uniformly 14% and 36% higher than that predicted by the Blasius equation respectively.

Yang and Webb develop predictive methods for friction factors of single-phase liquids, as well as two-phase fluids. Although experimental data show weak correlation with the Chisholm correlation using the Lockhart-Martinelli two-phase multiplier, they seem to be in good agreement with the equivalent mass velocity concept proposed by Akers et al.

The single-phase experiment took place in an adiabatic, horizontal channel, and thus no acceleration or gravity term is required in the pressure drop calculation. Thus, the total pressure drop is given as:

$$\Delta P_{obs} = \Delta P_{friction} + \Delta P_{entrance} + \Delta P_{exit} \tag{25}$$

where $\Delta P_{friction}$ is the friction pressure drop, and

$\Delta P_{entrance}$, ΔP_{exit} are due to the contraction and expansion of flow at the entrance and exit of the channel respectively, such that,

$$\Delta P_{entrance} = \frac{G^2}{2\rho}(1-\sigma^2+K_c) \tag{26}$$

$$\Delta P_{exit} = \frac{G^2}{2\rho}(1-\sigma^2-K_e) \tag{27}$$

where σ is the ratio of the cross-sectional area of test section to the frontal area of inlet and exit plenums.

The plain and micro-fin tubes are dimensionally identical, except for the presence of fins with height of 0.2 mm and pitch of 0.4 mm on the inner wall of the micro-fin tube. The cross-sectional areas of the planar and micro-fin channels are 27.27 mm^2 and 22.68 mm^2 respectively.

Experimental data in Yang and Webb [35] show that the empirical Fanning friction factors are respectively 14% and 36% above the Fanning friction factors predicted by the Blasius equation ($f = 0.079\,\mathrm{Re}^{-0.25}$). Empirical correlations are thus proposed for single-phase liquids in plain and micro-fin tubes as follows:

$$f_p = 0.0676\,\mathrm{Re}_D^{-0.22}, \text{ for } 2500 \le \mathrm{Re}_D \le 30000 \text{ in plane tubes, and} \quad (28)$$

$$f_{mf} = 0.0814\,\mathrm{Re}_D^{-0.22}, \text{ for } 2500 \le \mathrm{Re}_D \le 30000 \text{ in micro-fin tubes.} \quad (29)$$

where Re_D is the Reynolds number using smooth or pseudo-smooth equivalent hydraulic diameter D.

2.5.2. Non-Newtonian fluid in duct with arbitrary constant cross-sectional area

Several friction factor correlations for purely viscous non-Newtonian fluids in ducts with arbitrary but longitudinally constant cross sectional areas have been proposed [27, 36-38]. The friction factor correlations are based on experimental data for turbulent fluids in pipes and square ducts. Power-law constant, as well as dimensionless geometric parameters are used in the correlations.

2.6. Entrance Length

2.6.1. Background

In high heat flux applications, large fluid flow rates are often used to maintain small increases in the stream-wise temperature of the heat sink

and the wall of fluid channel. Depending on the hydraulic diameter and geometry, the length of the developing region may be of similar magnitude as the length of the fluid channel. To understand the friction pressure drop characteristics of fully developed flow in rectangular ducts with longitudinal rectangular fins, it is crucial to design the experiment such that sufficient length of the duct is provided in the upstream of the test section.

2.6.2. Entrance length of laminar flow

In single-phase fluid flow for channels with uniform cross section, a developing region, where an initial velocity profile at the inlet of the channel gradually changes to an invariant velocity profile downstream, is often observed. It is suggested in [39] that the length of the developing region for laminar flow in circular ducts extends to a maximum axial distance z, which can be predicted as follows:

$$\left(\frac{z}{D_e}\right)_{lam} \approx \frac{\mathrm{Re}}{20}, \text{ for } \mathrm{Re} < 2000. \tag{30}$$

For laminar flow in rectangular ducts with uniform velocity profile at the inlet, the length of developing region is approximated by Shah and London [40], where

$$L_d = (0.06 + 0.07\beta + 0.04\beta^2)\,\mathrm{Re}\cdot d_h \tag{31}$$

where β is the channel aspect ratio,

Re is the Reynolds number, and

d_h is the channel hydraulic diameter.

2.6.3. Entrance region effect of laminar flow

The relationship among friction factors (f_{fd}, f_{app}) and dimensionless parameters of incremental pressure drop (K_∞, K_x) are defined in

Hesselgreaves [41], where the apparent fanning friction factor f_{app} is used to include the friction pressure drop in the developing laminar flow:

$$\Delta P = \left[\frac{4 f_{app} L}{d_h}\right] \frac{G^2}{2\rho} \tag{32}$$

Definition of the hydrodynamic entrance length L_{hy} is given as the axial flow distance at which 99% of the fully developed flow velocity is attained at the centerline of the duct [41], where the dimensionless parameter L_{hy}^{+} is given as

$$L_{hy}^{+} = \frac{L_{hy}}{\mathrm{Re} \cdot D_h} \tag{33}$$

Moreover, for $x < L_{hy}$, the dimensionless x^{+} is defined by

$$x^{+} = \frac{x}{\mathrm{Re} \cdot D_h} \tag{34}$$

2.6.4. Entrance length of turbulent flow

In the turbulent flow, the velocity boundary layer develops faster and, hence, the following is suggested in [13]:

$$\left(\frac{z}{D_e}\right)_{turb} = 25 \sim 40 \tag{35}$$

The empirical and computational investigation of flow development and pressure drop in rectangular micro-channel, by Qu and Mudawar [42], finds that at high Reynolds numbers, sharp entrance effects generate pronounced vortices immediately downstream of the inlet, which have significant influence on flow development.

2.7. Comparison of Friction Factor Correlations

Many friction factor correlations have been proposed for laminar and turbulent flows in different channel geometries. The most common

flow channel geometries are commercial tubes and pipes, where the friction pressure drop is characterized by correlations in [13, 21-23]. Other common flow channel geometries include plain, as well as finned, rectangular and double-pipe ducts. Friction pressure drops in these flow channels are described by correlations in [15, 17, 26, 27, 33-35].

The friction factor correlations mentioned are summarized in Figure 6 and Figure 7. The friction factors for turbulent flows may be divided into two groups. The first group includes five correlations that describe the friction factors for flows in smooth circular conduits, as well as two correlations that describe the friction factors in shrouded longitudinal rectangular fin array at low flow rates. The second group includes four friction factor correlations for several finned channels.

Group one correlations are found, on average, about 50% lower than the ones in group two (with the exception of the Braga equation for finned annular region) when Reynolds number is between 3000 and 10^5. This finding provides a ball park estimate of the effect of fins on friction factor.

Table 1: Friction factor correlations divided into two groups by their magnitude.

Group 1 Correlations	**Group 2 Correlations**
Karman-Nikuradse	Michna
Blasius	Thombre (Re>15000)
McAdams	Yang and Webb
Kostic and Hartnett	Braga (finned annular)
Braga (unfinned)	
Naik	
Thombre (Re<15000)	

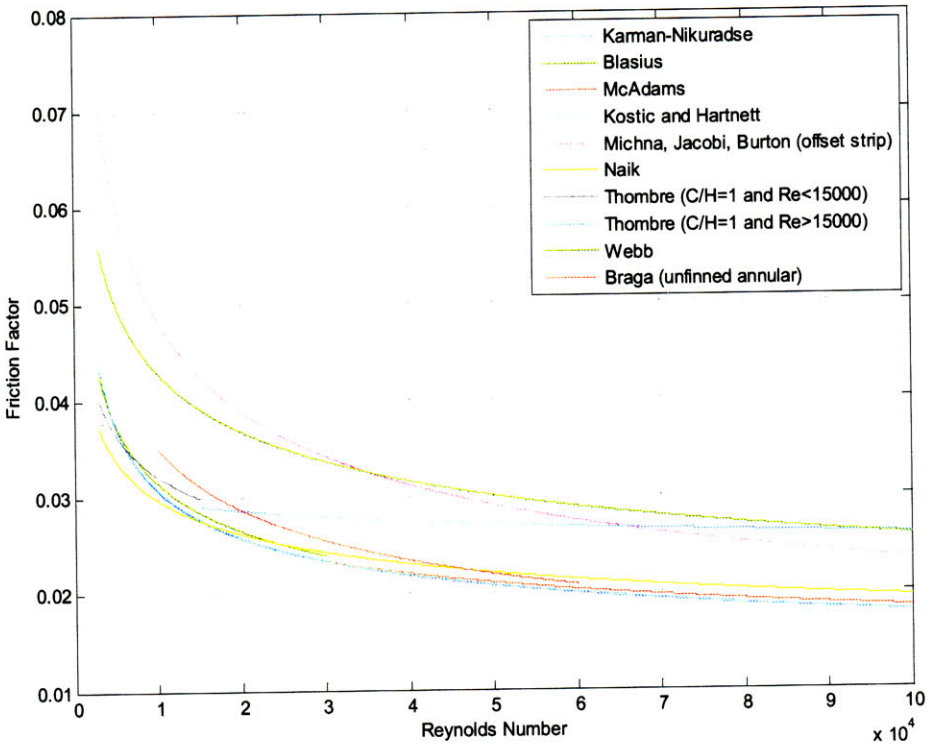

Figure 6: Friction factor correlations for turbulent flows.

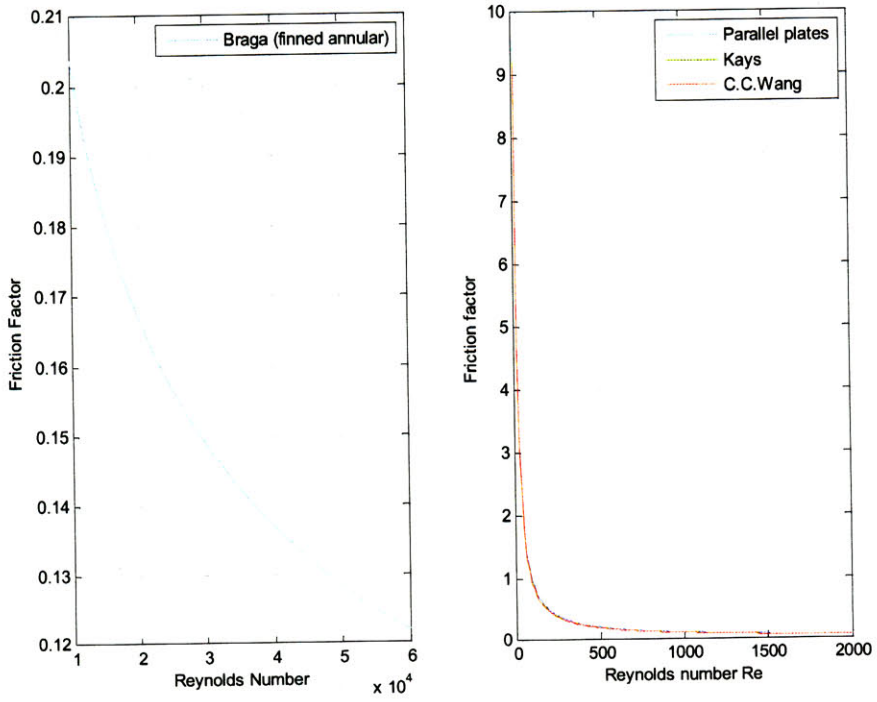

Figure 7: Friction factor correlations for turbulent flow in annual region with longitudinal fins [26] (left), and for laminar flow in rectangular channels [13, 17, 43] (right).

3. Experiment Design

3.1. Overview

A friction pressure drop experiment is designed and set-up at NW13-112, at the MIT Nuclear Reactor Laboratory, to obtain experiment data of friction factors for turbulent, laminar and transition flows in rectangular ducts with continuous longitudinal rectangular fins.

The experiment loop includes a test section that consists of two aluminium plates with continuous longitudinal rectangular fins, and two aluminium spacers that held the gap between the finned plates. Water is pumped through the experiment loop, and static differential pressure is measured from the side of the test section.

Four pairs of aluminium spacers of 0.040", 0.080", 0.120" and 0.150" high, are fabricated for the experiment to study the effect of equivalent hydraulic diameter on friction factors.

3.1.1. Major component of experiment loop

Figure 8 and Figure 9 show the major components of the friction pressure drop experiment loop. They include a test assembly made of aluminium alloy, turbine flow meters, differential pressure transducers, thermocouples, a de-ionized water storage tank, a centrifugal pump and a VFD controller as shown in Figure 11.

Water is pumped from the de-ionized water storage tank and is circulated through the 1" stainless steel tube to the turbine flow meter, thermocouples, and test assembly that includes the upstream and downstream plenums; and it is finally circulated back to the de-ionized water storage tank.

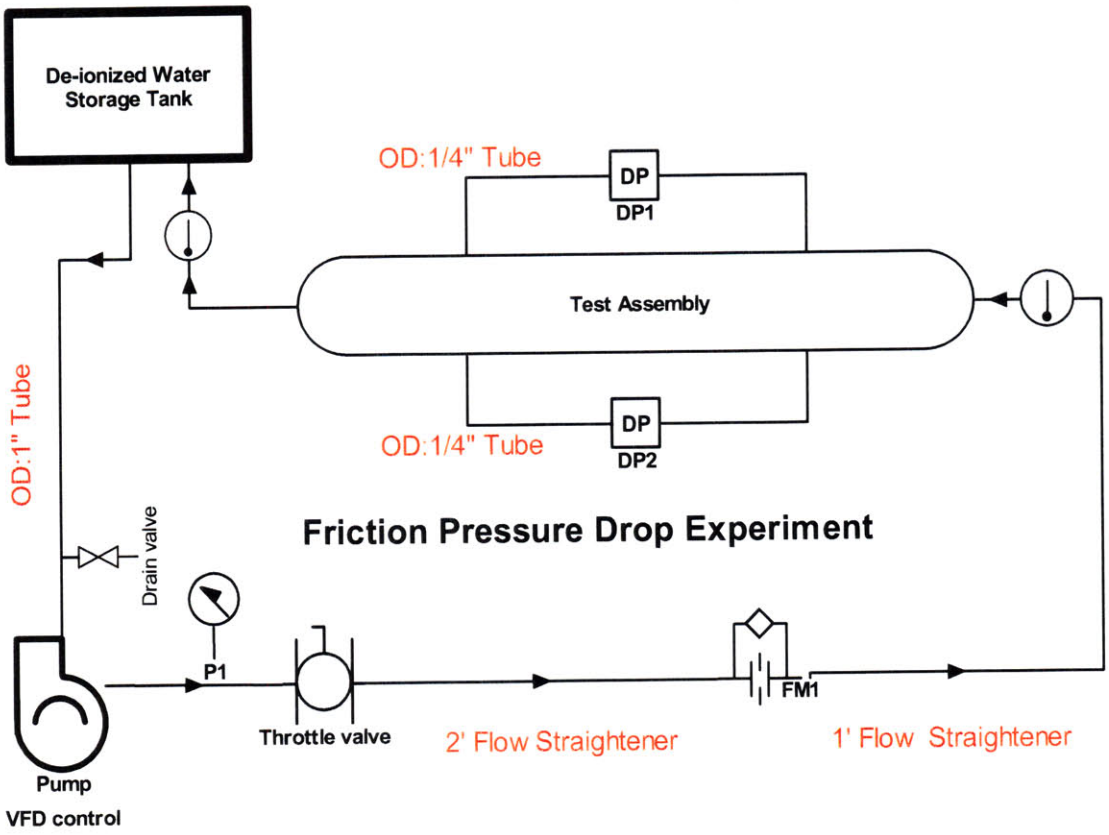

Figure 8: Schematic diagram of experiment loop for friction factor study.

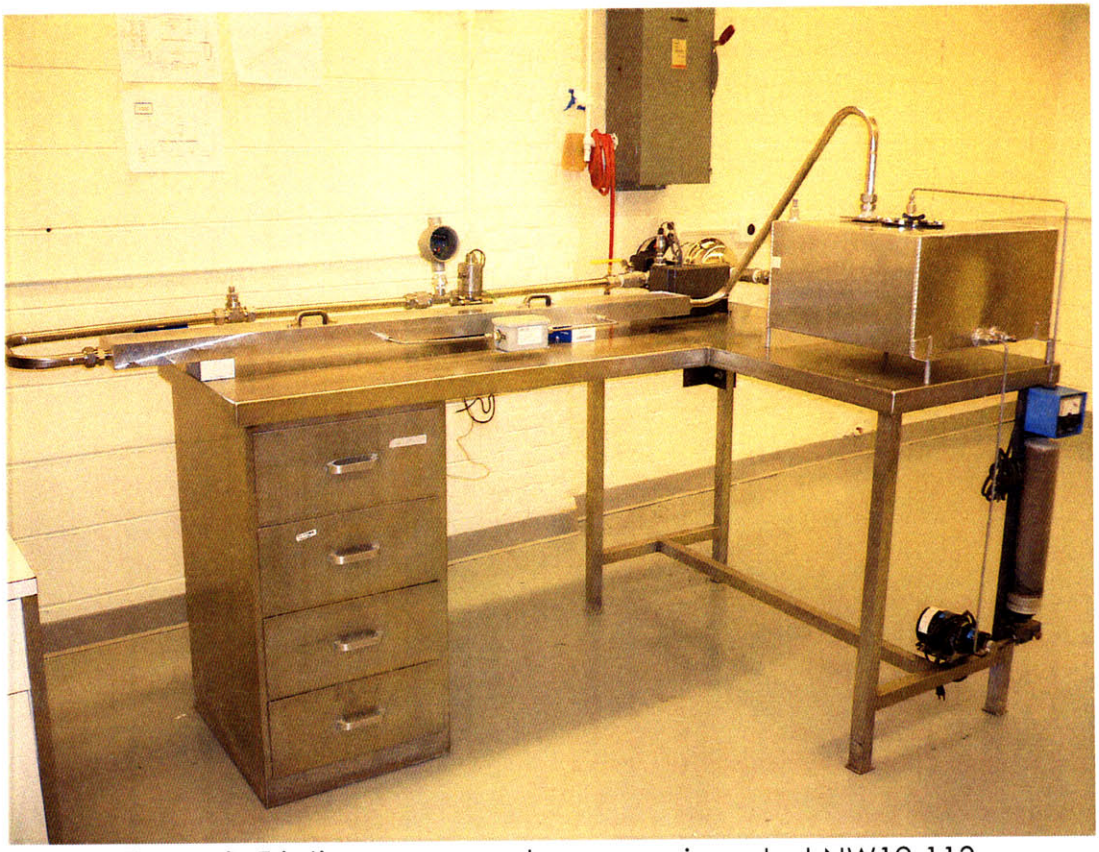

Figure 9: Friction pressure drop experiment at NW12-113.

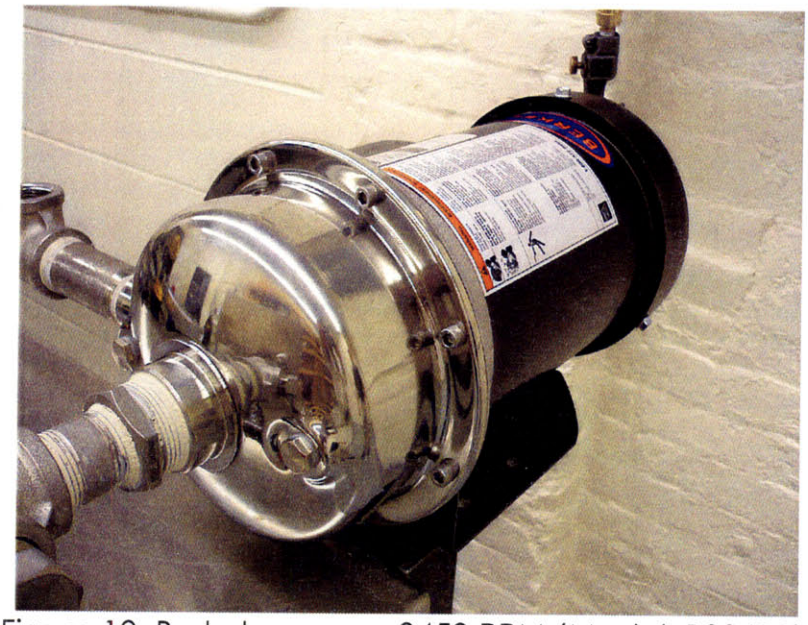

Figure 10: Berkeley pump 3450 RPM (Model: B82418).

Figure 11: VFD control (Model Fuji Electric AF-300 P11).

3.2. Test Assembly

The most critical parts of the experiment loop are located in the test assembly. The test assembly contains 10 pieces of components: aluminium bath, cover, upstream plenum, downstream plenum, lift, two plain or finned

plates, two spacers, and rubber gasket. The 5' by 5.2" test assembly is entirely made of aluminium alloy for the ease of machining (see Figure 13).

De-ionized water enters the front end of the test assembly via the 0.5" NPT inlet into the upstream plenum, the finned channel and the downstream plenum, before de-ionized water exits via the 0.5" NPT outlet on the back end of the test assembly.

To collect the data of pressure drop measurements in rectangular ducts with continuous longitudinal rectangular fins, four 0.125" NPT static pressure taps of 0.350" deep, with concentric through holes of 0.025" diameter, are made on the two sides of the test assembly (see Figure 14). Each pair of static pressure taps is connected to a differential pressure transducer to measure the pressure drop in the test section.

3.2.1. Finned channel region

The finned channel region consists of two aluminium dummy plates with continuous longitudinal rectangular fins on one side, and two aluminium spacers that determine the size of the gap between the finned plates. Eight aluminium spacers of four different heights, 0.040", 0.080", 0.120" and 0.150", are considered in the experiment to help study the effects of aspect ratio and hydraulic diameter on friction factors for flows in rectangular ducts with continuous longitudinal rectangular fins. The finned plates and the spacers are made of aluminium 6061.

3.2.1.1. Continuous longitudinal rectangular fin

The single-sided finned plates, manufactured by the Idaho National Laboratory, are arranged with their longitudinal rectangular fins facing each other to imitate the flow channel between two fuel plates at the MIT Reactor. The finned plates are 0.250" thick, with 110 continuous longitudinal rectangular fin spacing on each finned surface. The longitudinal rectangular fin spacing is 0.010" by width, 0.010" by depth, and 0.010" apart from one another (see Figure 16). The finned plates are

separated by a pair of aluminium spacers machined by the MIT Machine Shop (see Figure 18). The height of the aluminium spacers determines the base-to-base channel height between the finned plates and, thus, the aspect ratio and hydraulic diameter of the flow channel (see Table 2).

3.2.1.2. Aluminium spacer

Eight aluminium spacers of four different heights, 0.040", 0.080", 0.120" and 0.150", are considered. On each aluminium spacer, two through holes of 0.020" diameter, which are also concentric to the 0.025" through holes in Figure 14, are made to allow for static differential pressure measurements in the test section. The through holes are 24" apart from each other.

3.2.2. Test Section

Within the test assembly, the test section refers to the 24" of rectangular duct, with or without the continuous longitudinal rectangular fins, between the static pressure taps from which the pressure drop measurements are taken. The test section begins at 12" from the inlet of the finned channel region.

The 12" finned channel region at the upstream of the test section allows for the length of the developing region, where an initial velocity profile at the inlet of the channel gradually changes to an invariant velocity profile in the test section.

A total of 4 through holes of 0.020" diameter are made on the aluminium spacers (two through holes on each spacer) in Figure 14. Hence, as many as two differential pressure transducers may be installed to the test assembly simultaneously.

3.2.3. Upstream plenum region

The upstream plenum region is located between the 0.5" NPT inlet o the front end of the test assembly and the inlet of the finned channel

region. It allows for the space needed to develop a more uniform velocity profile before the flow reaches the finned channel region.

3.2.4. Downstream plenum region

The downstream plenum region collects the flow from the outlet of the finned channel region and feeds it through the 0.5" NPT outlet on the back end of the test assembly.

3.2.5. Entrance length of finned channel

The hydrodynamic boundary layer for the developing region is often assumed to begin developing at the entrance of the channel. The boundary layer then continues to grow from the wall of the channel until it meets the lines of symmetry of the channel.

The test section, essentially a 24" long rectangular duct with continuous longitudinal rectangular fins, is located at 12" from the inlet of the finned channel region. The 12" long channel between the inlet of the test section and the inlet of the finned channel region allows for the hydrodynamic boundary layer of the flow to grow, until a fully developed flow is achieved before reaching the test section.

3.2.5.1. Developing laminar flow

In developing laminar flow, the steady state velocity distribution and friction factor coefficients can be obtained from the equation suggested in [13]:

$$\frac{\mu}{r}\frac{\delta}{dr}\left(r\frac{\delta v_z}{dr}\right) = \rho v_z \frac{\delta v_z}{dz} + \frac{\delta p}{dz} \tag{36}$$

where $\frac{\delta v_z}{dz}$ is non-zero in the developing region.

Langhaar and No have suggested in [39] that the product of the local Fanning friction factor and Reynolds number $\left(f_z' \mathrm{Re}\right)$ stays relatively

constant as non-dimensional parameter $\frac{\mathrm{Re}}{z/D}$ approaches 20. It is, hence, concluded that the flow becomes fully developed when

$$\frac{z}{D_e} \approx \frac{\mathrm{Re}}{20} \tag{37}$$

Consider $\mathrm{Re} = 132$ and $D_e = 2.236 \times 10^{-3} m$ (Appendix [1]), the entrance length for developing laminar flow is approximately 1.5 cm.

3.2.5.2. Developing turbulent flow

In developing turbulent flows, the hydrodynamic boundary layers tend to develop quicker than that of developing laminar flow of similar range of Reynolds number. In [13], it is proposed that

$$\left(\frac{z}{D_e}\right)_{turb} = 25 \sim 40 \tag{38}$$

Hence, consider $\mathrm{Re} = 33{,}000$ and $D_e = 2.236 \times 10^{-3} m$, the entrance length is estimated to be between 5.6 and 8.9 cm.

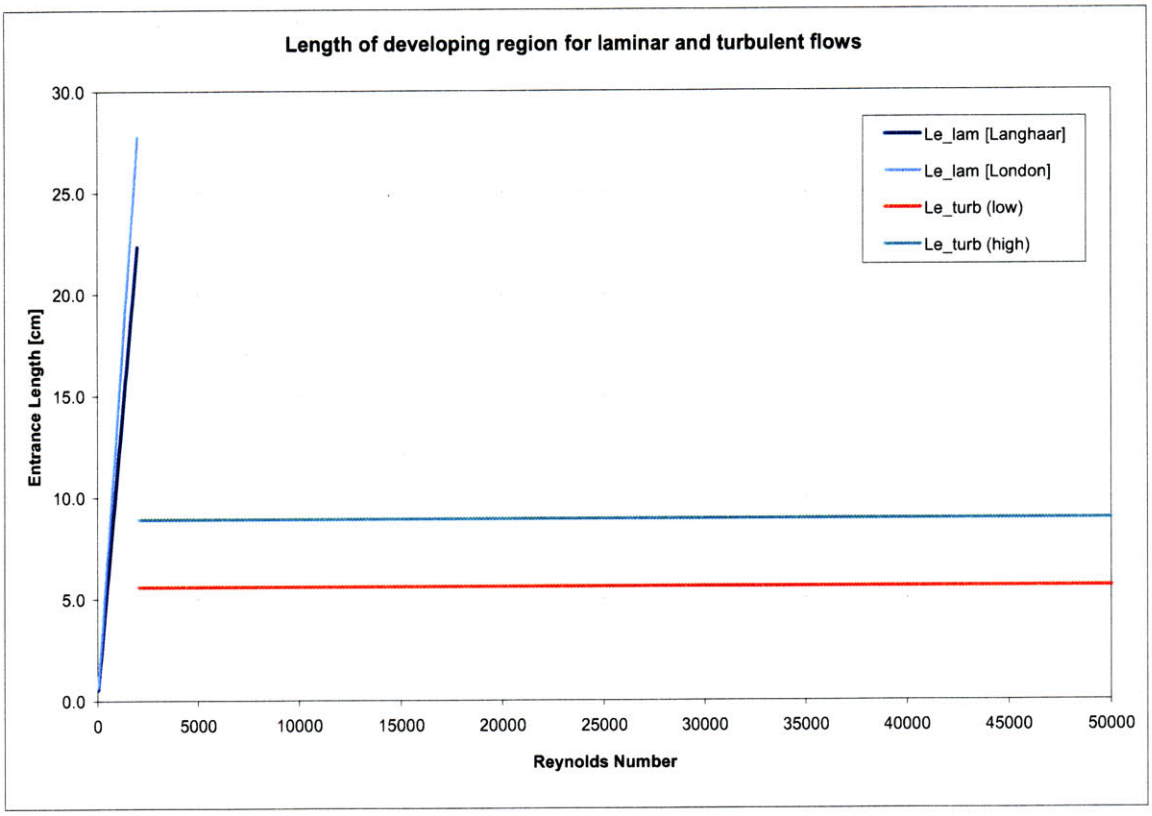

Figure 12: Length of developing region for laminar and turbulent flows.

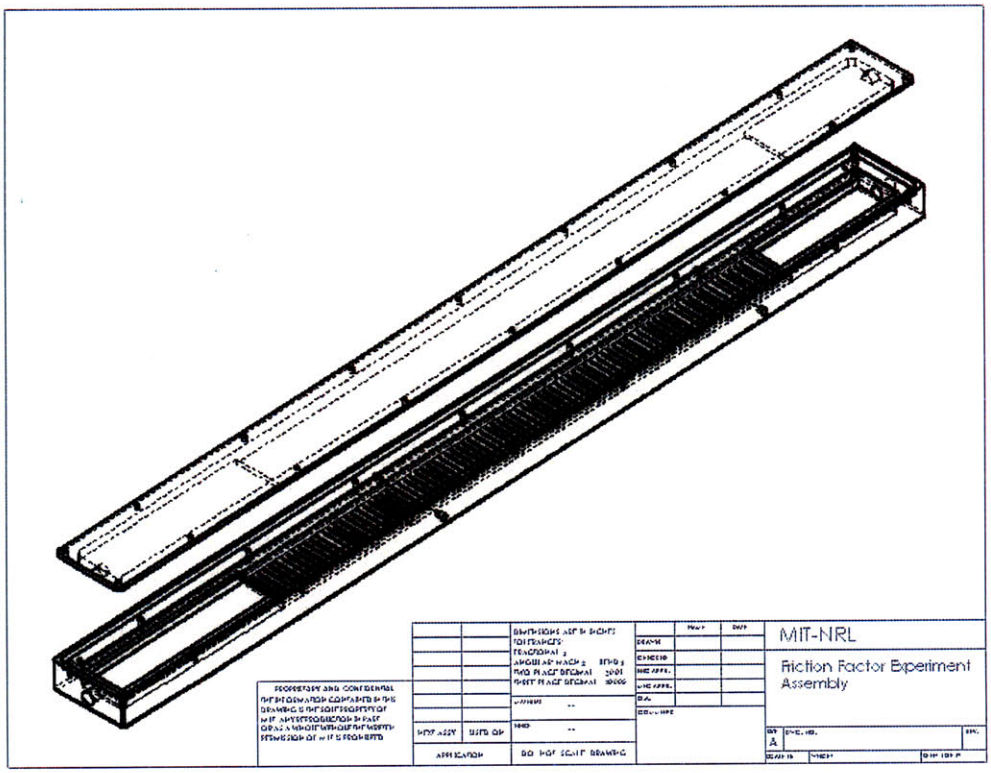

Figure 13: Test assembly made of Al 6061.

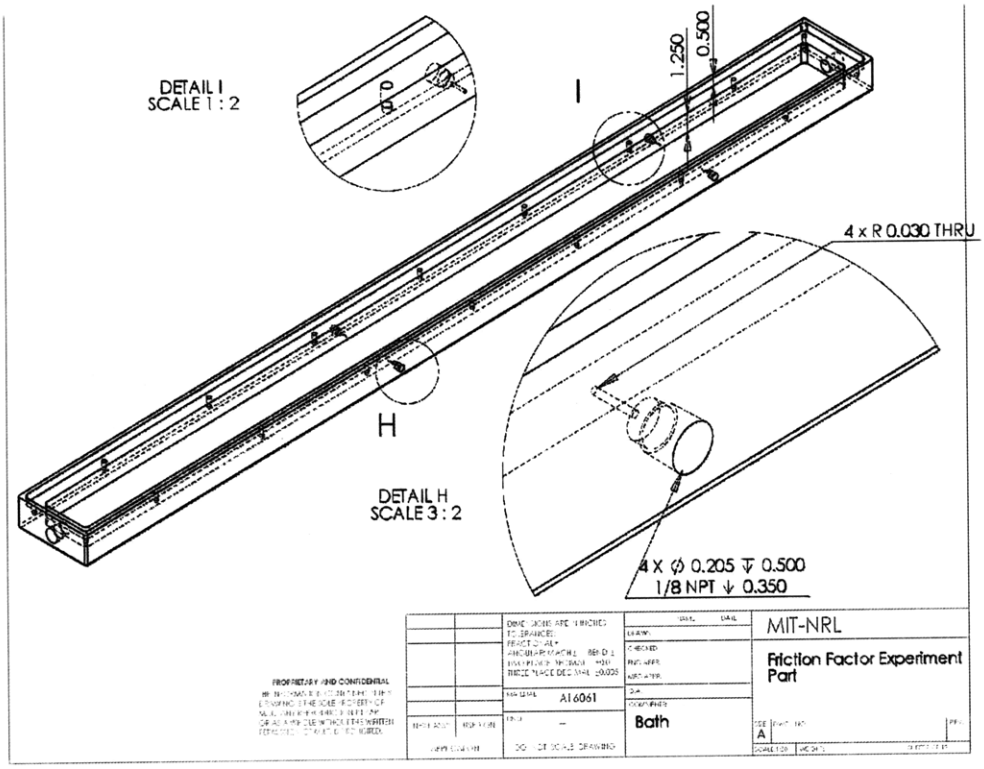

Figure 14: Four static pressure taps on two sides of the bath component of the test assembly.

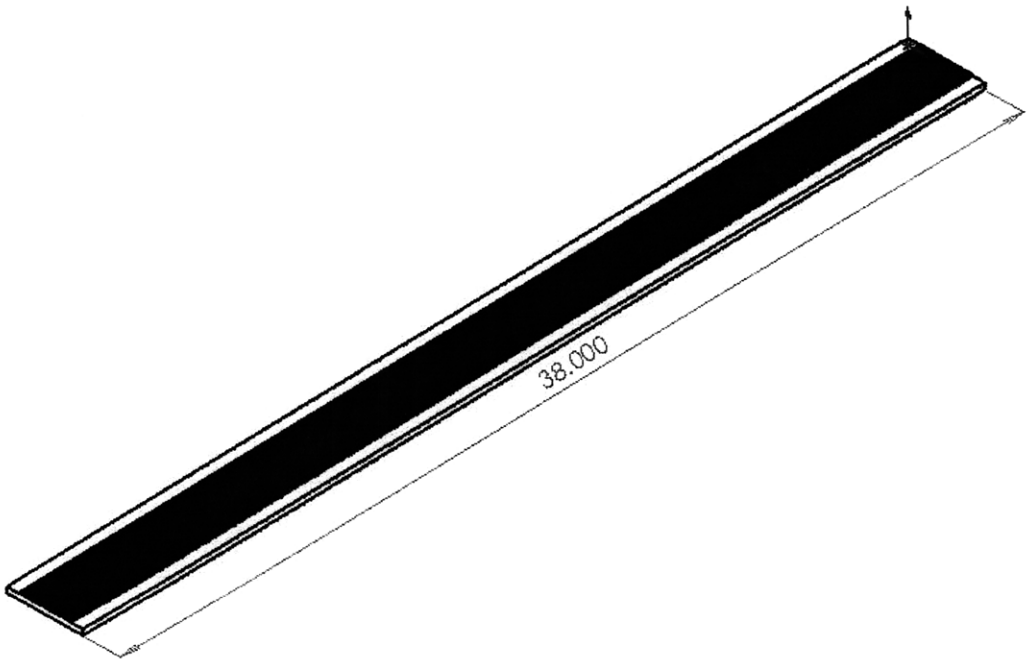

Figure 15: A 0.25" Al 6061 plate with 110 continuous longitudinal rectangular fin spacing.

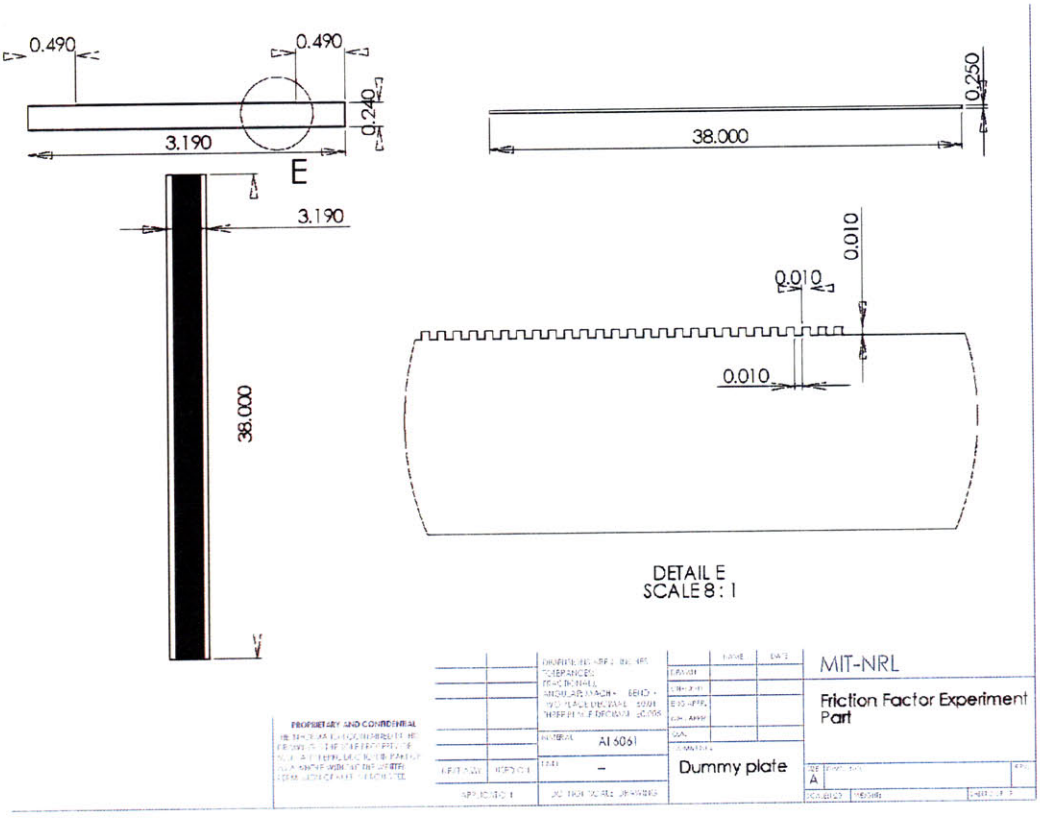

Figure 16: Engineering drawing of Al 6061 finned plate with fin dimensions.

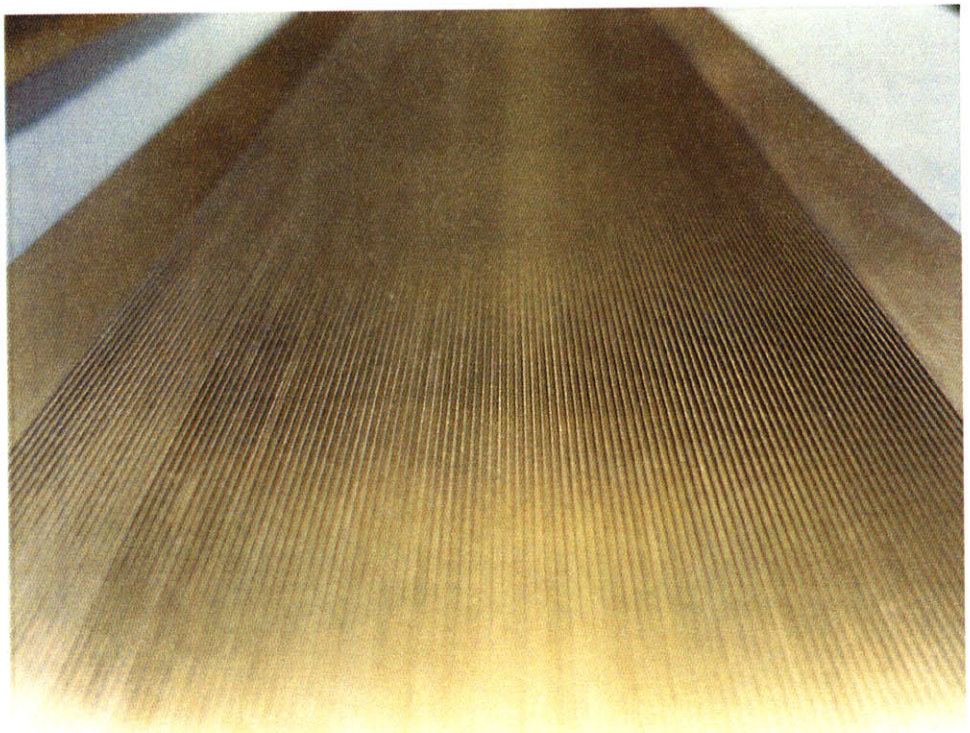

Figure 17: Two 0.25" Al 6061 plates each with 110 continuous longitudinal rectangular fin spacing. Manufactured by Idaho National Laboratory.

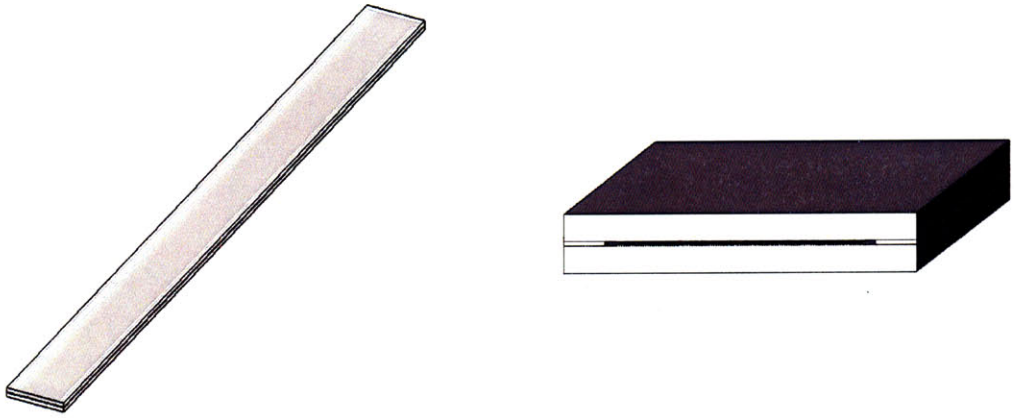

Figure 18: Two single-sided finned plates made of Al 6061, separated by two aluminium spacers.

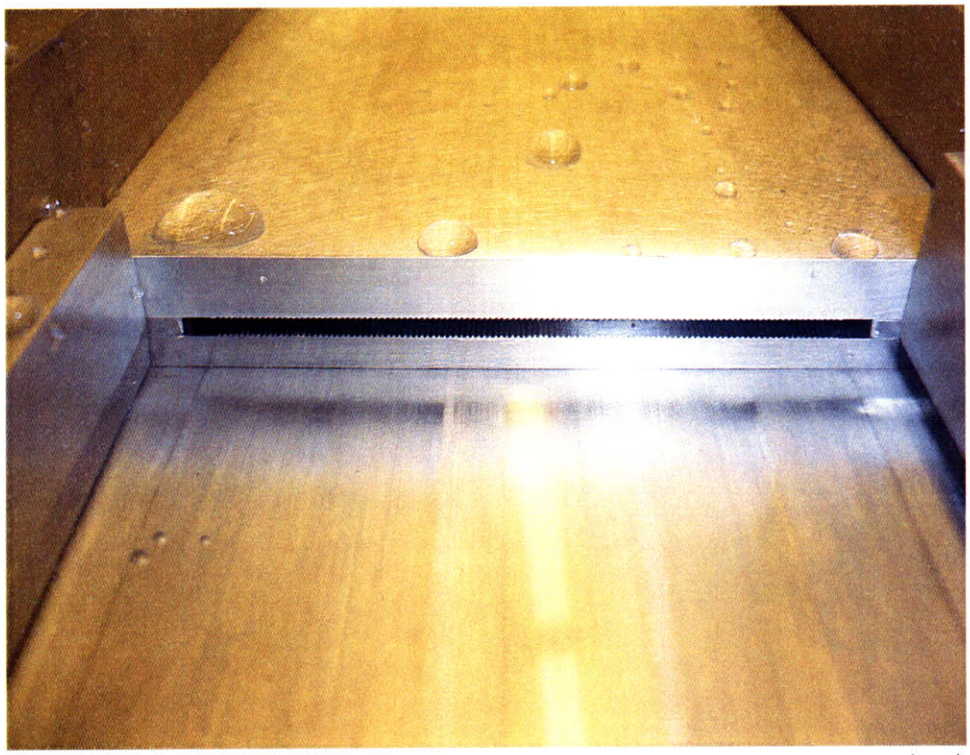

Figure 19: Two single-sided finned plates made of Al 6061, separated by two aluminium spacers, in experiment loop.

Table 2: Hydraulic diameter of flow channel with different base-to-base channel height.

Base to base channel gap [mils]	Hydraulic diameter [mm]
40	0.780
50	1.035
60	1.287
70	1.539
75	1.664
80	1.789
85	1.914
90	2.038
95	2.162
100	2.286
105	2.409
110	2.532
115	2.655
120	2.778
130	3.022
140	3.265
150	3.506

3.3. Pressure Drop Loop

The arrangement of the major components of the experiment loop is shown in a schematic diagram in Figure 8. The loop consists of a test assembly made of aluminium alloy 6061, turbine flow meters, a gauge pressure transducer (

Figure 22), differential pressure transmitters (Figure 20), thermocouples, a 20 gal. de-ionized water storage tank (Figure 24), a centrifugal pump and a VFD controller. Water is pumped from the de-ionized water storage tank and is circulated through the 1" stainless steel tube to a turbine flow meter, two thermocouples, and a test assembly that includes an upstream plenum, a finned channel region and a downstream plenum; and it is finally circulated back to the de-ionized water storage tank.

3.3.1. Turbine flow meters

The flow rates of water through the experiment loop are obtained by FTB-904 ball bearing liquid turbine flow meter for high flow rates (1.75 to 16 gpm), as well as FTB9511 ball bearing turbine flow meter for low flow rates (0.106 to 2.11 gpm).

The turbine flow meters come with NIST certification. The output of each meter is connected with a FLSC-60 signal conditioner, before it is fed to the data acquisition system.

3.3.2. Differential pressure transducers

The pressure drop measurements for flows in the finned test section are obtained using PD3000 sealed adjustable different pressure transmitter for high pressure drop range (0-40 to 0-200" H_2O), as well as PX154 low differential pressure transmitter (Figure 20) for low pressure drop range (0 to 6.23 kPa).

The differential pressure transmitters are connected to equal lengths of 0.25" tube, which are then connected to the 0.125" National Pipe Thread (NPT) static pressure taps on the sides of the test assembly (see Figure 14). For each pressure drop measurement of given flow rate and channel height, only one differential pressure transmitter is required to be online with the test assembly for data acquisition.

Figure 20: Low-range differential pressure transmitter PX154-025DI.

3.3.3. Thermocouples

Although the loop is not heated, a slight temperature change is expected due to the dissipated heat from the pump. Since the fluid viscosity varies appreciably with temperature, two 3" type K thermocouples are used in the experiment loop to monitor the change in fluid temperature between the inlet and the outlet of the test assembly. Type K thermocouples are commonly used general purpose thermocouples, and are available between the range of $-200^{\circ}C$ and $1350^{\circ}C$.

3.3.4. Stainless steel tubes

Stainless steel tubes of 1" outer diameter are used to connect the major components of the experiment loop. Stainless steel tubes, instead of pipes, are selected for this experiment because tubes often have smoother finishes than pipes and, thus, give lower pressure drops when all other factors are the same [44]. The friction factor correlation for turbulent flows in tubes is given by Drew, Koo and McAdams within $\pm 5\%$ in [44]:

$$f = 0.00140 + \frac{0.125}{\mathrm{Re}^{0.32}} \tag{39}$$

For clean commercial iron and steel pipes, friction factor correlation is given by Wilson, McAdams and Seltzer within $\pm 10\%$ in [44]:

$$f = 0.0035 + \frac{0.264}{\mathrm{Re}^{0.42}} \tag{40}$$

Lower head loss in the tubing of the experiment loop helps improve the performance of the pump and maximize the flow rates that are allowed to travel through the test assembly.

A VFD controller and a throttling valve are also installed at the outlet of the centrifugal pump to help adjust the flow rate through the loop.

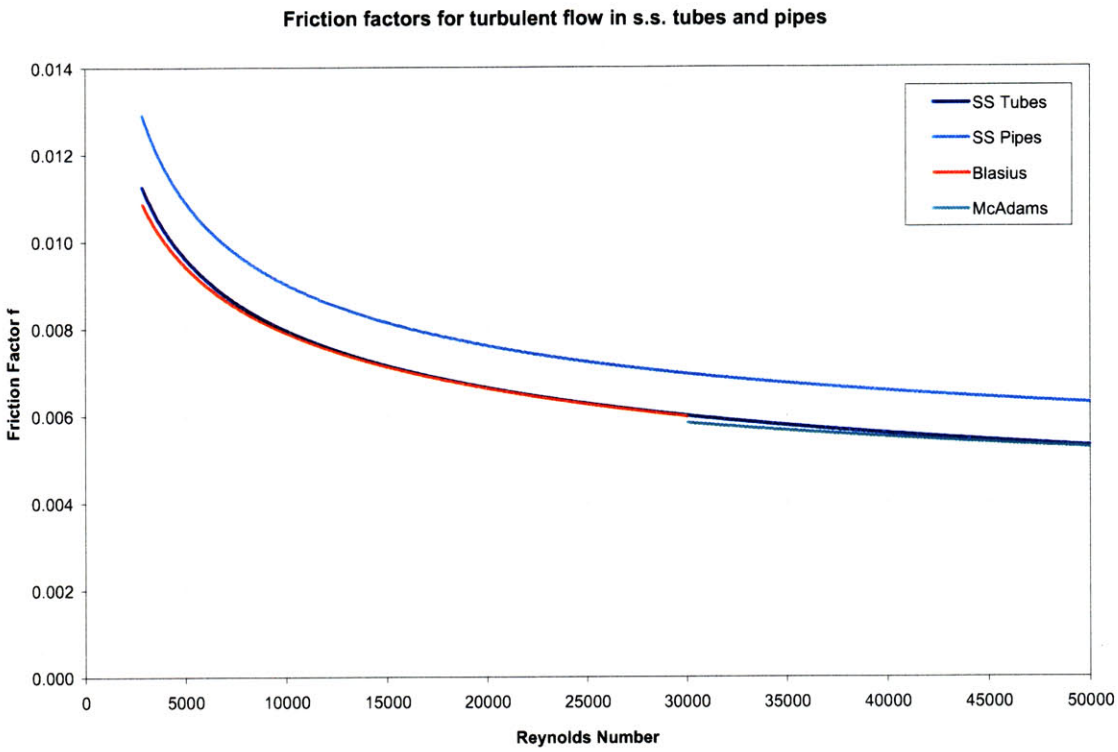

Figure 21: Friction factors for turbulent water flow in stainless steel tubes and pipes.

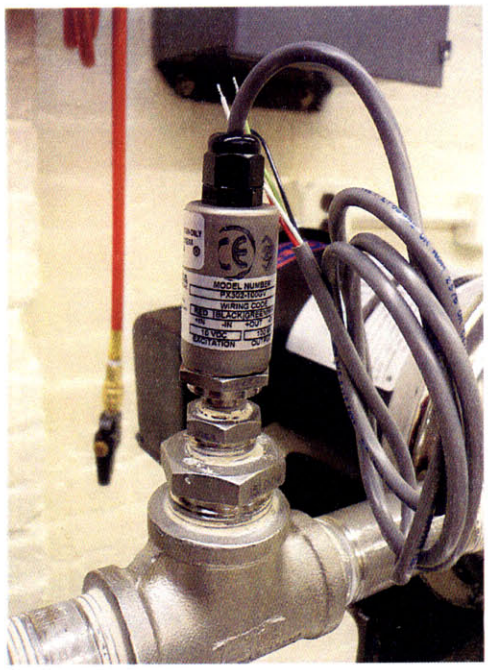

Figure 22: System pressure transducer PX302-100GV.

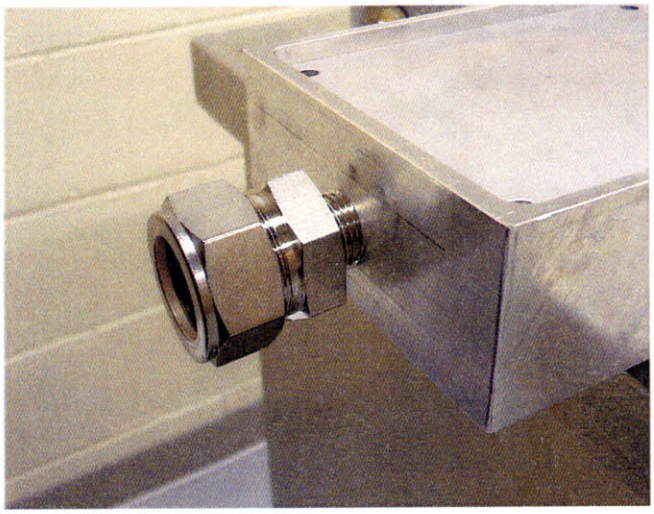

Figure 23: 0.5" NPT inlet into the upstream plenum of test assembly.

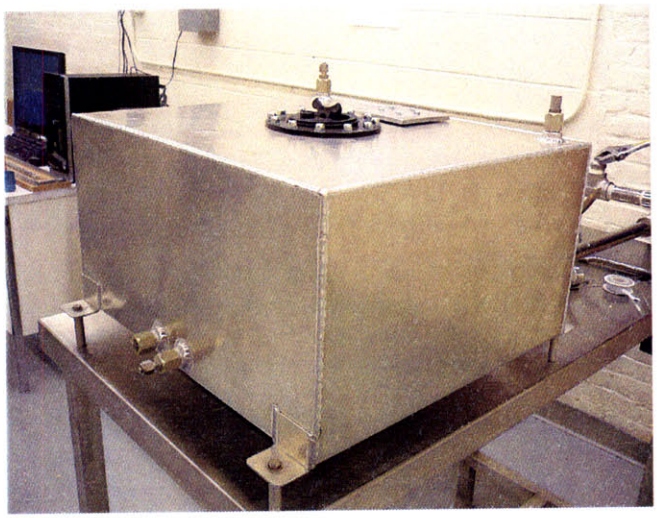

Figure 24: 20 gal. de-ionized water storage tank.

4. Experiment Result and Discussion

4.1. Overview

The friction pressure drop experiment loop is set-up at the MIT Nuclear Reactor Laboratory to obtain experiment data for the study of friction factors for different flows in rectangular ducts with continuous, longitudinal, rectangular fins. In addition to the finned rectangular channels, experiments are also performed using smooth rectangular channels for validation purposes. The experiment data are then used to compare and evaluate the effect of continuous, longitudinal and rectangular fins on friction pressure drop.

Experiment data are acquired using a National Instruments data acquisition (DAQ) system. A brief description of the design of the data acquisition interface, instrumentation calibration, and sampling frequency optimization is given in Appendix 8.7. Analysis of experiment errors and uncertainties can also be found in Section 4.4.

4.2. Experiment Result

In this study, two types of flow channel geometries, flow rates and several channel heights are investigated. The experiment data are organized into the following groups:

1. Laminar flow in smooth rectangular channel,
2. Laminar flow in finned rectangular channel,
3. Turbulent flow in smooth rectangular channel, and
4. Turbulent flow in finned rectangular channel.

4.2.1. Smooth rectangular channel

Data of the friction pressure drop for laminar and turbulent flows in smooth rectangular channels are measured for different channel heights between 0.078" and 0.125". The Darcy friction factors f_d, defined in Eq.(1),

are plotted against Reynolds number in Figure 25 for laminar flow, and in Figure 26 for turbulent flow. The friction factors are also compared to the correlation for rectangular ducts in Eqs.(10) and (12) respectively.

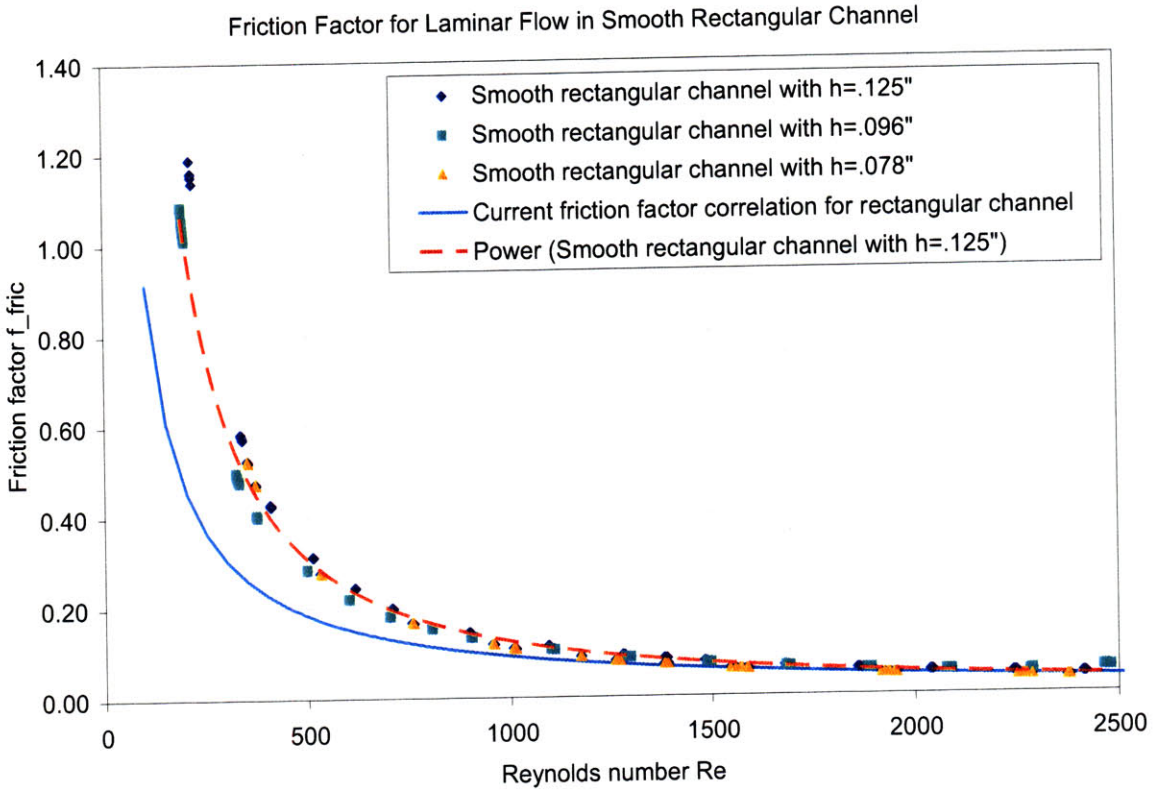

Figure 25: Friction factor for laminar flow (Re<2500) in smooth rectangular channels, with channel height of 78, 96 and 125 mils.

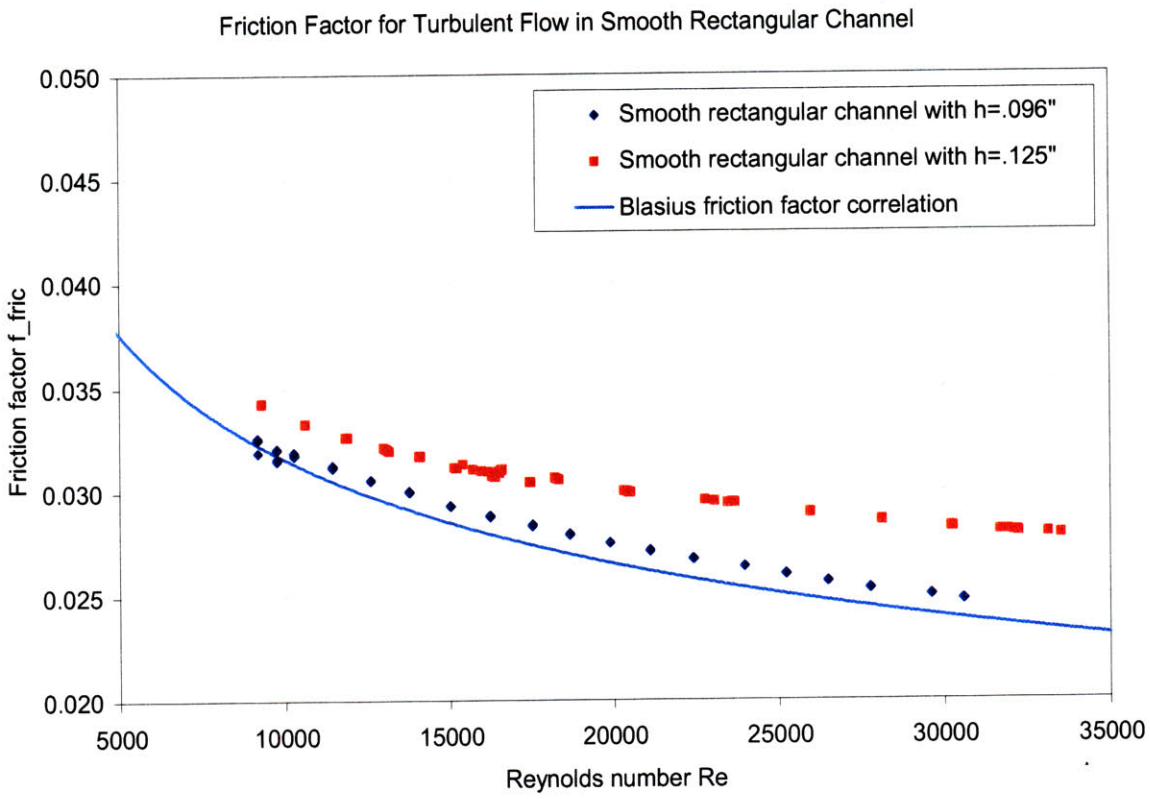

Figure 26: Friction factor for turbulent flow (Re>10,000) in smooth rectangular channels, with channel height of 96 mils and 125 mils.

In Figure 25, it is shown that the friction factors f_d for laminar flow in smooth rectangular channel seem independent of the different channel heights. It is due to the insignificant difference in the aspect ratios of the channels as they are applied to Eq.(10).

4.2.2. Finned rectangular channels with finned equivalent hydraulic diameter D_f^{finned}

In the study of finned rectangular channels, two approaches are attempted in the calculation of the equivalent hydraulic diameters. The first approach uses the definition of equivalent hydraulic diameter in Eq.(4) and Eq.(6), where the rectangular fins are included as a form in the calculation of the total perimeter P_w^{finned}.

$$P_w^{finned} = \left[w_{ch} + h_{ch} + \left(2n_f\right)\cdot h_f\right]\cdot 2 \tag{41}$$

where w_{ch} is the width of the flow channel,

h_{ch} is the base-to-base height of the finned flow channel,

h_f is the height of a rectangular fin, and

n_f is the number of rectangular fins on each plate.

4.2.2.1. Laminar flow

The friction factors for laminar flow in finned rectangular channels of 96 mils and 125 mils channel height are shown in

Figure 27 and Figure 28 respectively.

The friction factors f_d, calculated using the actual equivalent hydraulic diameter D_f^{finned}, are approximately half of the predicted values using the friction factor correlations in (9) and (10). This raises the concern that the actual equivalent hydraulic diameter D_f^{finned}, which is about twice as large as the equivalent hydraulic diameter of a smooth rectangular channel of similar height, might have caused the friction factors to deviate from the predicted values.

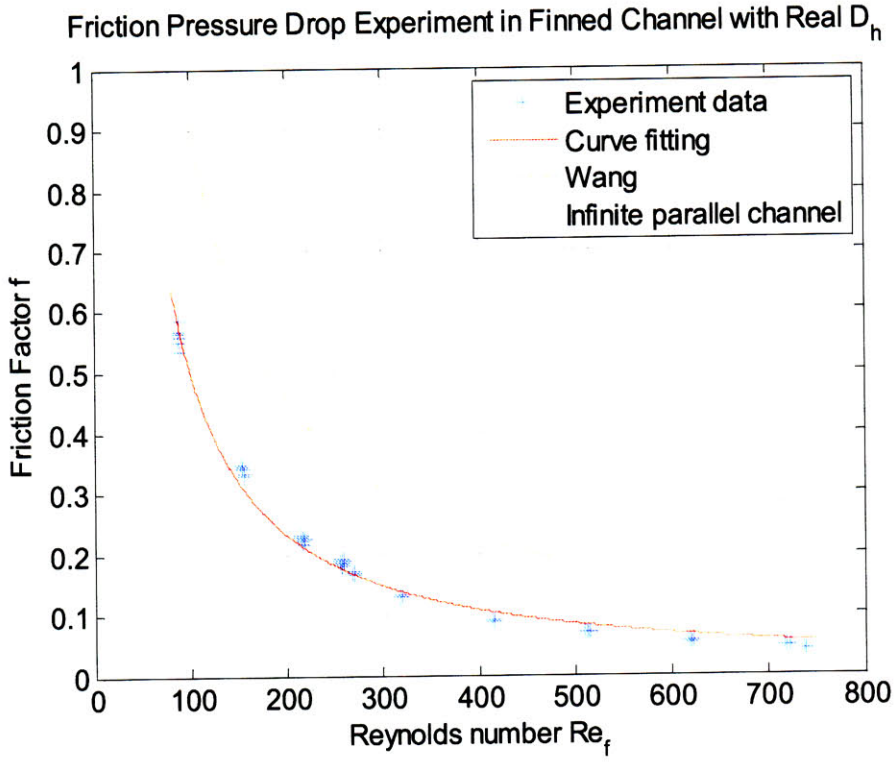

Figure 27: Friction factor for laminar flow (Re<750) in rectangular channel of 96 mils height with continuous longitudinal fins with actual equivalent hydraulic diameter.

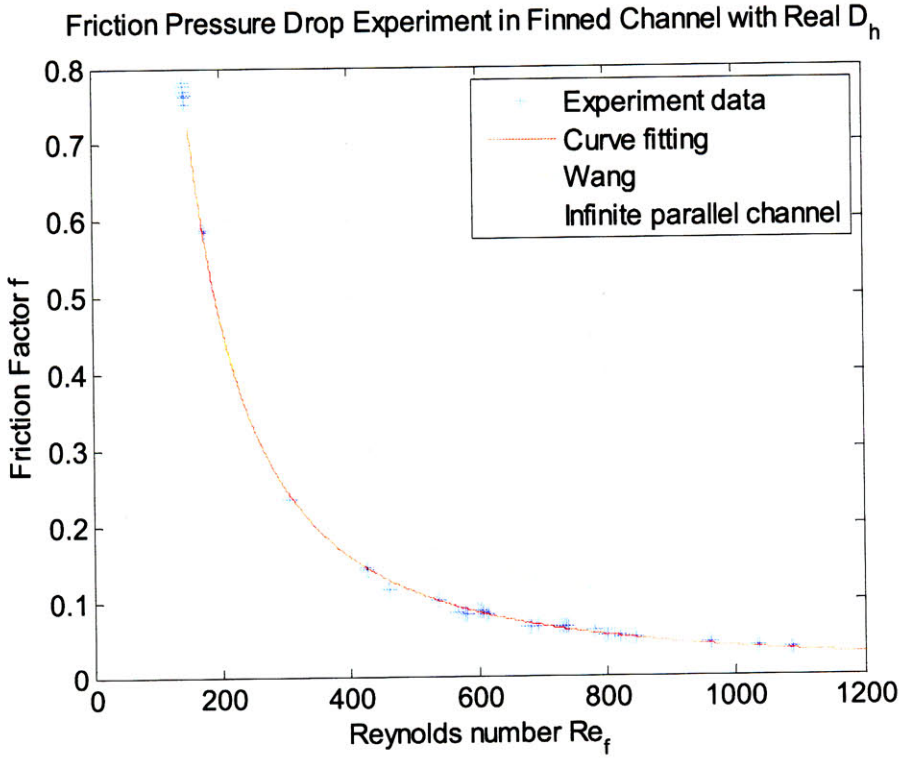

Figure 28: Friction factor for laminar flow (Re<1200) in rectangular channel of 125 mils height with continuous longitudinal fins with the actual equivalent hydraulic diameter.

4.2.2.2. Turbulent flow

The friction factors for turbulent flow in finned rectangular channels of 96 mils and 125 mils channel height are shown in Figure 29 and Figure 30 respectively.

The Darcy friction factors f_d, calculated using the experiment data, along with the actual equivalent hydraulic diameter D_f^{finned}, are about 20% below the Blasius friction factors in Eq.(12). Given that the continuous longitudinal rectangular fins of the flow channel lower the actual equivalent hydraulic diameter D_f^{finned} by almost a factor of 2, it is necessary to investigate in whether the rectangular fins should be treated as a form or surface roughness of the flow channel in the study of friction pressure drop characteristics.

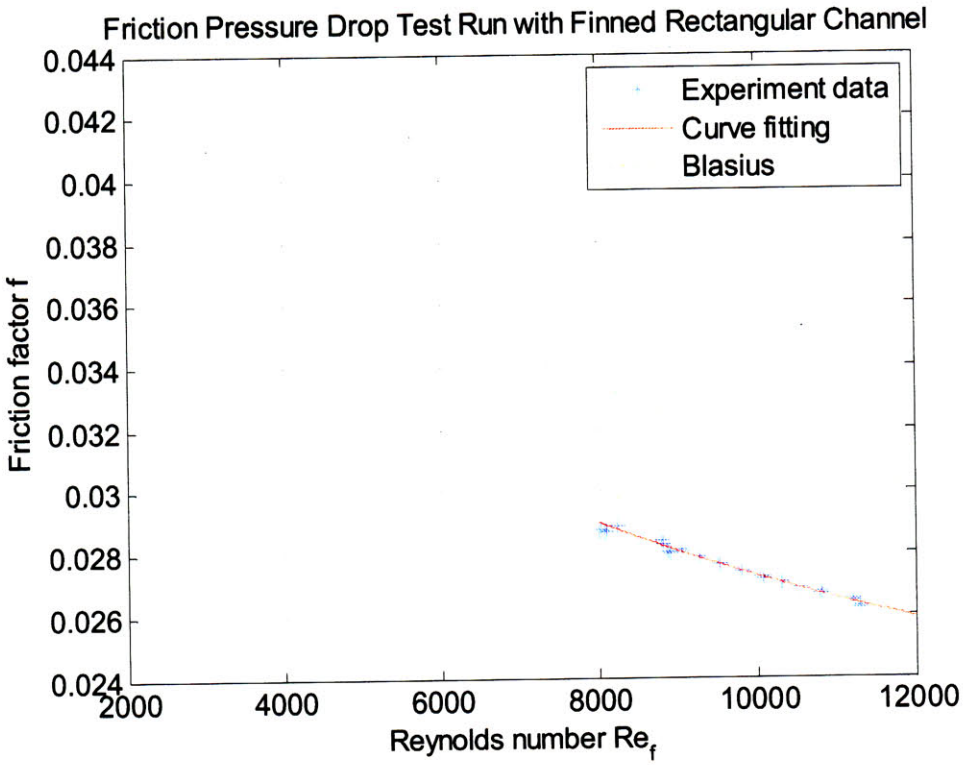

Figure 29: Friction factor for turbulent flow (Re<8,000) in rectangular channel of 96 mils height with continuous longitudinal fins with the actual equivalent hydraulic diameter.

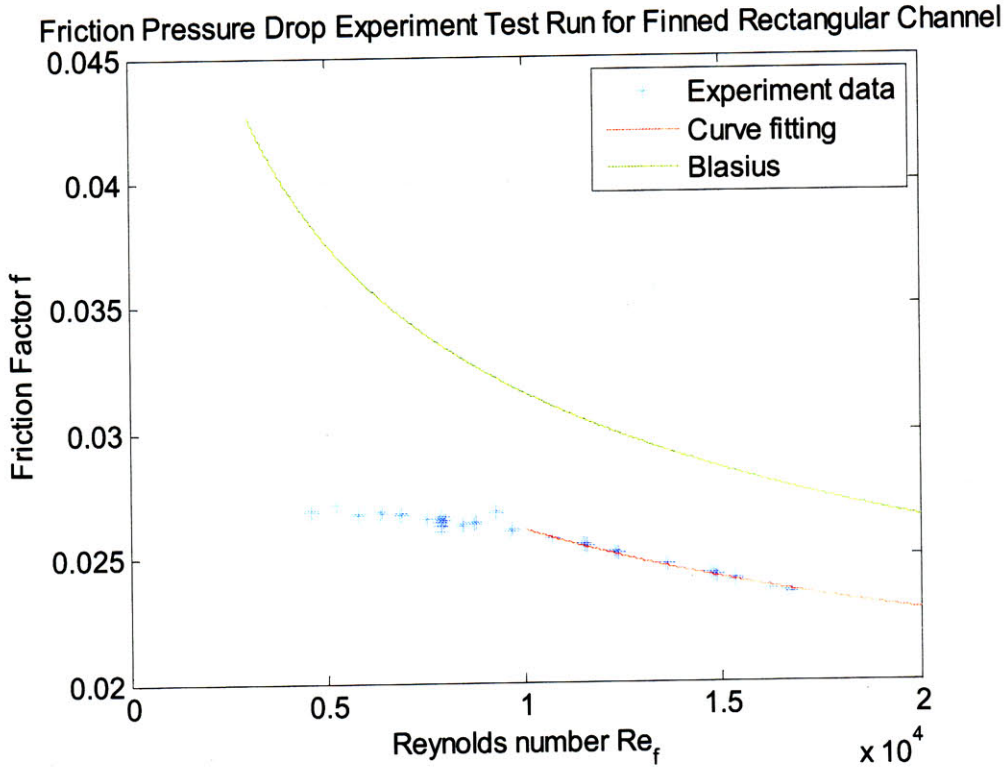

Figure 30: Friction factor for laminar flow (Re<10,000) in rectangular channel of 125 mils height with continuous longitudinal fins with the actual equivalent hydraulic diameter.

4.2.3. Finned rectangular channels with pseudo equivalent hydraulic diameter D_s^{finned}

A possible reason for the discrepancy between the calculated and measured friction is that the longitudinal fins affects the pressure drop due to surface roughness effect, not a form effect. Therefore, the second approach in the calculation of equivalent hydraulic diameter utilizes the actual cross-sectional area of finned rectangular channel A_c, and the equivalent hydraulic diameter of plain rectangular channel adjusted for the height of fins, such that,

$$\tilde{P}_w^{finned} = \left(w_{ch} + h_{ch} - h_f\right) \cdot 2 \tag{42}$$

where w_{ch} is the width of the flow channel,

h_{ch} is the base-to-base height of the finned flow channel, and

h_f is the height of a rectangular fin.

The pseudo equivalent hydraulic diameter D_s^{finned} is thus calculated as follows:

$$D_s^{finned} = \frac{4A_c}{\tilde{P}_w^{finned}} \tag{43}$$

where A_c is the cross-sectional area of the flow channel.

4.2.3.1. Laminar flow

Calculated using the pseudo equivalent hydraulic diameter D_s^{finned}, the friction factors f_d for laminar flows in finned rectangular channels (in Figure 31 and Figure 32) show similar trends as the friction factors in smooth rectangular channels (shown in Figure 25). This may be justified by the physical characteristics of laminar flow, in which a fluid flows through a channel in thick organized boundary layers.

In laminar flow, fluid molecules stay in the same layer of fluid as they continue on their path, unaffected by the presence of continuous longitudinal rectangular fins in the flow channel. This is consistent with the existing theory that friction factors are independent of the surface roughness of the channel, and hence explains the similar friction pressure drop characteristics for laminar flows in smooth and finned rectangular channels.

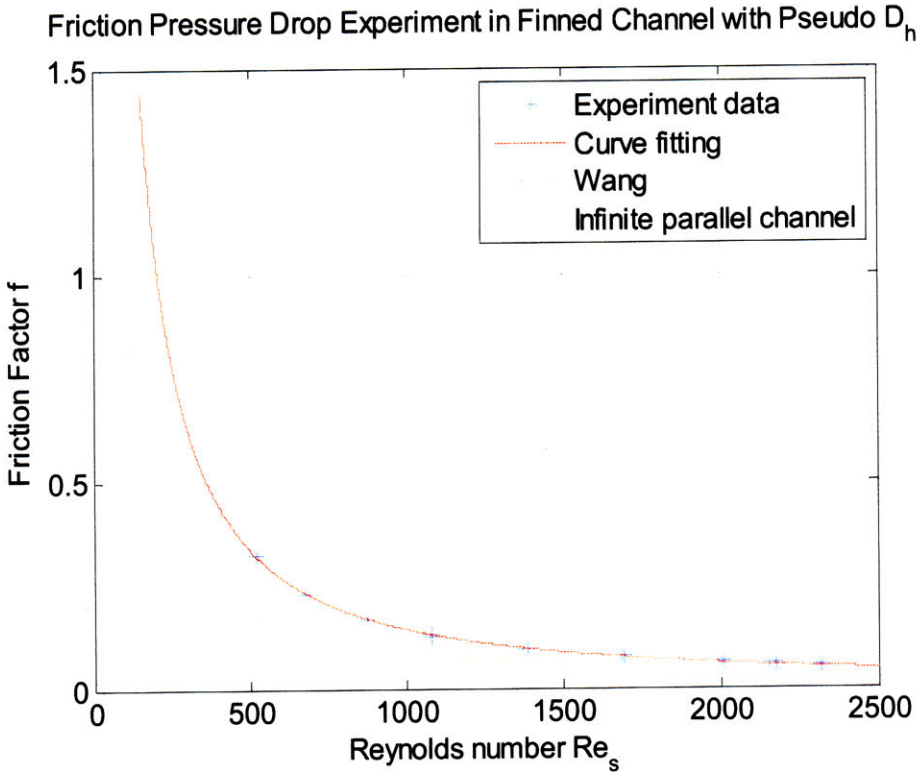

Figure 31: Friction factor for laminar flow (Re<2500) in rectangular channel of 78 mils height with continuous longitudinal fins with pseudo equivalent hydraulic diameter.

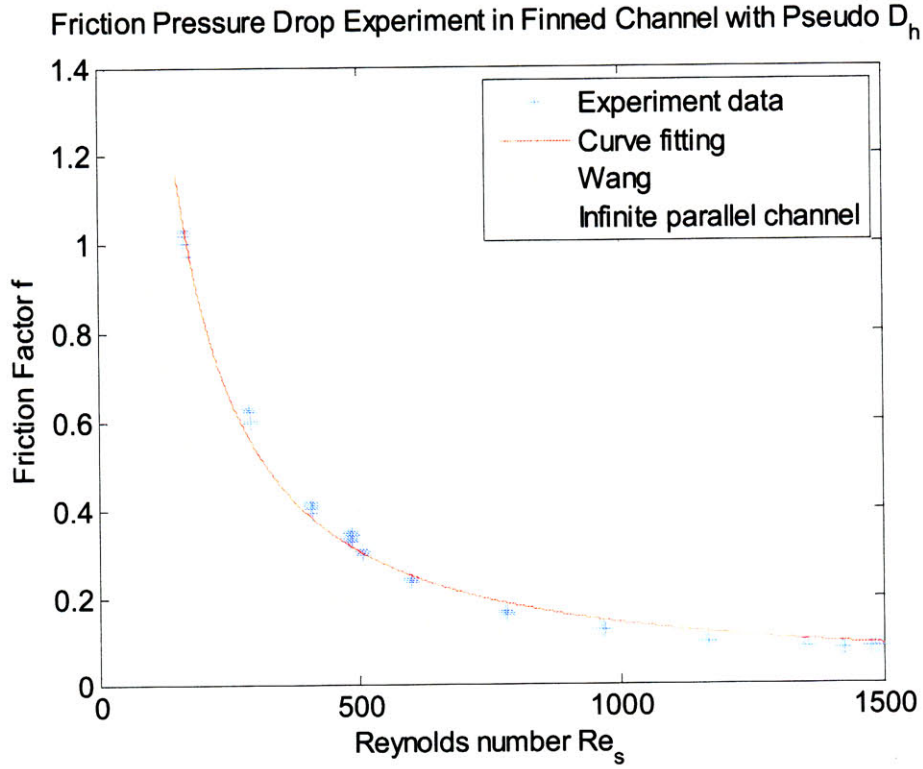

Figure 32: Friction factor for laminar flow (Re<2500) in rectangular channel of 96 mils height with continuous longitudinal fins with pseudo equivalent hydraulic diameter.

4.2.3.2. Turbulent flow

The friction factors f_d for turbulent flows in finned rectangular channels, calculated using the pseudo equivalent hydraulic diameter D_s^{finned} and assuming the rectangular fins to be a surface roughness, are shown in Figure 33 and Figure 34.

Unlike the laminar friction factors that seem to agree with those for smooth rectangular channel, the turbulent friction factors are significantly higher than the predicted values from the Blasius friction factor correlation in Eq.(12) due to the presence of the surface roughness. The trend of the turbulent friction factors versus the Reynolds number is consistent with that in Figure 29 and Figure 30.

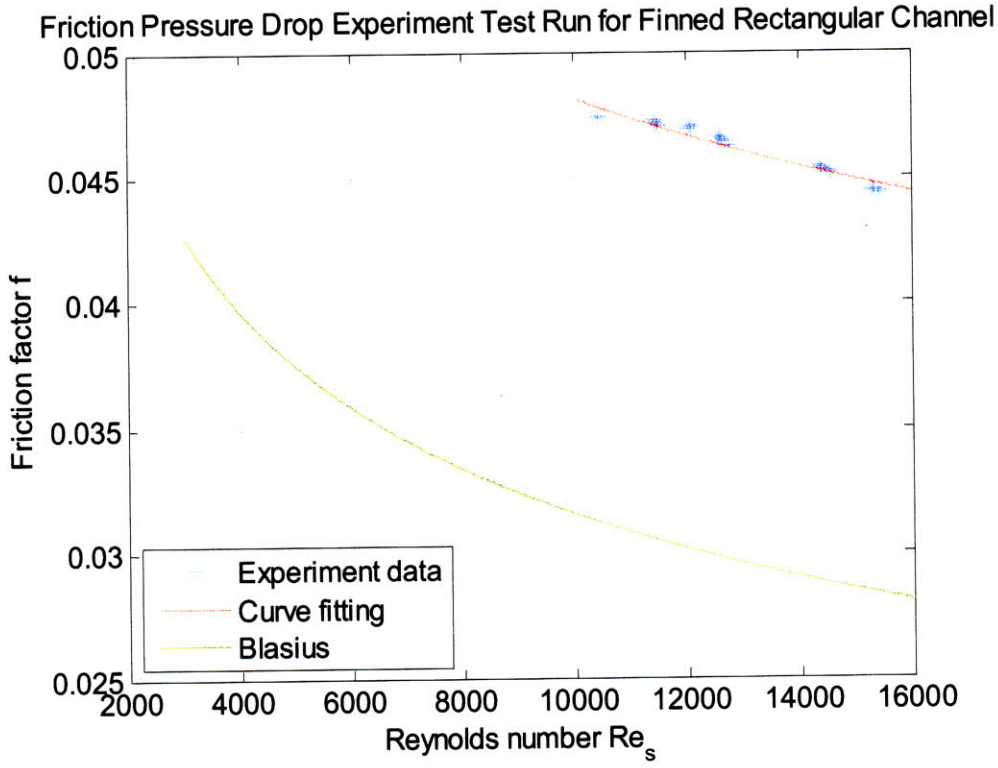

Figure 33: Friction factor for turbulent flow (Re>10,000) in rectangular channel of 78 mils height with continuous longitudinal fins with pseudo equivalent hydraulic diameter.

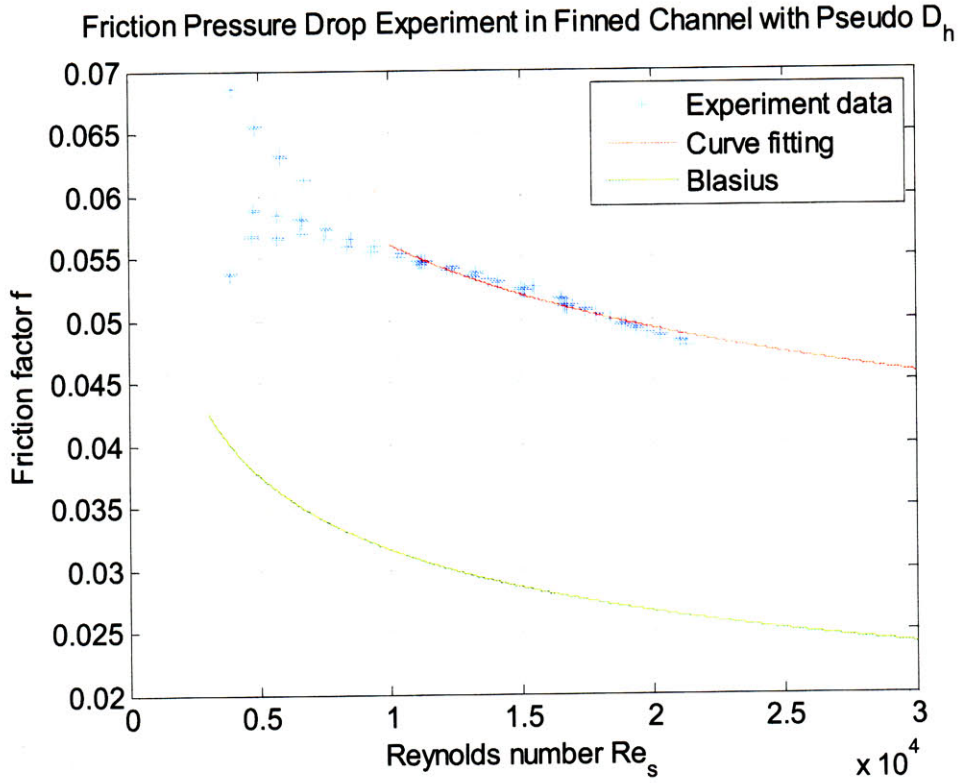

Figure 34: Friction factor for turbulent flow (Re>10,000) and transition flow (2500<Re<10,000) in rectangular channel of 96 mils height with continuous longitudinal fins with pseudo equivalent hydraulic diameter.

4.2.3.3. Transition flow

Figure 35 and Figure 36 show the friction factors for transition flows in finned rectangular channels, calculated using the pseudo equivalent hydraulic diameter D_s^{finned}, for channels with base-to-base heights of 78 mils and 96 mils respectively.

The significant levels of scattering of the transition friction factors in Figure 35 and Figure 36, as well as the difficulty in repeating the experiment data, cause tremendous challenge to drawing any meaningful conclusion to the friction pressure drop characteristics for transition flows in finned rectangular channels. More experiment data are needed to further study the characteristics of transition flows.

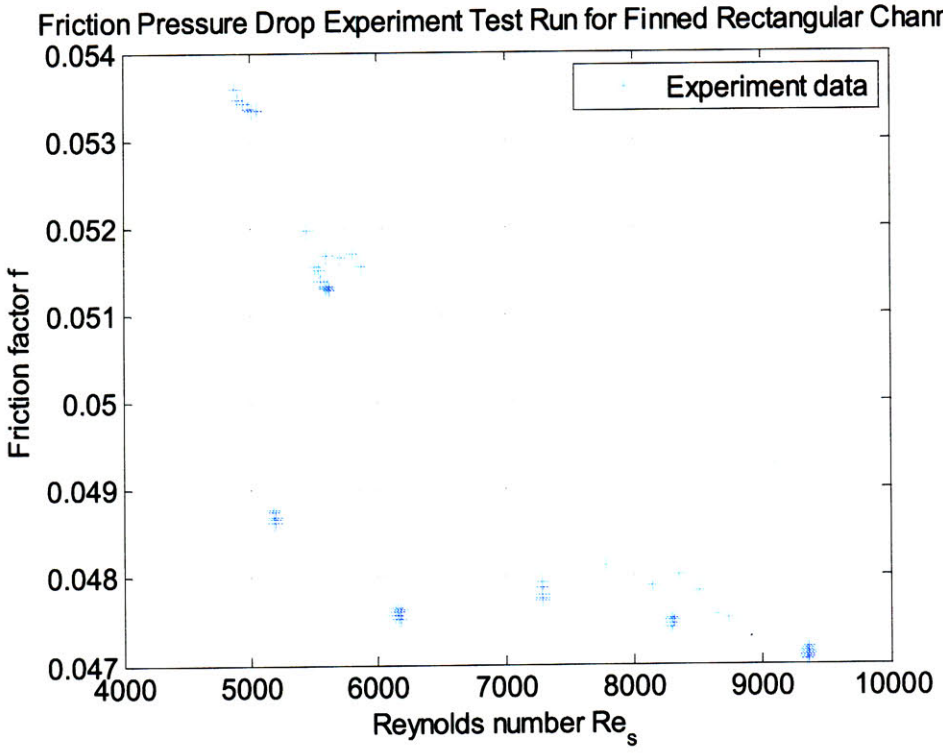

Figure 35: Friction factor for transition flow (2500<Re<10,000) in rectangular channel of 78 mils height with continuous longitudinal fins with pseudo equivalent hydraulic diameter.

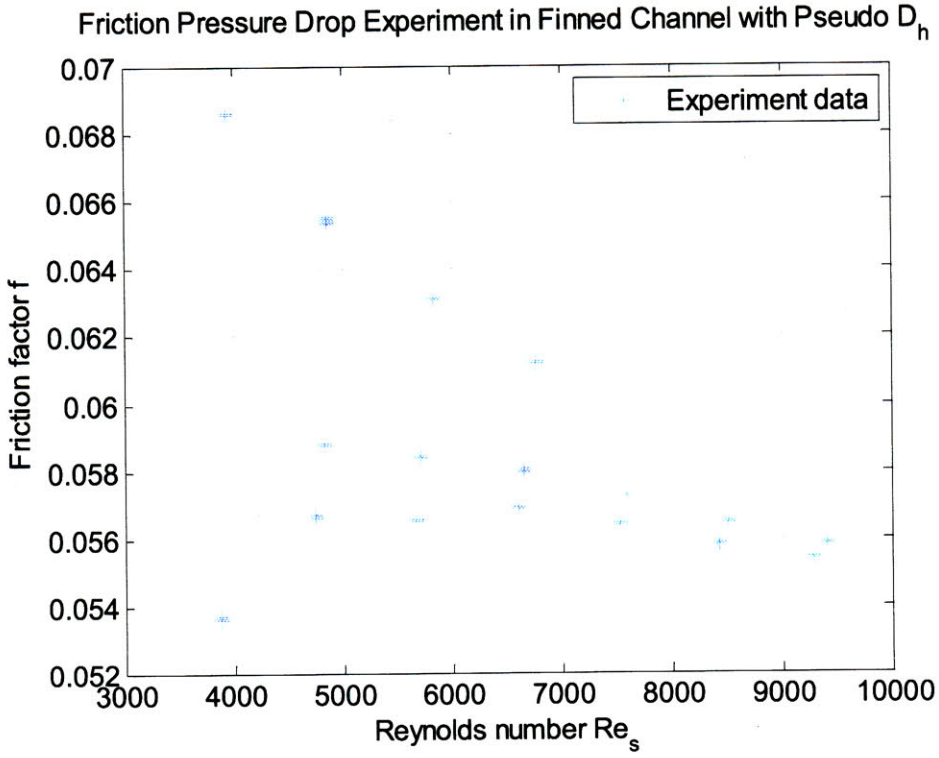

Figure 36: Friction factor for transition flow (2500<Re<10,000) in rectangular channel of 96 mils height with continuous longitudinal fins with pseudo equivalent hydraulic diameter.

4.3. Discussion

In this section, we will discuss the friction pressure drop characteristics for laminar and turbulent flows in smooth and finned rectangular channels, and propose new friction factor correlation for turbulent flow in finned rectangular ducts based on the experiment data.

4.3.1. Dimensionless parameter K_{fric}

In the study of the friction pressure drop characteristics in finned rectangular channels, it is discussed that the approach in the calculation of the equivalent hydraulic diameter has significant effect on the interpretation of the experiment data in Sections 4.2.2 and 4.2.3.

Reconsidering the definition of the Darcy friction factor f_d in (1) in Section 2, where the Darcy friction factor is linked to the pressure gradient $\frac{dP}{dz}$, fluid properties (ρ, v) and equivalent hydraulic diameter of flow channel D_e:

$$-\frac{dP}{dz} = \frac{f_d}{D_e}\frac{\rho v^2}{2} \tag{1}$$

It is possible to express the friction pressure drop characteristics in a different dimensionless parameter K_{fric}, in which the equivalent hydraulic diameter and axial length of the flow channel are no longer depended on, such that:

$$K_{fric} = \frac{f_d \cdot L}{D_e} = -\frac{2\Delta P}{\rho v^2} \tag{44}$$

where f_d is the Darcy friction factor,

L is the axial length of flow channel,

D_e is the equivalent hydraulic diameter,

ΔP is the friction pressure drop,

ρ is the fluid density, and

v is the average velocity of the fluid.

The utilization of friction factor K_{fric} in (44) instead of friction factor f_d in (1) to describe friction pressure drop characteristics in a flow channel, K_{fric} has the advantage of only depending on ΔP, ρ and v, but not the equivalent hydraulic diameter D_e.

4.3.2. Laminar flow

In Section 4.2.3.1, it is discussed that, in laminar flows, fluid molecules stay in the same layer of fluid as they continue on their path, independent of the continuous longitudinal rectangular fins of the flow channel and, thus, the similar friction pressure drop characteristics in smooth and finned rectangular channels.

4.3.2.1. Comparing f_d and K_{fric} for finned rectangular channel

Figure 37 shows a summary of friction factors f_d for laminar flows in smooth and finned rectangular channels with different channel heights (78 mils, 96 mils and 125 mils).

The inverse relationship between the friction factors f_d and Reynolds numbers (calculated using the actual and pseudo equivalent hydraulic diameters) in finned rectangular channels seems to be consistent with the trend in Figure 25. However, the significant difference between the actual equivalent hydraulic diameter D_f^{finned} and the pseudo equivalent hydraulic diameter D_s^{finned} leads to two interpretations of the friction factor curves in Figure 37. Another friction factor K_{fric}, defined in (44), is introduced in Section 4.3.1.

Figure 38 shows the friction factor K_{fric} for laminar flow in smooth and finned rectangular channels. The fact that K_{fric} only depends on the pressure drop ΔP, and the fluid properties ρ and ν, but not the equivalent hydraulic diameter D_e, reduces much of the deviation between two interpretations of the friction factors for laminar flow in finned rectangular channels. However, the embedded choice of D_e in the Reynolds number Re still remains as shown in Figure 38.

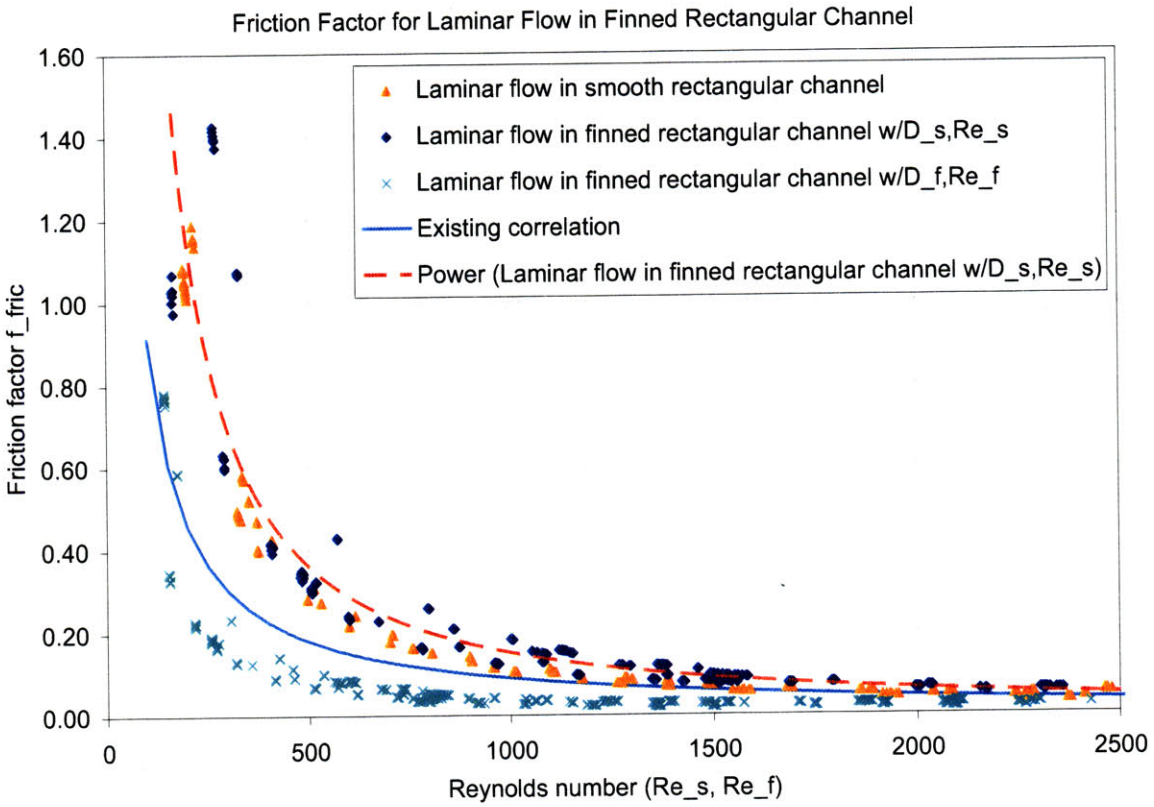

Figure 37: Friction factor f_d for laminar flow (Re<2500) in smooth and finned rectangular channels, with channel height of 78, 96 and 125 mils.

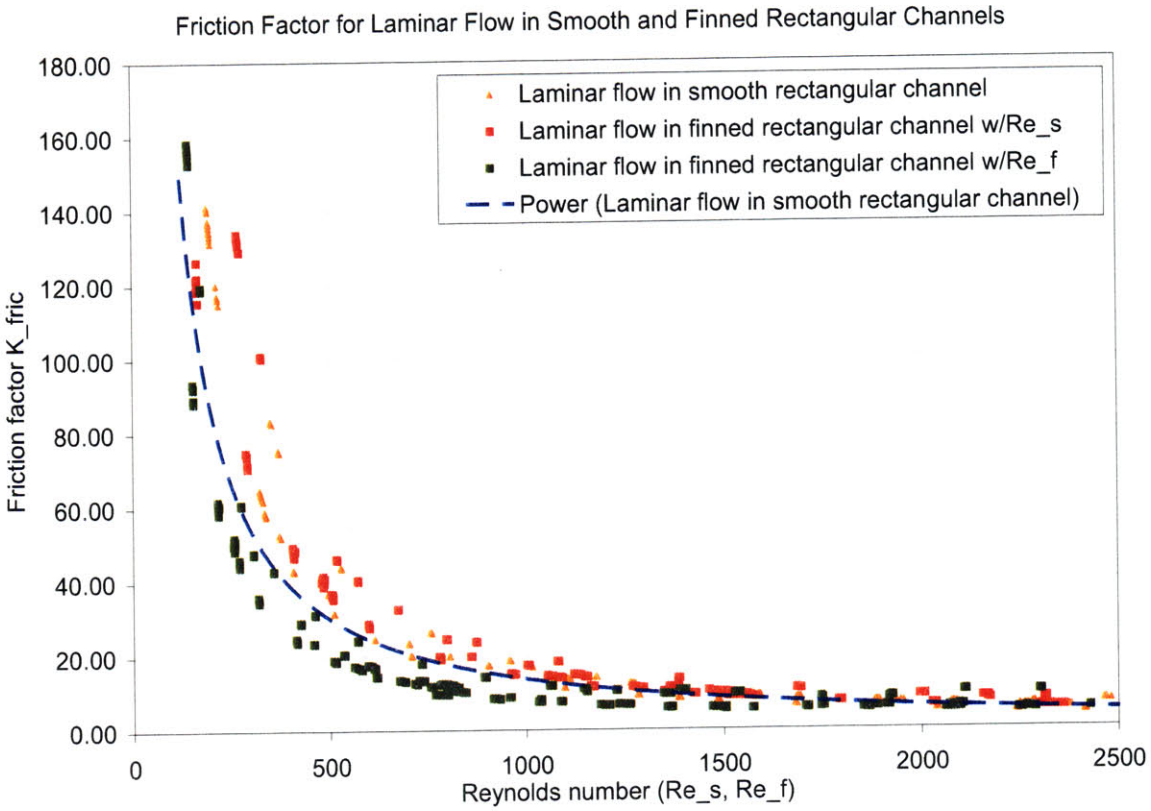

Figure 38: Friction factor K_{fric} for laminar flow (Re<2500) in smooth and finned rectangular channels, with channel height of 78, 96 and 125 mils.

4.3.3. Turbulent flow

In turbulent flow, fluid molecules rarely stay in the same layer as they continue on the path like they do in laminar flow. Instead, unsteady vortices and eddies appear on many scales and tend to interact with each other.

In this section, we will present and discuss the different friction pressure drop characteristics for turbulent flow in finned rectangular channels from smooth channels based on the experiment result.

4.3.3.1. Comparing f_d and the Colebrook friction factor for finned rectangular channel

Figure 39 shows the friction factors f_d for turbulent flows in finned rectangular channels with three different channel heights (78 mils, 96 mils

and 125 mils). The friction factors and the Reynolds numbers are calculated using the pseudo equivalent hydraulic diameter D_s^{finned}, as defined in (42) and (43) in Section 4.2.3, in which the finned rectangular channel is considered a pseudo-smooth channel with an adjusted channel height $h_{ch}^{'}$:

$$h_{ch}^{'} = h_{ch} - h_f \tag{45}$$

where h_{ch} is the base-to-base height of finned rectangular channel, and h_f is the height of the rectangular fins.

Figure 39 also shows the Blasius in (12) and Colebrook in (14) friction factor correlations for comparison. It is shown that the friction factors f_d, calculated using the pseudo equivalent hydraulic diameter D_s^{finned}, for turbulent flow in finned rectangular channel are about 60% – 80% higher than the Blasius friction factors, which although are intended for turbulent flow in smooth circular channels, are often used to describe the friction pressure drop for turbulent flow in other types of channel.

In a different comparison, the friction factors f_d from the experiment data are compared to the Colebrook correlation, which are intended for turbulent flow in circular channel with surface roughness r, where $r = \frac{\varepsilon}{D_e}$.

The Colebrook friction factor correlation in Figure 39 utilizes a surface roughness of $\varepsilon = h_f$. It is shown that the Colebrook correlation, while assuming the entire height of the continuous, longitudinal, rectangular fins as surface roughness, is flatter and higher than the friction factor f_d calculated from the experiment data.

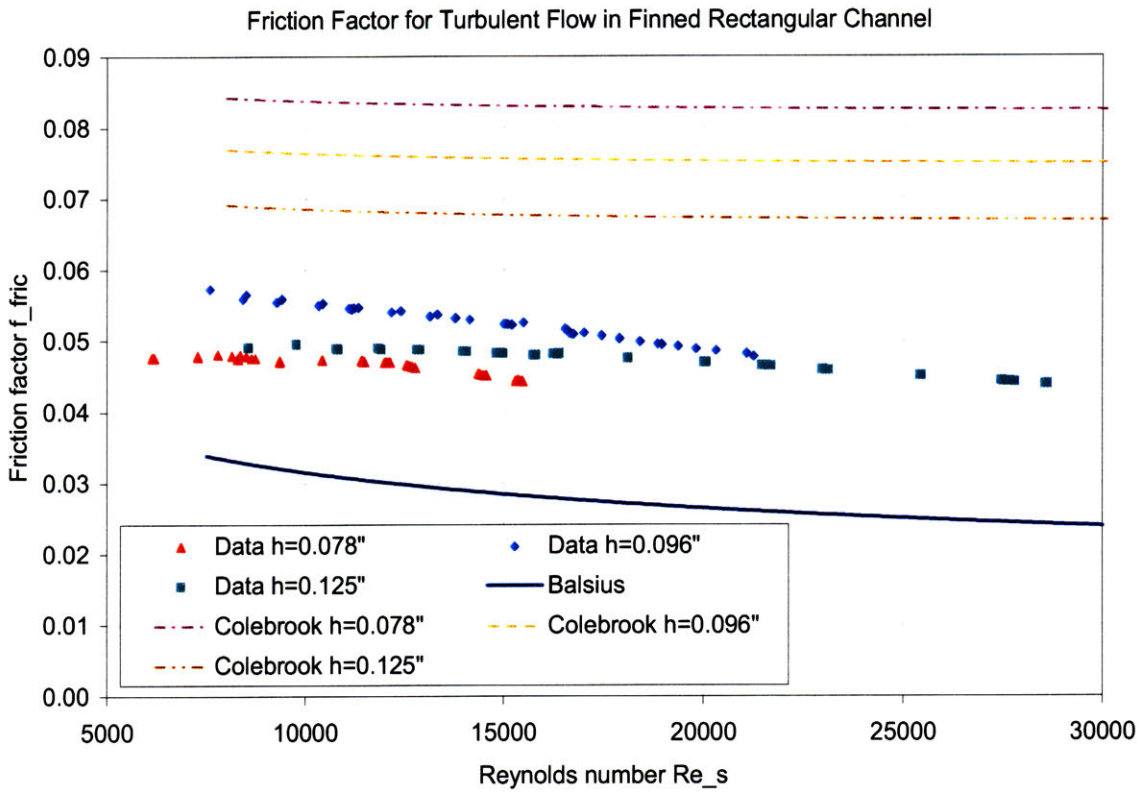

Figure 39: Friction factor for turbulent flow (Re>10,000) in finned rectangular channels, with channel height of 78, 96 and 125 mils.

4.3.3.2. Comparing f_d and a new friction factor for finned rectangular channel

Figure 40 shows a summary of the Darcy friction factors f_d, calculated using the actual and pseudo equivalent hydraulic diameters $\left(D_f^{finned}, D_s^{finned}\right)$ and assuming the continuous longitudinal rectangular fins to be a surface roughness, for turbulent flow in finned rectangular channels; the friction factors f_d for smooth rectangular channels are also shown in Figure 40 for comparison.

In addition, the Blasius friction factor correlation for turbulent flow from Eq.(12), as well as a new friction factor correlation, are plotted in the same figure for comparison. The new friction factor correlation uses the same exponential as the Blasius friction factor in Eq.(12). It is then multiplied

by a coefficient that characterizes the geometry of the channel and can be represented as follows:

$$f_d = C_j \cdot \mathrm{Re}^{-0.25} \tag{46}$$

where $C_j \approx 0.575$ is a dimensionless coefficient, and

$\mathrm{Re} < 35{,}000$.

The friction factors f_d for turbulent flow in finned rectangular channel seem to show good agreement with the method proposed in Eq.(46) for $15{,}000 < \mathrm{Re} < 35{,}000$. The deviation between friction factors f_d and the correlations proposed in Eq.(46) is also within the errors and uncertainties of the experiment data. The analysis of measurement errors and uncertainties will be discussed in Section 4.4.

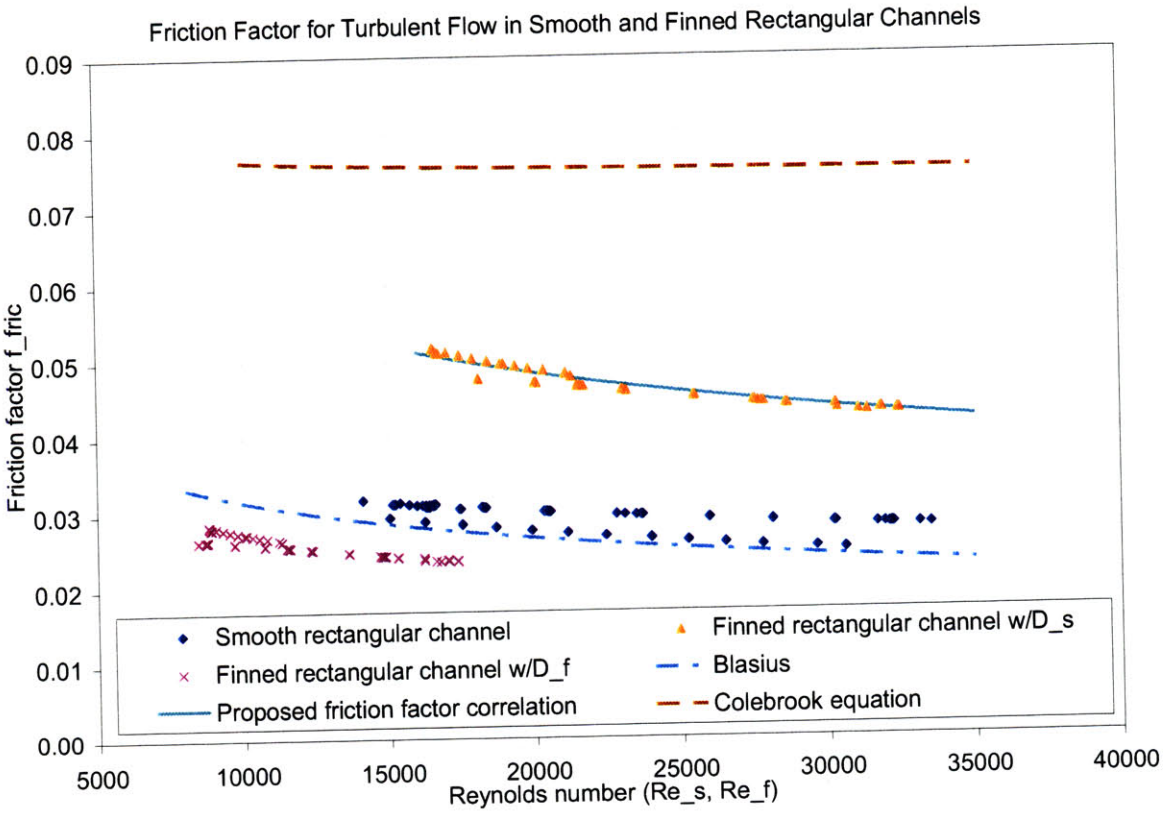

Figure 40: Friction factor for turbulent flow (Re>10,000) in finned rectangular channels.

4.3.3.3. Comparing friction factors f_d and K_{fric} for turbulent flow in finned rectangular channel

In Section 4.3.1, we discuss the advantage and disadvantage of considering friction factors K_{fric} in Eq.(44), as opposed to f_d in Eq.(1), for finned rectangular channels due to the different approaches to calculate the actual and pseudo equivalent hydraulic diameters $\left(D_f^{finned}, D_s^{finned}\right)$. Figure 41 shows a summary of the friction factors K_{fric} for turbulent flow in finned rectangular channels, with various channel heights of 78 mils, 96 mils and 125 mils.

For finned rectangular channel with smaller channel heights of 78 mils and 96 mils, the friction factors K_{fric} for turbulent flow show similar trends as shown in Figure 41, and can be characterized in the following equation:

$$K_{fric} = 114.7 \cdot \mathrm{Re}^{-0.3030} \tag{47}$$

for finned rectangular channel with channel height of 78 mils and 96 mils, and $8{,}000 < \mathrm{Re} < 22{,}000$.

For finned rectangular channel with larger channel height of 125 mils (and hence larger aspect ratio), however, the friction factors K_{fric} show slightly different trend and are found to be lower than the friction factors in (47).

$$K_{fric} = 31.76 \cdot \mathrm{Re}^{-0.1988} \tag{48}$$

for finned rectangular channel with channel height of 125 mils, and $8{,}000 < \mathrm{Re} < 35{,}000$.

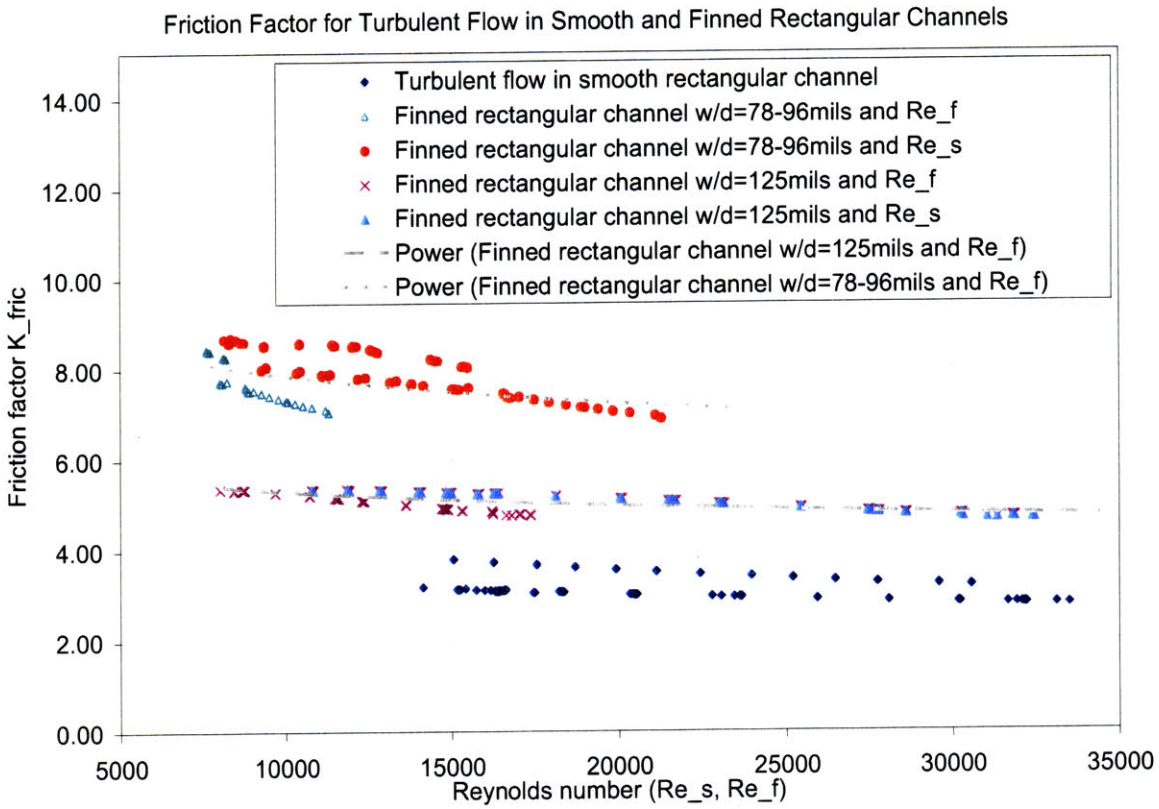

Figure 41: Friction factor K_{fric} for turbulent flow (Re>10,000) in finned rectangular channels.

4.4. Error Analysis

In previous sections, the design of the friction pressure drop experiment loop and the result are discussed in details. In this section, we will further consider the uncertainties of the experiment data, the sources of uncertainties and the propagation uncertainties from individual measurements to the friction factor estimates.

4.4.1. Instrumental uncertainties of data

In the friction pressure drop experiment, several independent variables are vital in the estimation of friction factors as it is defined in (1). The independent variables include the following:

1. velocity of flow,
2. pressure drop in test section,

3. fluid density, and
4. fluid viscosity.

Instrumental uncertainties arise when there is a lack of perfect precision in the physical instrument (shown in Table 3), or when there are fluctuations in the instrumental readings due electrical noise or human imprecision (shown in Figure 42), or a combination of both.

The precision of each physical instrument, as described in the specifications sheet, is summarized in Table 3. A set of sample tests is also performed to estimate the instrumental uncertainties due to electrical noise in the data acquisition system. It is found that the deviation of sample data remains at 1% to 2% for the flow meter and thermocouples; but reduces dramatically for the system pressure transducer as the number of acquired test data increases.

Ideally, as the number of sample data increases infinitely, the standard deviation of the sample population decreases for statistical reasons; but this also adds to the volume of data that the system needs to handle. To maintain a balance between the instrument uncertainties and speed of data processing, it is selected that 120 seconds of measurements collected at 20 Hz are used for a single datum.

Table 3: Accuracy of the instruments listed on the specification sheets.

Instrument	Model	Precision	Adjusted Instrument Uncertainties
System pressure transducer	PX-302	0.25%	9%
Differential pressure transmitter	PD 3000	0.25%	-
Thermocouple 1	Std K 3"	1.67%	1.67%
Thermocouple 2	Std K 3"	1.67%	1.67%
Flow meter (high range)	FTB-904	0.50%	2.50%

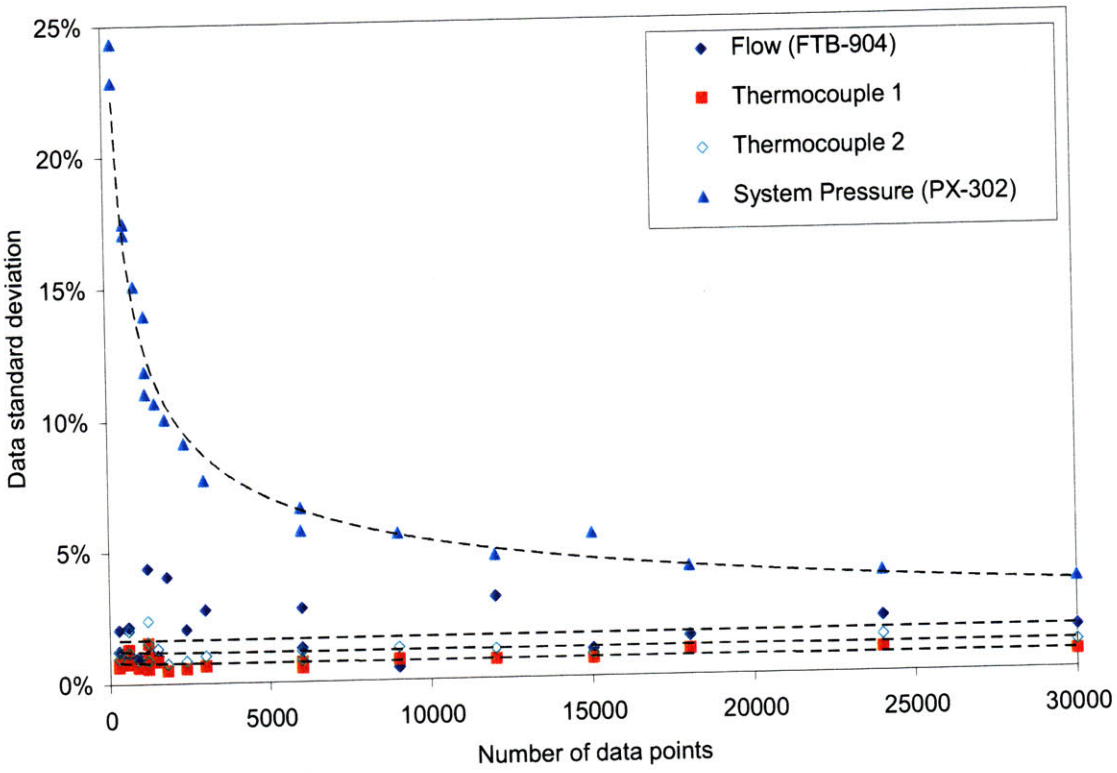

Figure 42: Instrument uncertainties due to electrical noise during zero-flow operation.

4.4.2. Propagation of errors

Using the uncertainties of individual physical instruments from Section 4.4.1, it is possible to determine the uncertainty in the dependent variables (K, f_d) via the method of error propagation in [45].

$$\Delta K \approx \frac{-2\Delta P}{\rho v^2} \cdot \frac{\Delta(\Delta P)}{\Delta P} + \frac{2\Delta P}{\rho v^2} \cdot \left(\frac{\Delta \rho}{\rho}\right) + \frac{4\Delta P}{\rho v^2} \cdot \left(\frac{\Delta v}{v}\right) \tag{49}$$

where ΔK is the uncertainties in the friction factor K,

$\Delta(\Delta P)$ is the uncertainties in the pressure drop,

$\Delta \rho$ is the uncertainties in the fluid density, and

Δv is the uncertainties in the fluid velocity.

Using the equation in (49), the percentage uncertainty $\frac{\Delta K}{K}$ of friction factor K is estimated to be about 5% (see Appendix). Moreover, the same method of error propagation can be applied in (50), where

$$\Delta f_d \approx \frac{KD_e}{L} \cdot \left(\frac{\Delta K}{K}\right) + \frac{KD_e}{L} \cdot \left(\frac{\Delta D_e}{D_e}\right) - \frac{KD_e}{L} \cdot \left(\frac{\Delta L}{L}\right) \tag{50}$$

where Δf_d is the uncertainties in the Darcy friction factor f_d,

ΔL is the uncertainties in the axial length of the flow channel, and

ΔD_e is the uncertainties in the equivalent hydraulic diameter.

Similarly, the percentage uncertainty $\frac{\Delta f_d}{f_d}$ of friction factor f_d is estimated to be between 7% and 15% for f_f^{finned}, f_s^{finned} and f_s^{smooth}.

Table 4: Percentage uncertainty of friction factor f_d.

	$\%\Delta f_d$
Laminar flow	14%
Turbulent flow	15%

4.5. Summary

For laminar flow in rectangular duct with continuous, longitudinal, rectangular fins, the pseudo equivalent hydraulic diameter D_s^{finned} should be considered, as opposed to the actual equivalent hydraulic diameter D_f^{finned}, to estimate the friction pressure drop behavior. Moreover, the correlation of friction factors f_d in Eq.(10), along with the use of D_s^{finned}, show good agreement with the experiment result.

For turbulent flow in finned rectangular channel, a new correlation for the Darcy friction factor f_d is proposed. The new friction factor correlation uses the same exponential as the Blasius friction factor in Eq.(12). It is then multiplied by a coefficient based on the geometry of the channel and can be represented as follows:

$$f_d = 0.575 \cdot \mathrm{Re}_s^{-0.25} \tag{46}$$

where $15{,}000 < \mathrm{Re}_s < 30{,}000$.

Moreover, another friction factors K_{fric} defined in Section 4.3.1 show different trends for channels of different heights and aspect ratios.

The friction factors for turbulent flow in finned rectangular channels with smaller channel height (78 mils and 96 mils) are found to be about 25% higher than those with larger channel height (125 mils), and are proposed in (47) and (48) respectively:

$$K_{fric} = 114.7 \cdot \mathrm{Re}^{-0.3030} \tag{47}$$

$$K_{fric} = 31.76 \cdot \mathrm{Re}^{-0.1988} \tag{48}$$

where Re is the Reynolds number, calculated using the actual or pseudo equivalent hydraulic diameter.

5. Reactor Core Flow Distribution Analysis

5.1. Homogenous Core Analysis

5.1.1. Overview

The distribution of flow of the primary coolant in the reactor core can be determined by the various pressure drop characteristics. [13] suggests that these pressure drop characteristics include the friction effect due to the surface interaction between fluid and wall of the channel, the form effect due to changes in geometry of the channel, the acceleration effect due to changes in the fluid density, as well as the gravitation effect.

A well documented knowledge of friction factors for laminar and turbulent flows in channels of different geometries and surface roughness have been made and is shown in Figure 72. In the design studies of the MITR-II, two Darcy friction factor correlations (shown below) have been used for the calculation of friction pressure drop in laminar and turbulent flows.

$$f_d = \frac{91.5}{\mathrm{Re}} \tag{51}$$

$$f_d = 0.316 \cdot \mathrm{Re}^{-0.25} \tag{12}$$

where Re is Reynolds number.

Equation (51), which agrees with equation (10), was used in a study of laminar pressure drop in 1975, while equation (12) was used in calculating the friction factor for turbulent flows in [1, 2, 11, 12].

5.1.2. Effect of Channel Height in Homogenous Core

The friction pressure drop in rectangular ducts with continuous longitudinal rectangular fins is modeled using a MATLAB script. In this analysis, Blasius [13] and Braga [26] friction factor correlations are selected to compare the friction pressure drop for turbulent flows in both plain and

finned channels of various channel heights. Channel height is referred to as the distance between the fin bases of two opposing finned plates.

5.1.2.1. HEU reactor core

The hexagonal core of the MIT Reactor contains 27 positions, among which 24 positions are filled with fuel elements, leaving 3 positions available for in-core experiments. Each fuel element has 14 full flow channels and 2 half-channels.

The boundary of a full channel is formed by two rectangular HEU fuel plates with continuous longitudinal rectangular fins, separated by two side plates of 0.188" thick. The fin-to-fin distance between two opposing fuel plates is 0.078" in a full flow channel, or 0.088" in two neighboring half-channels; and the base-to-base channel height is thus 0.098" in a full flow channel, or 0.108" in two neighboring half-channels.

In this section, "channel height" is referred to as the base-to-base channel height unless specified otherwise. The friction pressure drop for turbulent water flow in finned rectangular ducts in the core of the MIT reactor is shown in Figure 46.

Using Blasius friction factor correlation for turbulent flows at $\mathrm{Re} < 30{,}000$, the friction pressure drops in the HEU channel during normal reactor operation (2 pumps) and low flow primary coolant (2 pumps) are estimated to be around 3.29×10^4 Pa and 2.32×10^4 Pa respectively.

During natural convection operation when the reactor power is below 100 kW, the friction pressure drop for laminar flow in the HEU channel is estimated to be around 89.6 Pa.

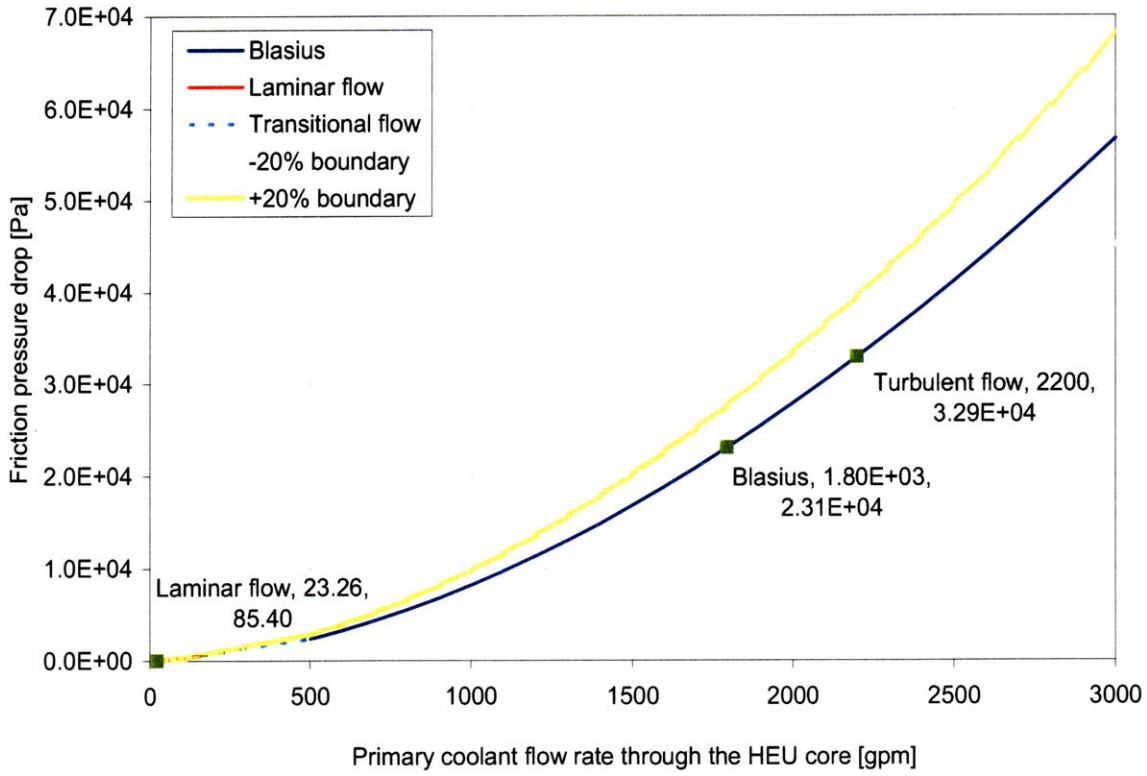

Figure 43: Estimated friction pressure drop in the HEU core of the MIT Reactor with the use of Eq.(51) and Eq.(12) for laminar and turbulent flows respectively.

Table 5: Primary coolant flow rate and estimated friction pressure drop for various operating conditions.

Operating condition	**Primary coolant flow rate [gpm]**	**Friction pressure drop [Pa]**
Normal reactor operation (2 pumps)	2200	3.29E+04
Low flow primary coolant (2 pumps)	1800	2.32E+04
Natural convection condition	20.85	8.96E+01

5.1.2.2. LEU reactor core

In the design of the LEU core, thinner fuel meat and aluminium cladding are used in the finned rectangular fuel plates [1]. The proposed design of the LEU fuel element contains 18 fuel plates, with 17 full flow channels and 2 half-channels. Each finned rectangular fuel plate contains

a 0.020" thick fuel meat, with a 0.010" thick aluminium cladding. Similar to the HEU design, continuous longitudinal rectangular fins of 0.010" by width, 0.010" by height, and 0.010" apart from one another are added to the surface of the aluminium cladding.

The increase in the number of fuel plates per element in the LEU core design proposed in [1, 2, 8, 9] reduces the heights of the flow channels, but are slightly offset by the reduced thicknesses of the fuel meat and the aluminium cladding. The base-to-base channel height decreases to about 0.092" as compared to 0.098" in HEU fuel element [8, 9].

Using Blasius and McAdams friction factor correlations for turbulent flows in smooth circular conduits, the reduction in the equivalent hydraulic diameter D_e of the LEU flow channel has an immediate effect on the friction pressure drop expressed as follows:

$$-\frac{dP}{dz} = \frac{f_d}{D_e}\frac{\rho v^2}{2} \tag{52}$$

where f_d is Darcy friction factor,

v is the mean velocity of flow, and

D_e is the equivalent hydraulic diameter of the finned channel.

Figure 44 shows that the friction pressure drop in rectangular ducts with continuous longitudinal rectangular fins decreases dramatically as the channel height increases from 0.040" to 0.100", while keeping the number of plates per fuel element constant at 15 (Figure 44) and 18 (Figure 45).

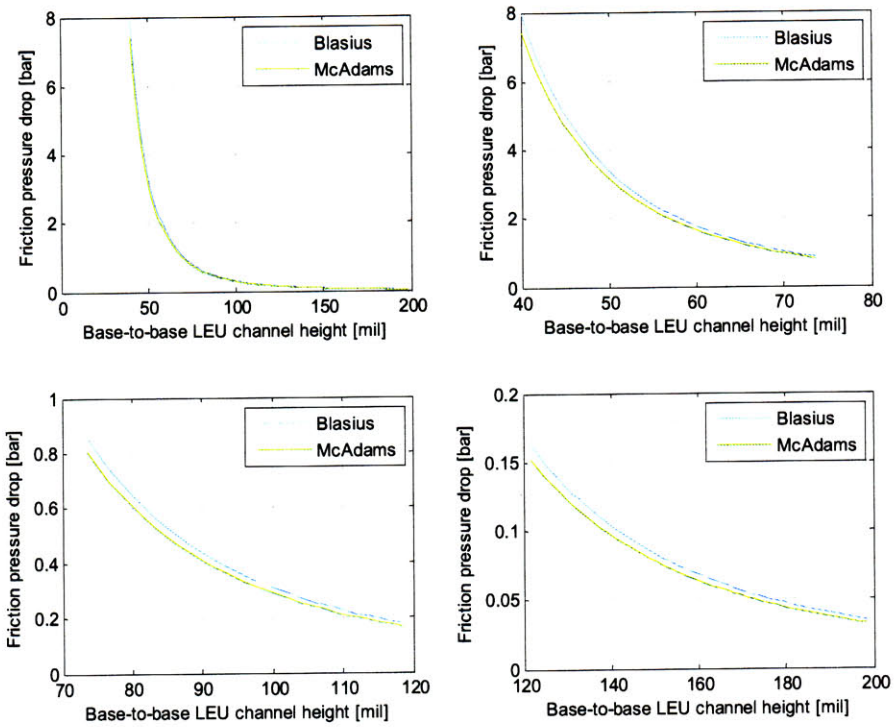

Figure 44: Friction pressure drop for turbulent water flow in aluminium ducts with continuous longitudinal rectangular fins, with 15-plate fuel element design.

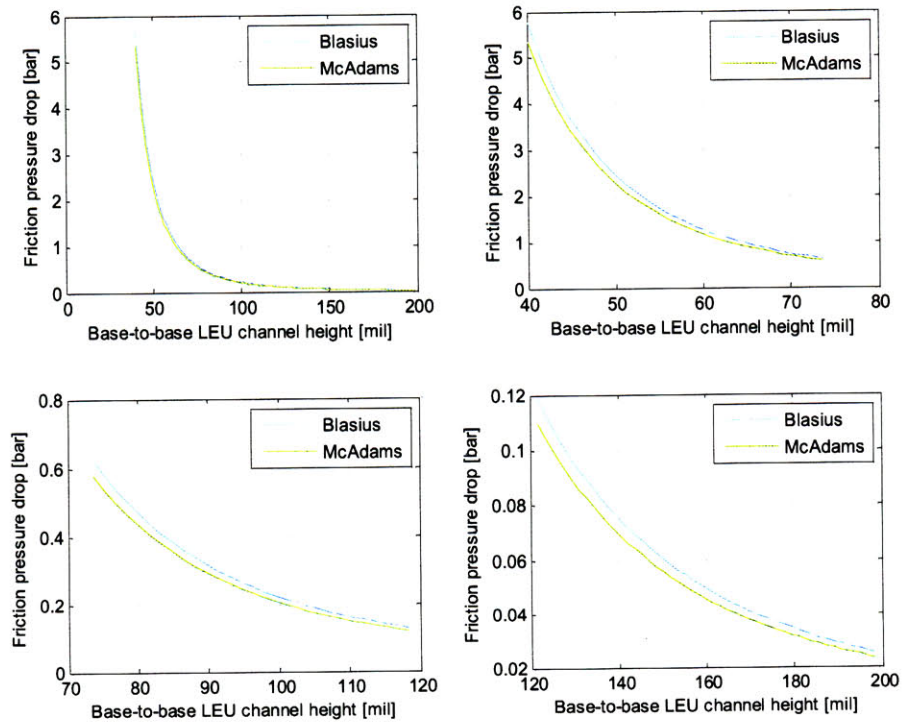

Figure 45: Friction pressure drop for turbulent water flow in aluminium ducts with continuous longitudinal rectangular fins, with 18-plate fuel element design.

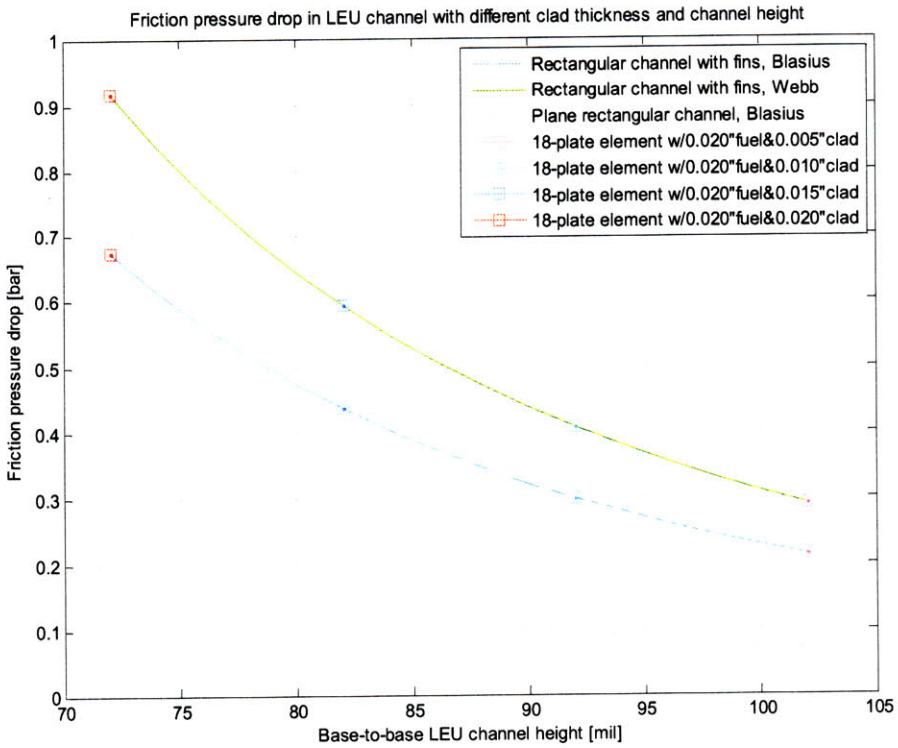

Figure 46: Friction pressure drop for turbulent water flow through 18-plate LEU element.

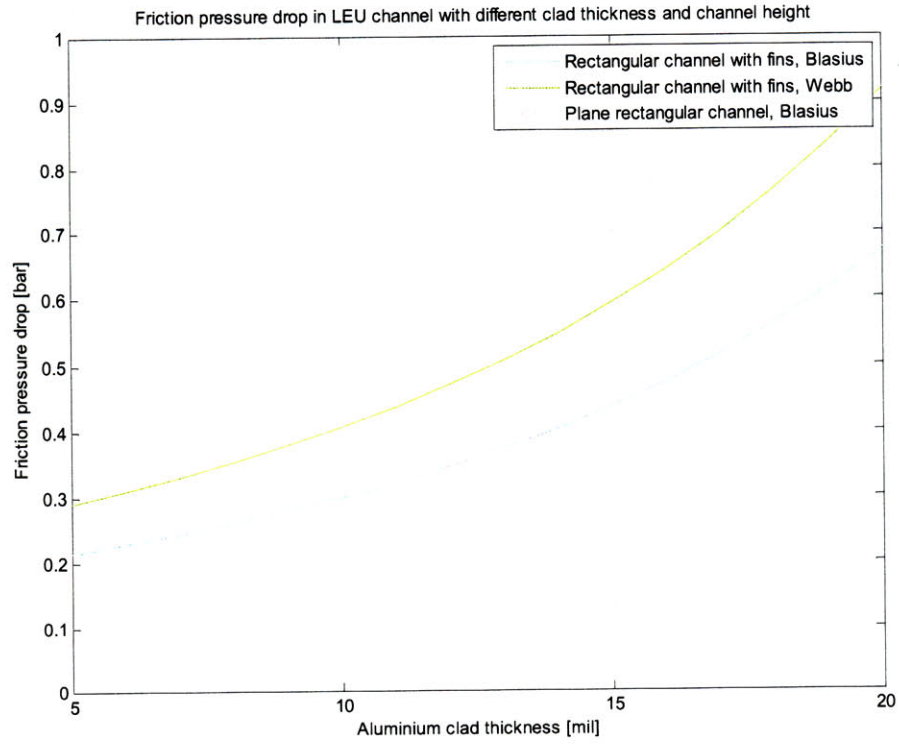

Figure 47: Friction pressure drop for turbulent water flow through 18-plate LEU element with respect to the aluminium clad thickness.

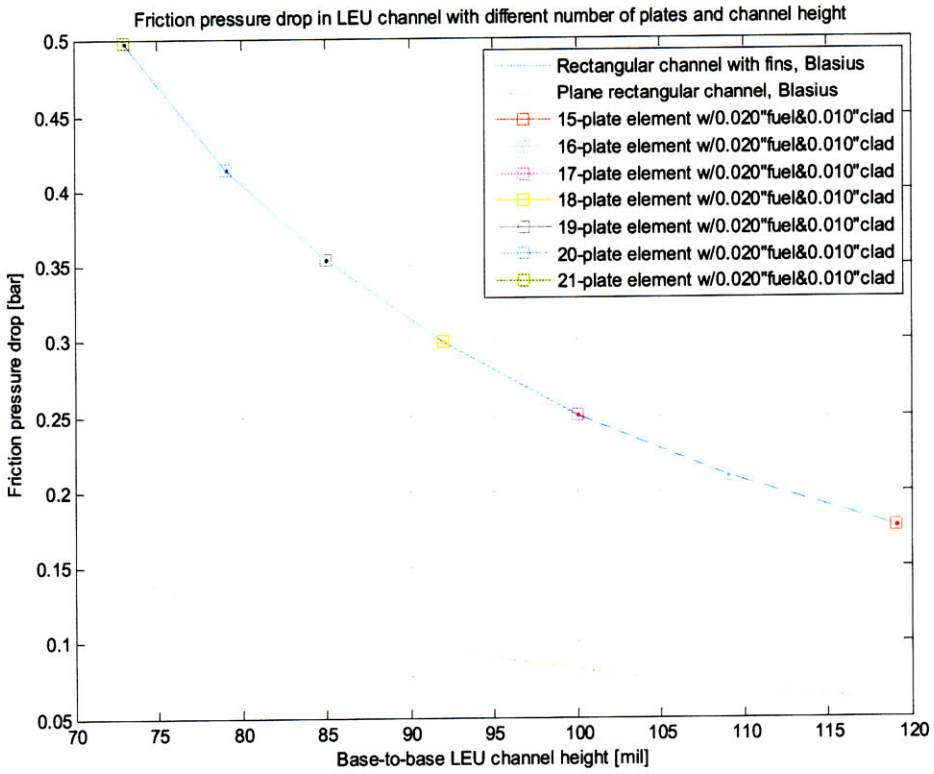

Figure 48: Friction pressure drop for turbulent water flow through LEU elements with different number of plates.

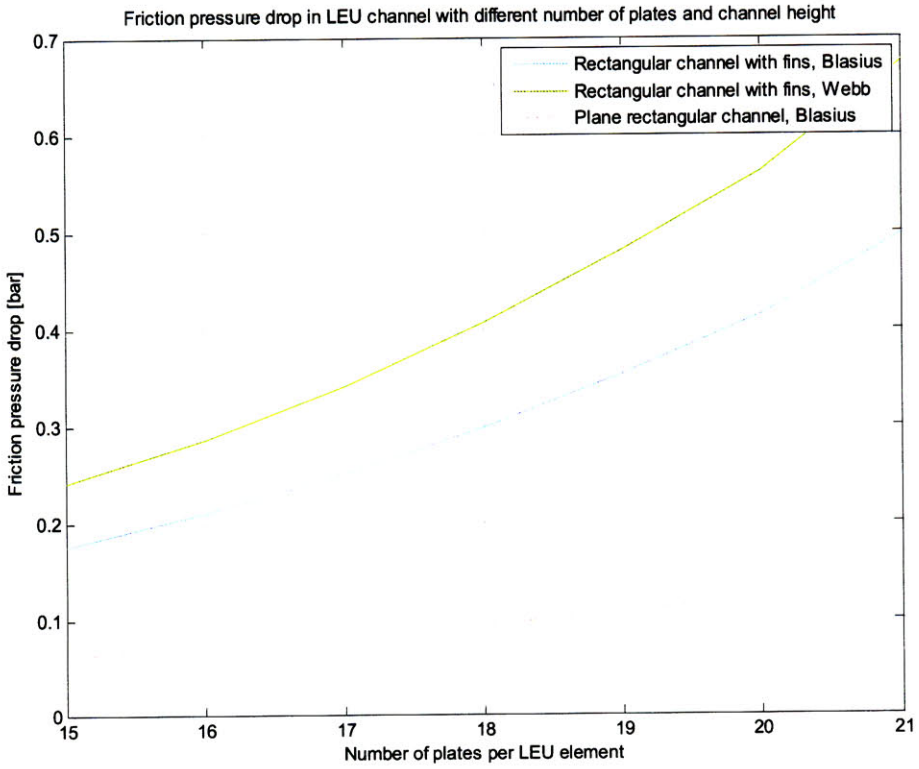

Figure 49: Friction pressure drop for turbulent water flow through LEU elements with respect to the number of fuel plates per element.

5.1.2.3. Effects on mean velocity of flow

The velocity of flow depends heavily on the cross sectional area of the flow channel at any given volumetric flow rate. The sensitivities of the mean velocity of flow at different base-to-base channel heights in homogenous core with 15-plate and 18-plate fuel elements are illustrated in Figure 50 and Figure 51.

5.1.2.3.1. 15-plate fuel element

As the channel height decreases, the mean velocity of flow through the homogenous core with 15-plate fuel elements varies as shown in Figure 50. For instance, should the thickness of the aluminium cladding on each plate be reduced to 0.010" from 0.015" while keeping the same number of plates per element, the height of flow channel would increase. The increase in the channel height, as well as the cross sectional area of the flow channel, result in about 10% drop in the mean velocity of primary coolant in a flow channel during normal reactor operations (2 pumps) in Figure 50.

5.1.2.3.2. 18-plate fuel element

Based on the assumption of the design of LEU fuel in [1], similar calculations are made for the mean velocity of primary coolant through twenty-four 18-plate fuel elements, during normal reactor operations (2 pumps) at the MIT Reactor.

The thickness of LEU fuel meat, as proposed in [1], is reduced to 0.020" from 0.030", and the aluminium cladding reduced to 0.010" from 0.015". The base-to-base height of the flow channel in the 18-plate element also decreases to 0.092" from 0.098" in the current 15-plate HEU element design.

Figure 51 shows similar trend of decreasing velocity of flow with decreasing aluminium clad thickness and increasing channel height. In the

design of LEU fuel in [1], the base-to-base channel height is 0.092". The mean velocity of primary coolant in the flow channel during normal reactor operations (2 pumps) is $2.62\ ms^{-1}$, which is approximately 10% lower than the mean velocity of flow at the HEU core of the MIT Reactor.

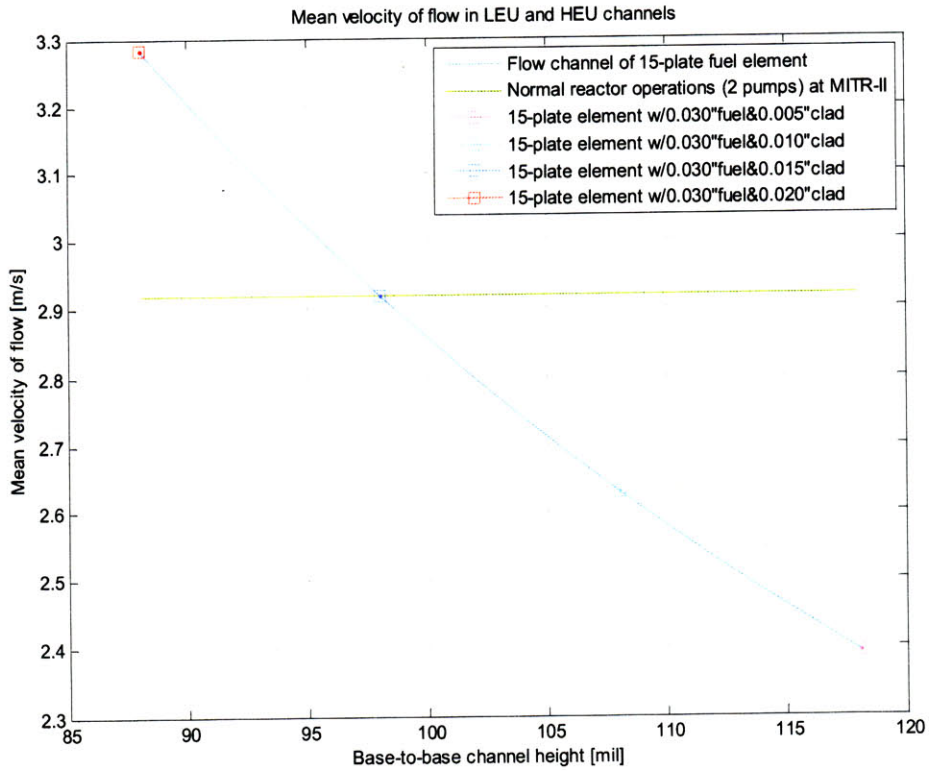

Figure 50: Estimated flow velocity in homogenous core with 15-plate fuel elements.

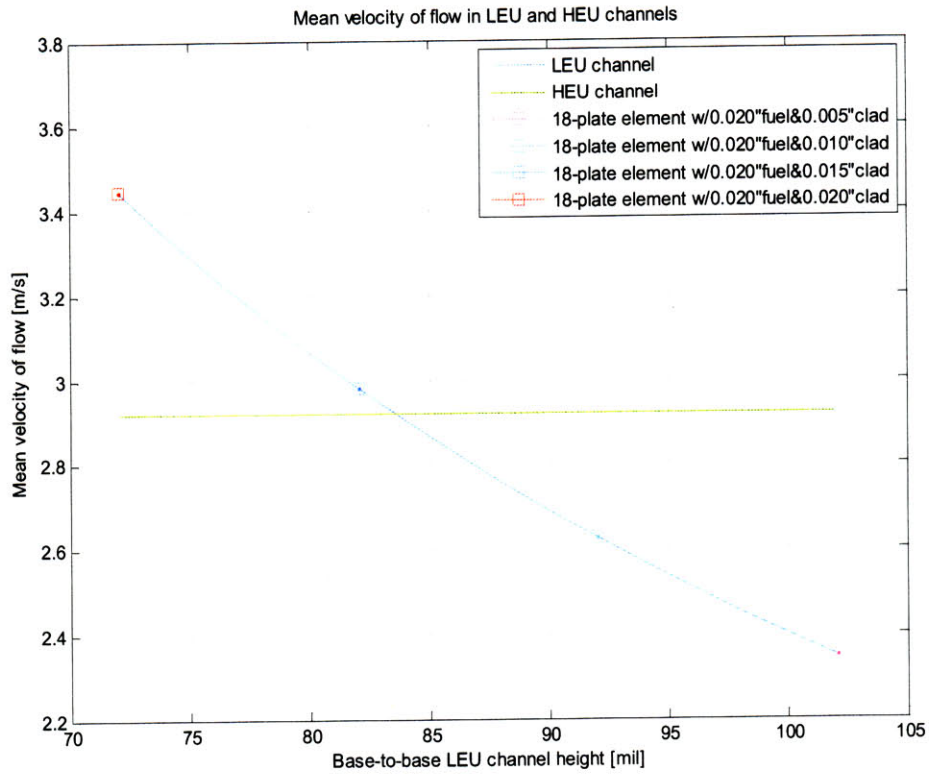

Figure 51: Estimated flow velocity in homogenous core with 18-plate fuel elements.

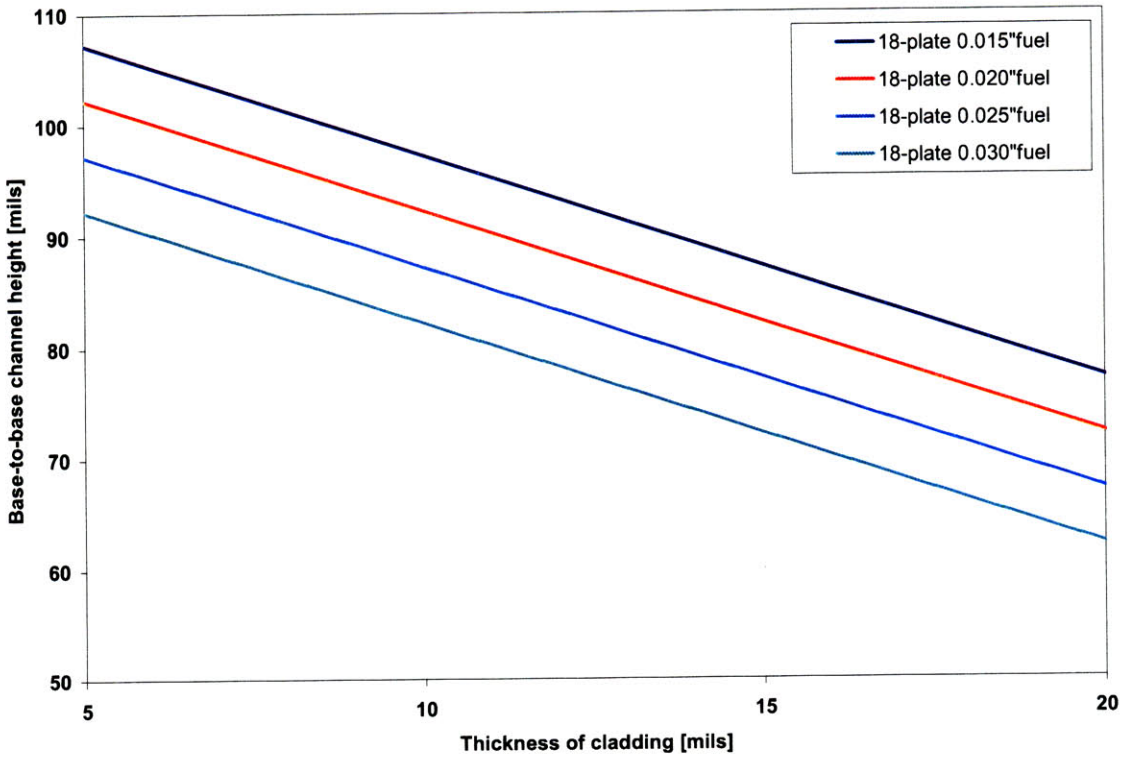

Figure 52: Height of flow channel with respect to fuel meat and cladding thickness.

5.2. Transitional Core Analysis

5.2.1. Overview

The Reduced Enrichment for Research and Test Reactors (RERTR) program was initiated by the Department of Energy in 1978 to develop the technology necessary to reduce the use of High Enriched Uranium (HEU) fuel in research reactors by converting them to Low Enriched Uranium (LEU) fuel from Ref.[46].

As partial fulfillment of the goal of the reactor conversion program to design a suitable LEU fuel assembly [1], as well as to perform a safety analysis of the conversion from HEU to LEU fuels, it is of importance to ensure that the transition from HEU to LEU fuels can be performed safely, without interrupting the normal operations of the MIT Reactor.

The objectives of the transitional core analysis is to estimate the friction pressure drop and the flow distribution of the primary coolant in the reactor core during the progressive conversion from HEU to LEU fuels, as well as to demonstrate the feasibility of the transitional core from a thermal hydraulic perspective.

5.2.2. Transitional Core with HEU and LEU fuels

The hexagonal MIT Reactor core contains 27 positions; they are normally filled with 24 fuel elements, leaving 3 positions available for in-core experiments. The process of the conversion of the reactor core is likely to undergo the following phases:

1. a homogenous core with HEU fuel,
2. a transitional core with HEU and LEU fuels, and
3. a homogenous core with LEU fuel.

Among the three different phases, the first phase refers to the current HEU core design of the MIT Reactor. The second phase, also known as the partial conversion phase, refers to the gradual transition from HEU to LEU

fuels, starting from a small number of LEU fuel elements and slowly increasing to a more significant presence of the LEU fuels in the transitional core. The final phase is the complete conversion phase, which refers to the homogenous core with LEU-only fuel.

There are several benefits of this transitional core conversion strategy. These are given as follows:

(1) Manufacturing and shipping of the LEU fuel are limited to a few fuel elements per transitional core. This reduces the burden of receiving, inspecting, and storing a large number of new fuel elements during a given refueling cycle.

(2) The excess reactivity due to gradual addition of new fuel elements is more manageable a whole core.

(3) The LEU fuel will be operated at a lower neutron peaking factor which allows for an opportunity to monitor the performance of this first-of-its-kind LEU fuel element. In the event of a failure, the core configuration can be returned to HEU core to minimize its impact on the reactor utilization program.

(4) Since each spent fuel shipment is limited to eight elements due to the capacity of the spent fuel cask, gradual discharge of the HEU fuel will minimize the number of HEU fuel elements stored in the spent fuel pool which is the current practice of the MITR security plan.

From the operational perspective, thermal hydraulic operation limits of the HEU core and the LEU are governed by the respective safety analysis reports that are approved by the US Nuclear Regulatory Commission. The main challenges associated with transitional core operation are in nuclear power peaking and primary flow distribution. Both need to be considered in the context of the established HEU and LEU core operating limits in order to ensure that the 10CFR50.59 requirements are met and that a license amendment is not required.

5.2.2.1. Transitional core with 3 LEU elements

In the transitional core, owing to the differences in the channel heights and equivalent hydraulic diameters of the flow channels in HEU and LEU fuels, the mean velocities of flow and the volumetric flow rates are likely to be different from the homogenous core analysis. In the transitional core, where the flow channels of the HEU and LEU fuels are parallel to each other, the following condition has to be satisfied:

$$\Delta P_{tot} = \int_{in}^{out} \frac{dP_{heu}}{dz} = \int_{in}^{out} \frac{dP_{leu}}{dz} \tag{53}$$

where ΔP_{tot} is the total friction pressure drop in the reactor core, and $\int_{in}^{out} \frac{dP_{heu}}{dz}$, $\int_{in}^{out} \frac{dP_{leu}}{dz}$ are the friction pressure drop in HEU and LEU flow channels between the inlet and outlet of the reactor core.

Figure 53 shows the estimated mean velocity of flow in HEU (15-plate) and LEU (18-plate) fuels in the transitional core with 3 LEU fuel elements. During normal reactor operations (2 pumps), as the base-to-base height of the flow channel in LEU fuel increases due to a reduction in the thickness of the aluminium cladding, the mean velocity of flow in LEU (18-plate) fuel increases, whereas the velocity in HEU (15-plate) fuel decreases.

Moreover, the two curves in Figure 53 intersect when the channel height in the LEU fuel is equal to 0.098", which is the same as the channel height of the current HEU design at the MIT Reactor. The intersection implies when the channel heights of the HEU and LEU fuels are equal, there is no disparity of flow in the reactor core due to the equal Reynolds numbers and equivalent hydraulic diameters in the HEU and LEU fuels.

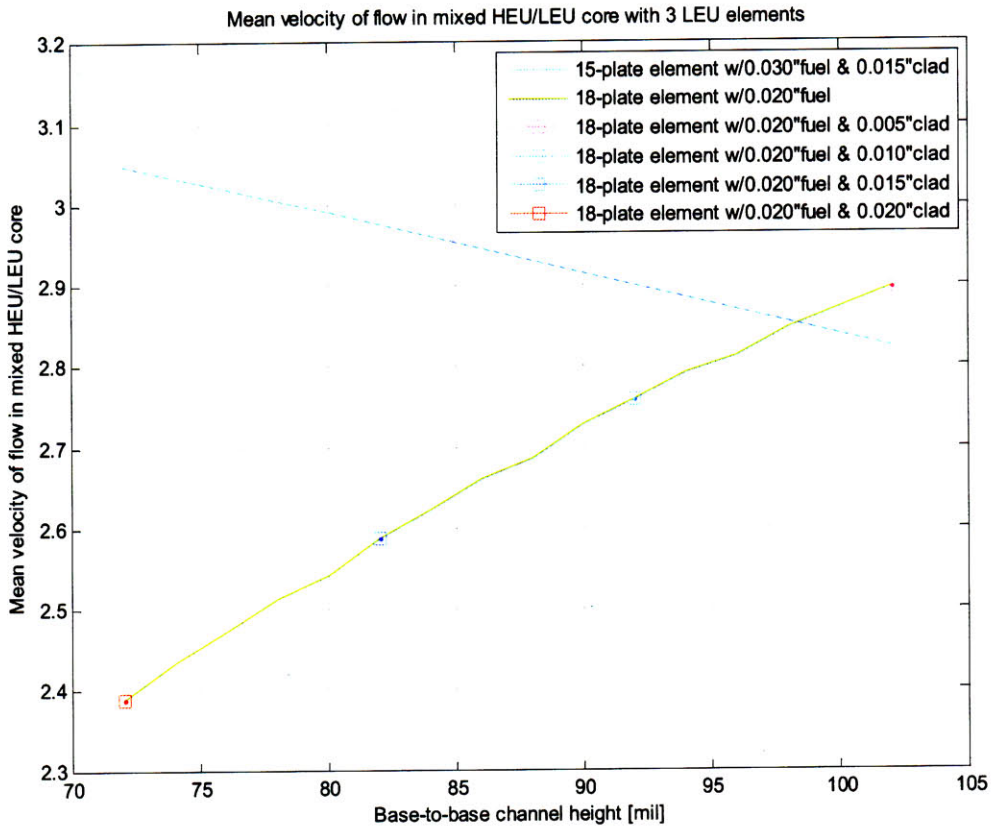

Figure 53: Mean velocity of flow in transitional core with 3 LEU fuel elements during normal reactor operations (2 pumps).

Figure 54 shows the estimated volumetric flow rate per channel in the HEU (15-plate) and LEU (18-plate) fuels in the transitional core with 3 LEU fuel elements, during normal reactor operations (2 pumps). Similar to the trend in Figure 53, as the base-to-base height of the flow channel in LEU fuel increases, the per channel volumetric flow rate in the LEU fuel element increases, whereas the flow rate in the HEU fuel element decreases with a lower sensitivity. The opposing trends in Figure 54 agree with the law of conservation of mass.

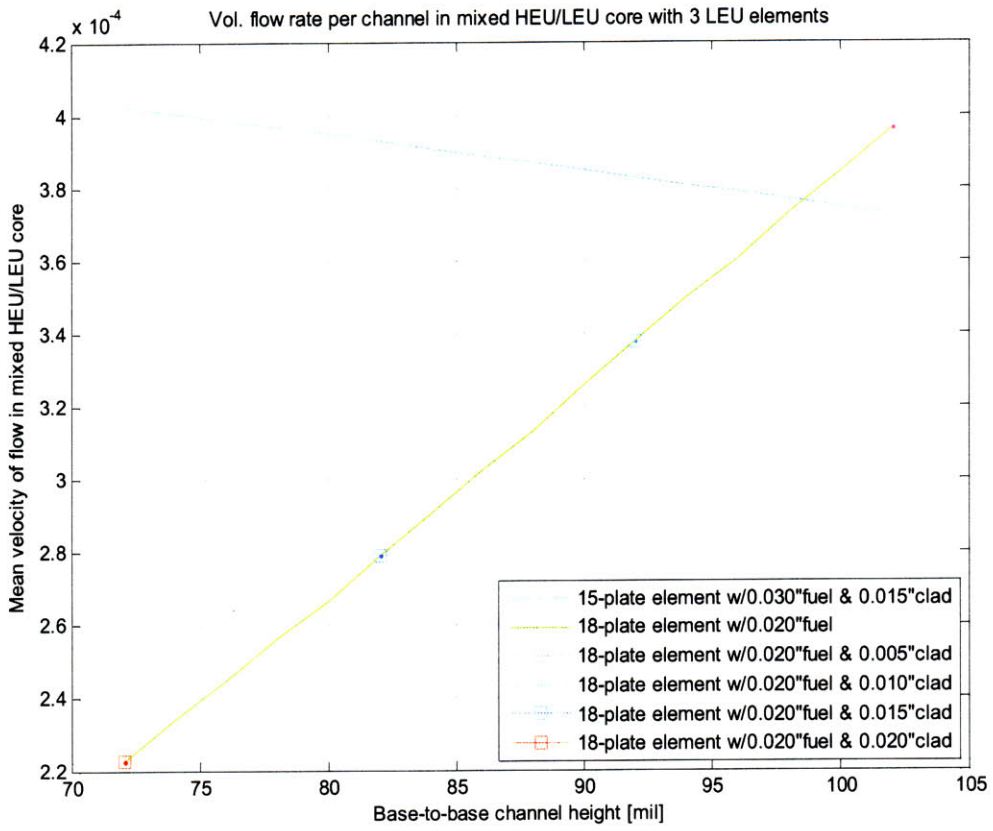

Figure 54: Volumetric flow rate per flow channel in the transitional core with 3 LEU fuel elements during normal reactor operations (2 pumps).

It is noted in (53) that the friction pressure drops in the parallel flow channels of the HEU and LEU fuels in the transitional core have to be the same, and is verified in Figure 55. As the height of the flow channel in LEU fuel increases due to a reduction in the thickness of the aluminium cladding, the friction pressure drops in both HEU and LEU fuels decrease simultaneously.

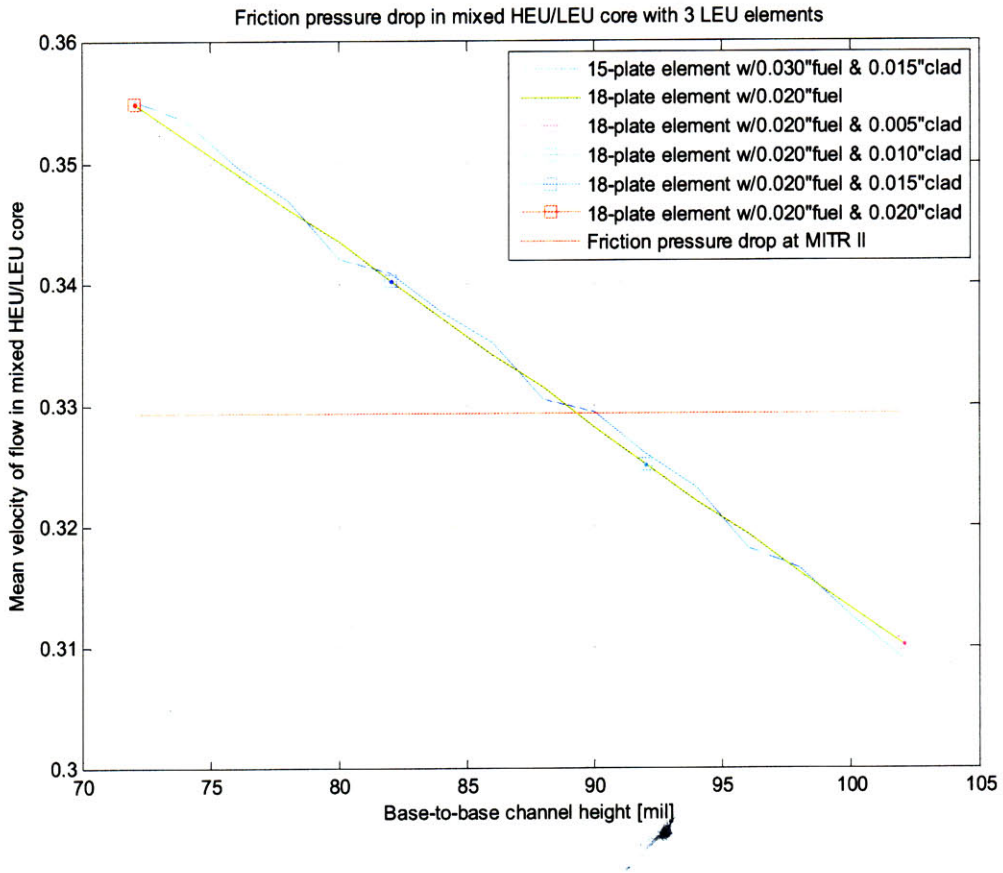

Figure 55: Estimated friction pressure drop in the transitional core with 3 LEU fuel elements during normal reactor operations (2 pumps).

5.2.2.2. Transitional core with more than 3 LEU elements

Similar analyses have been performed to estimate the friction pressure drop and the flow disparity of the primary coolant in the transitional core with 6 and 9 LEU fuel elements.

The more significant presence of LEU fuel in the transitional core causes the mean velocity of flow in HEU fuel to respond to changes in the height of the flow channel in LEU fuel with greater sensitivity as shown in Figure 56 and Figure 58. For instance, in the transitional core with 9 LEU fuel elements (and thus 15 HEU fuel elements), a ± 0.004" manufacturing tolerance leads to about $\pm 6.2\%$ and $\pm 3.1\%$ uncertainties in the friction pressure drop and the mean velocity of flow in HEU fuel respectively.

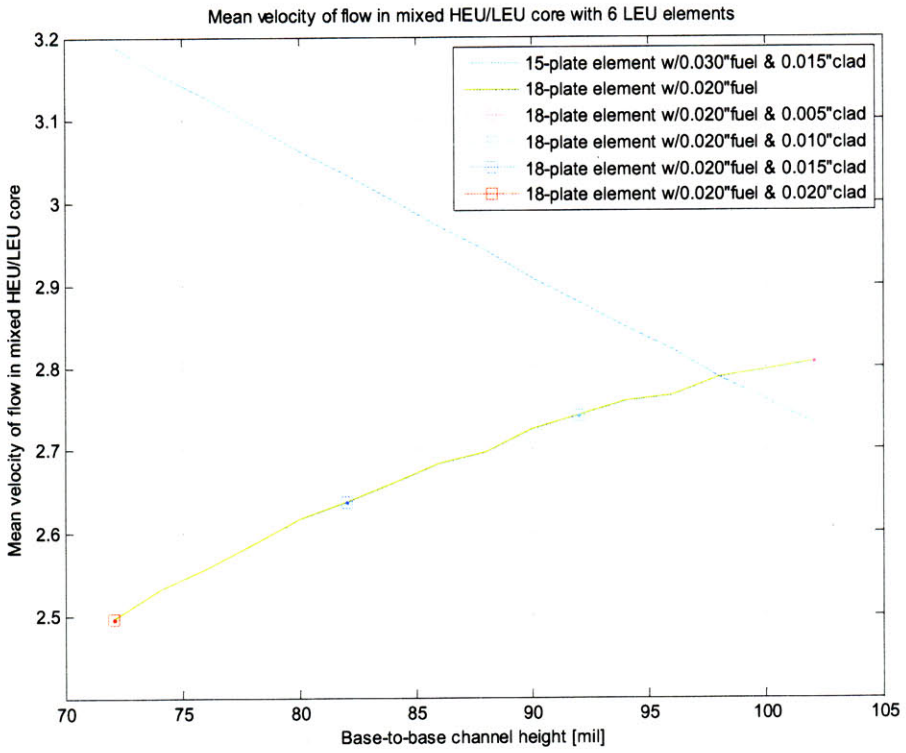

Figure 56: Mean velocity of flow in transitional core with 6 LEU fuel elements during normal reactor operations (2 pumps).

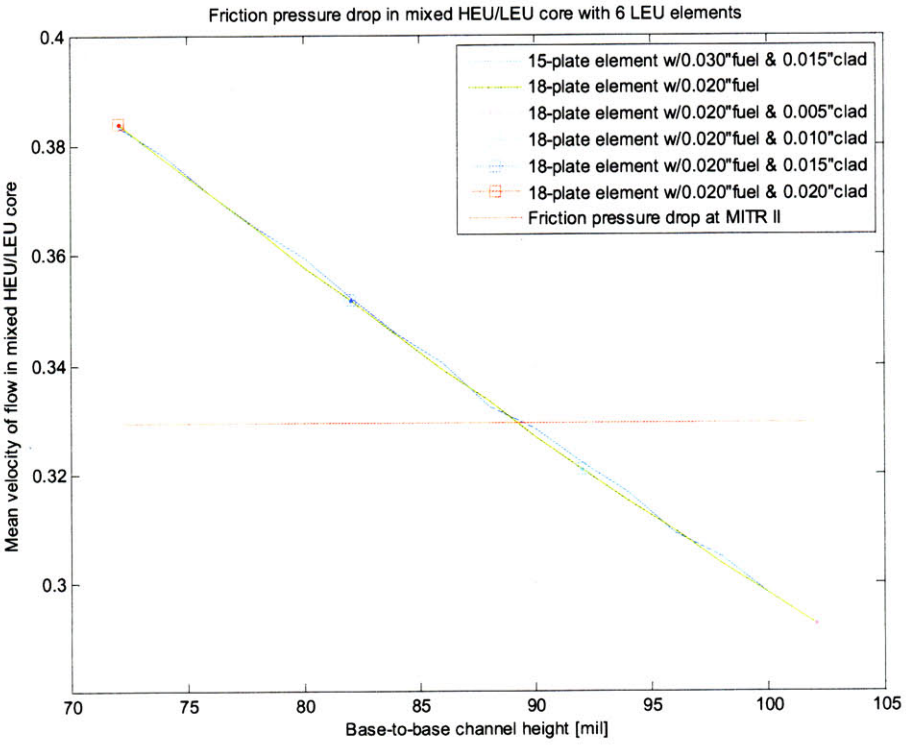

Figure 57: Friction pressure drop in transitional core with 6 LEU fuel elements during normal reactor operations (2 pumps).

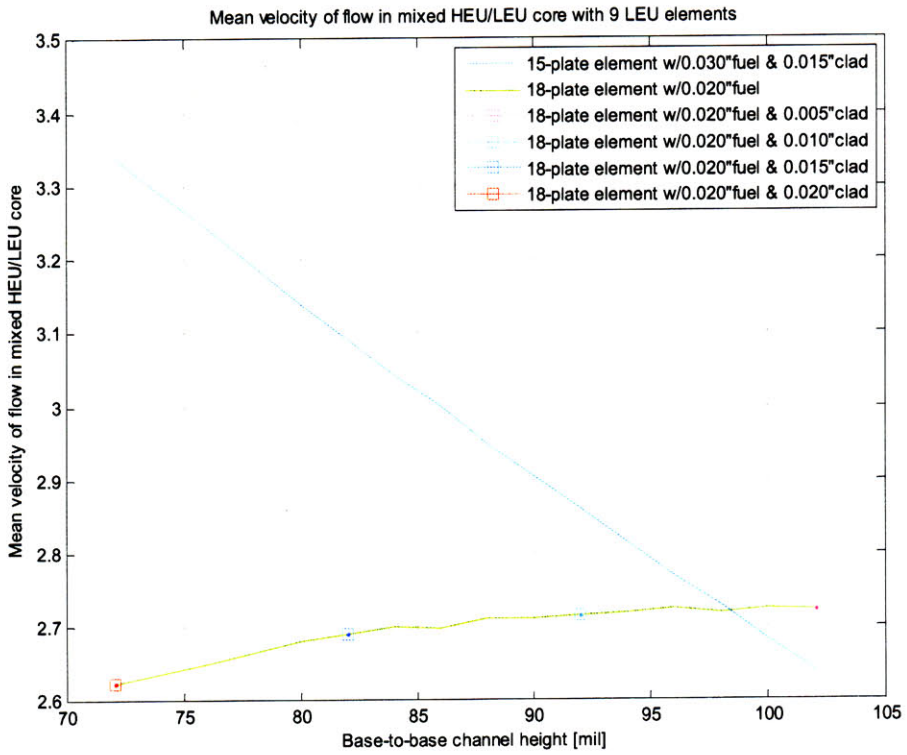

Figure 58: Mean velocity of flow in transitional core with 9 LEU fuel elements during normal reactor operations (2 pumps).

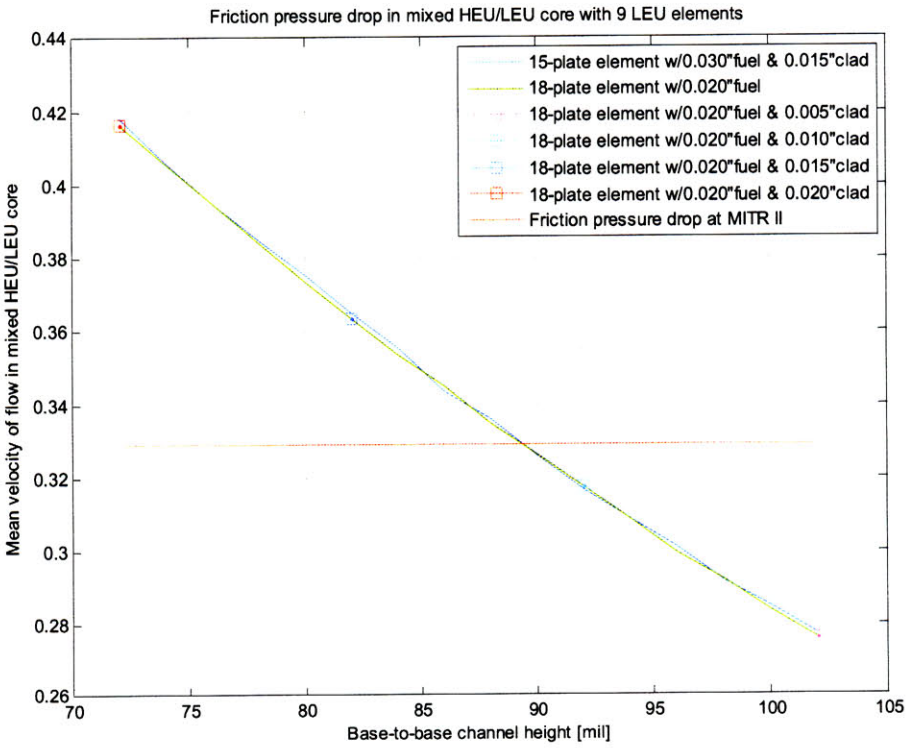

Figure 59: Friction pressure drop in transitional core with 9 LEU fuel elements during normal reactor operations (2 pumps).

5.2.3. Progressive transition from HEU to LEU fuel

According to the proposed design of the LEU fuel in [1, 2, 8, 9], a LEU fuel element contains 18 fuel plates, with 17 full flow channels and 2 half-channels. Each finned rectangular fuel plate contains a 0.020" thick fuel meat, with a 0.010" thick aluminium cladding. Continuous longitudinal rectangular fins of 0.010" by width, 0.010" by height, and 0.010" apart from one another are also added to the surface of the aluminium cladding to enhance heat transfer of the fuel plates.

A plausible approach to the transition from HEU to LEU fuel at the MIT Reactor is a progressive process of the partial conversion phase, in which a small number of HEU fuel (15-plate) elements are first replaced with LEU fuel (18-plate) elements, and then more HEU fuel elements are replaced in the following operating periods, until the reactor core becomes homogenous core with LEU-only fuel.

5.2.3.1. Effects on friction pressure drop

The friction pressure drop in the transitional core with different number of LEU fuel elements during normal reactor operations (2 pumps) is calculated using the design parameters described in this section, and the results are shown in Figure 60.

5.2.3.2. Effects on flow disparity

As the number of LEU fuel elements increases, the friction pressure drops in the HEU and LEU fuels drop simultaneously, which agree with (53). The total decrease in the friction pressure drop towards the end of the conversion, where the number of LEU fuel elements is 23, is around 10% of the friction pressure drop of the current HEU core at the MIT Reactor.

Figure 61 shows the estimated mean velocity of flow in the transitional core with different number of LEU fuel elements during normal reactor operations (2 pumps). The mean velocity of flow in the HEU fuel is always higher than that in the LEU fuel. This implies that the flow of primary

coolant in the reactor core tends to be bypassed to the flow channels in the HEU fuel, from the ones in the LEU fuel, where the channel height is smaller.

Combining the results in Figure 61 and the respective areas of the flow channels, it is possible to calculate the volumetric flow rates per channel in the HEU and LEU fuels as shown in Figure 62, and to estimate the distribution of flow in the transitional core during normal reactor operation (2 pumps).

The volumetric flow rate of the primary coolant per flow channel in the LEU fuel is about 12% lower than that in the HEU fuel in a transitional core. The lower volumetric flow rate in the LEU fuel can affect the temperature increase in a channel $\Delta T_{ch,i}$, depending on the distribution of reactor thermal power in the HEU and LEU fuel plates.

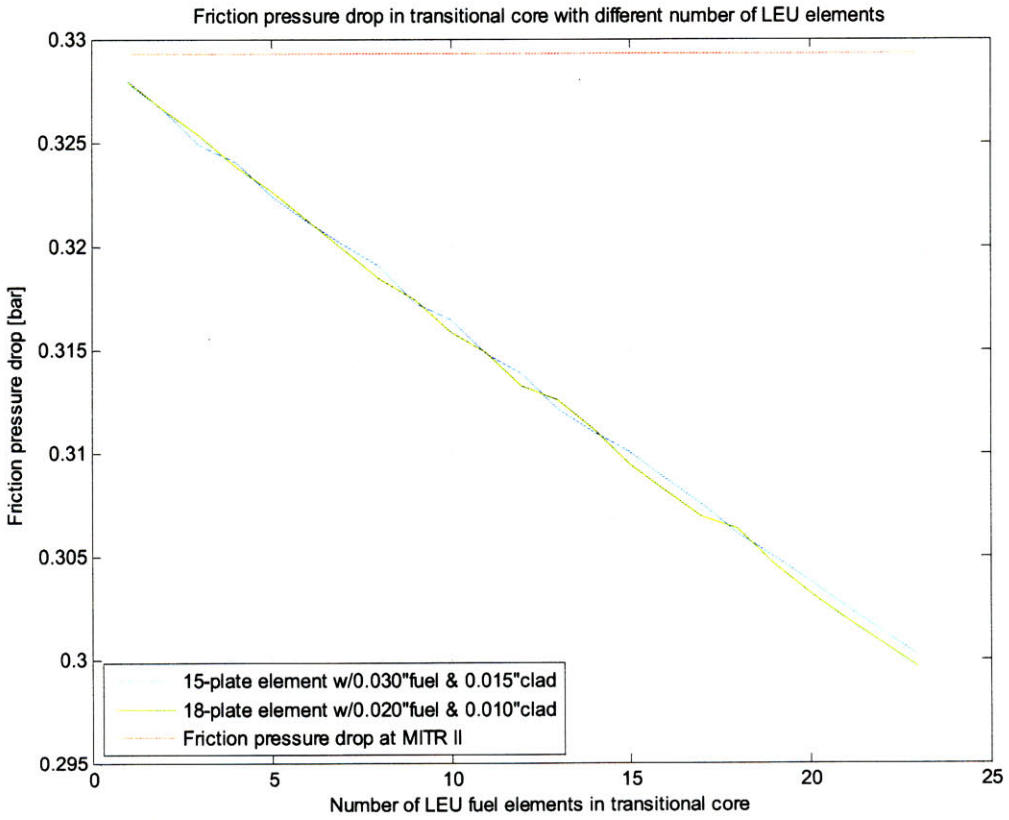

Figure 60: Estimated friction pressure drop in the transitional core with different number of fuel elements during normal reactor operations (2 pumps).

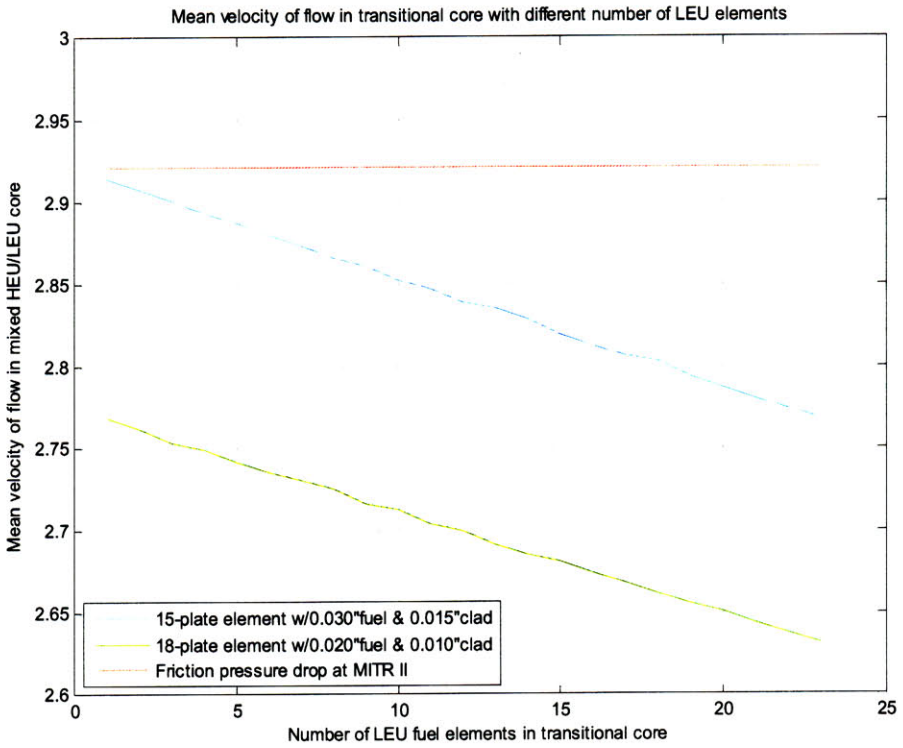

Figure 61: Estimated mean velocity of flow in the transitional core with different number of fuel elements during normal reactor operations (2 pumps).

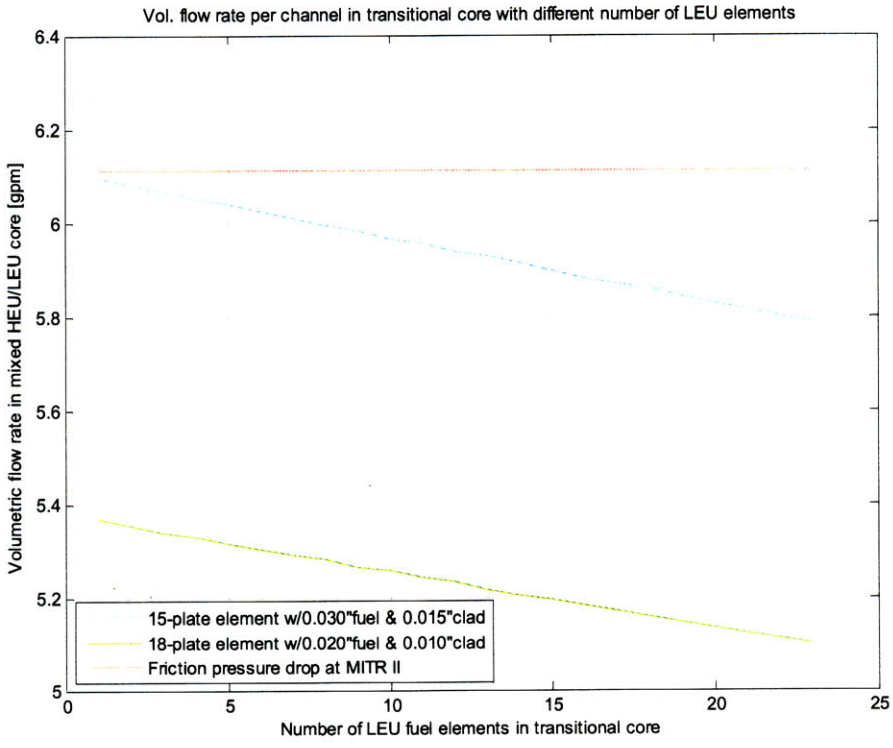

Figure 62: Estimated volumetric flow rate per channel in the transitional core with different number of fuel elements during normal reactor operations (2 pumps).

6. Thermal-hydraulic Limits Analysis for Transitional Core Operation

6.1. Safety Limits

The high enrichment uranium (HEU) core of the MITR-II, as well as the low enrichment uranium (LEU) core of the MITR-III, consist of 22 to 24 fuel elements, with each element containing 15 (HEU) to 18 (LEU) fuel plates. Primary coolant flows through between 330 and 432 parallel flow channels in the fuel to provide sufficient cooling during normal operations and power transients.

The multi-channel design, however, leads to the possibility that the onset of flow instability (OFI) occurs before the critical heat flux (CHF), which may undesirably reduce the flow rate of primary coolant in the hot channel and, thus, lower the critical heat flux. It is necessary to calculate both OFI and CHF to determine the more conservative safety limits, within which the integrity of the fuel clad is maintained.

6.1.1. Transitional core

The transitional core of the MIT Reactor contains a combination of HEU and LEU fuel elements during the gradual transition from homogenous HEU core of the MITR-II to homogenous LEU core of the MITR-III. The gradual transition could take as long as several years.

Sample mixed core (#107) contains 3 new LEU elements in the B1, B5 and B7 positions, and three dummy elements in the A1, A3 and B4 positions. 21 HEU elements are located in the rest of 27 positions in the core.

6.1.2. Objective

The objective of this exercise is to re-calculate the safety limits for forced convection operation in the transitional core of the MIT Reactor,

and to demonstrate the feasibility of transitional core from a thermal-hydraulic perspective.

6.1.3. Methods and assumption

It is assumed that the hot channel receives the minimum flow of all coolant channels to provide the most conservative estimation of the safety limits.

The transitional core consists of In the case of a transitional core, due to the differences in the number of fuel plates per element and the size of the flow channels, the average flow rates of the primary coolant through HEU and LEU fuel elements differ. New parameters $\left(F_{mf,heu}, F_{mf,leu}\right)$ are introduced and the following equation is proposed for the safety limits calculations for transitional core:

$$\frac{P_{rx}}{W_p} = \frac{\rho_{pf} c_{pf} \left(T_{sat}^{H} - T_{out}\right)}{F_{core}\left(\frac{F_r^j F_h}{R \cdot F_f F_{mf}^j d_f^j} - 1\right)} \tag{54}$$

where the variables are defined below.

P_{rx} is the total reactor power

$\overline{P_{plate}}$ is the average power per fuel plate

$$\overline{P_{plate}} = \frac{P_{rx}}{N_{plate}^{all}} \tag{55}$$

P_{hc}^{heu} is the power of the hot channel fuel plate in the HEU fuel, where

$$P_{hc}^{heu} = \overline{P_{plate}} \cdot F_r^{heu} \tag{56}$$

P_{hc}^{leu} is the power of the hot channel fuel plate in the HEU fuel, where

$$P_{hc}^{leu} = \overline{P_{plate}} \cdot F_r^{leu} \tag{57}$$

W_p is the total primary flow

$\overline{w_p}$ Is the average primary flow per flow channel in the transitional core, where

$$\overline{w_p} = \frac{W_p}{N_{plate}^{all}} \tag{58}$$

$w_{p,i}^{heu}$ is the primary flow in an HEU flow channel *i*

$w_{p,i}^{leu}$ is the primary flow in a LEU flow channel *i*

F_{core} is the fraction of reactor power deposited in the core

F_r^{heu} is the hot channel factor in the HEU fuel in the transitional core

F_r^{leu} is the hot channel factor in the LEU fuel in the transitional core

F_h is the engineering hot channel factor for enthalpy rise

F_f is the fraction of the total primary flow through the fuel

F_{mf}^{heu} is the ratio of the average primary flow in HEU flow channels to the average primary flow per flow channel in the transitional core, where

$$F_{mf}^{heu} = \frac{\overline{w_p^{heu}}}{\overline{w_p}} \tag{59}$$

F_{mf}^{leu} is the ratio of the average primary flow in LEU flow channels to the average primary flow per flow channel in the transitional core, where

$$F_{mf}^{leu} = \frac{\overline{w_p^{leu}}}{\overline{w_p}} \tag{60}$$

d_f^{heu} is the ratio of the minimum primary flow to the average primary flow in the HEU flow channels, where

$$d_f^{heu} = \frac{w_{p,\min}^{heu}}{\overline{w_p^{heu}}} \tag{61}$$

d_f^{leu} is the ratio of the minimum primary flow to the average primary flow in the LEU flow channels, where

$$d_f^{leu} = \frac{w_{p,\min}^{leu}}{\overline{w_p^{leu}}} \tag{62}$$

R is the subcooling ratio

N_{fuel}^{heu} is the number of HEU fuel elements in the transitional core

N_{fuel}^{leu} is the number of LEU fuel elements in the transitional core

N_{fuel}^{all} is the total number of fuel elements in the core, where

$$N_{fuel}^{all} = N_{fuel}^{heu} + N_{fuel}^{leu} \tag{63}$$

$N_{plate}^{heu} = 15$ is the number of fuel plates in an HEU element

$N_{plate}^{leu} = 18$ is the number of fuel plates in a LEU element

N_{plate}^{all} is the total number of fuel plates in the transitional core, where

$$N_{plate}^{all} = N_{fuel}^{heu} \cdot N_{plate}^{heu} + N_{fuel}^{leu} \cdot N_{plate}^{leu} \tag{64}$$

ρ_{pf} is the density of the primary coolant

c_{pf} is the specific heat capacity of the primary coolant

T_{sat}^{H} is the saturation temperature of the primary coolant at core outlet, given core tank level H

T_{out} is the core outlet temperature of the primary coolant

H is the core tank level in feet

Table 6: Assumption of variables.

Variables		Unit
P_rx	5.0	MW
P_plate_avg	13.6	kW
P_hc_heu	22.1	kW
P_hc_leu	23.8	kW
W_p	1800	gpm
w_p_avg	4.88	gpm
w_p_heu_avg	4.97	gpm
w_p_leu_avg	4.37	gpm
F_core	1.00	
F_r_heu	1.63	
F_r_leu	1.76	
F_mp_heu	1.32	
F_mp_leu	1.53	
F_h	1.173	
F_mf_heu	1.0179	
F_mf_leu	0.8956	
d_f_heu	0.864	
d_f_leu	0.864	
den_pf_10	983	kg/m3
den_pf_6	983	kg/m3
c_pf	4180	J/kg
T_sat_10	107.11	deg-C
T_sat_6	104.78	deg-C
T_out	60	deg-C
N_fuel_heu	21	
N_fuel_leu	3	
N_plate_heu	15	
N_plate_leu	18	
N_all	369	
H	6 or 10	feet

6.1.4. Results

6.1.4.1. Case 1 (10 ft. primary coolant above core outlet)

During normal conditions, the core tank level remains at about 10 feet above the reactor core outlet. The absolute pressure at the reactor core outlet is thus about 1.3 bar, which is slightly higher than the atmospheric pressure.

Although the higher hot channel factor and distribution of primary flow in the transitional core of the MIT Reactor seem to challenge the safety limits of the MITR-II, Figure 63. The reactor thermal power P for transitional core operations must be lowered, so that the power to flow ratio $\frac{P}{W_p}$ must not go above the more conservative safety limits suggested in Figure 63.

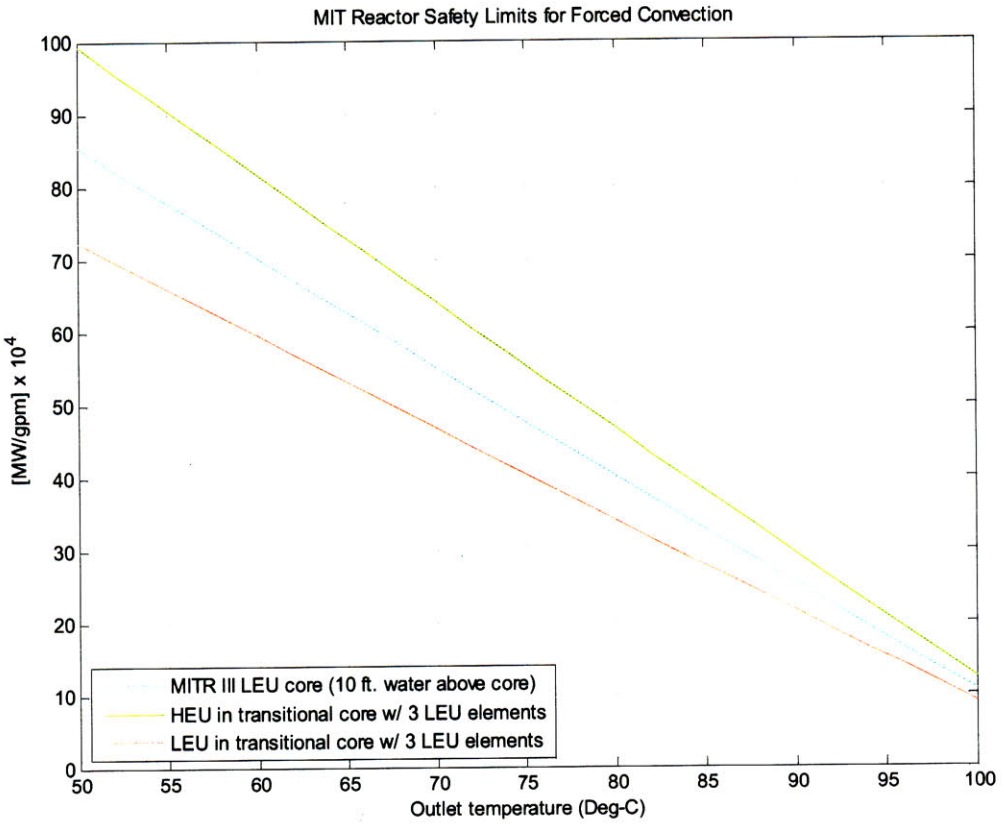

Figure 63: MITR safety limits for forced convection in transitional core with 3 LEU elements, with 10 ft. water above core outlet.

6.1.4.2. Case 2 (6 ft. primary coolant above core outlet)

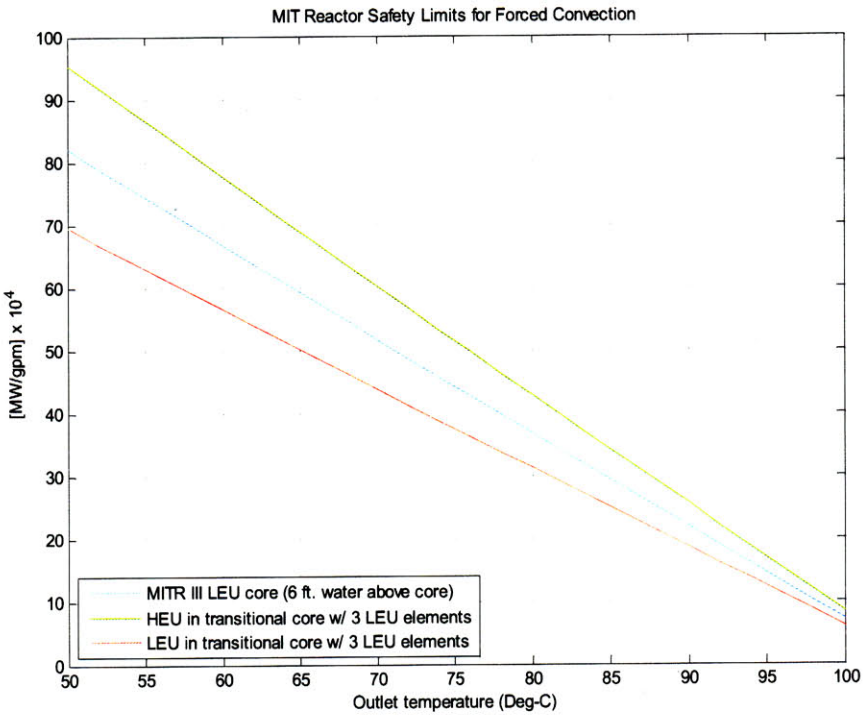

Figure 64: MITR safety limits for forced convection in transitional core with 3 LEU elements, with 6 ft. water above core outlet.

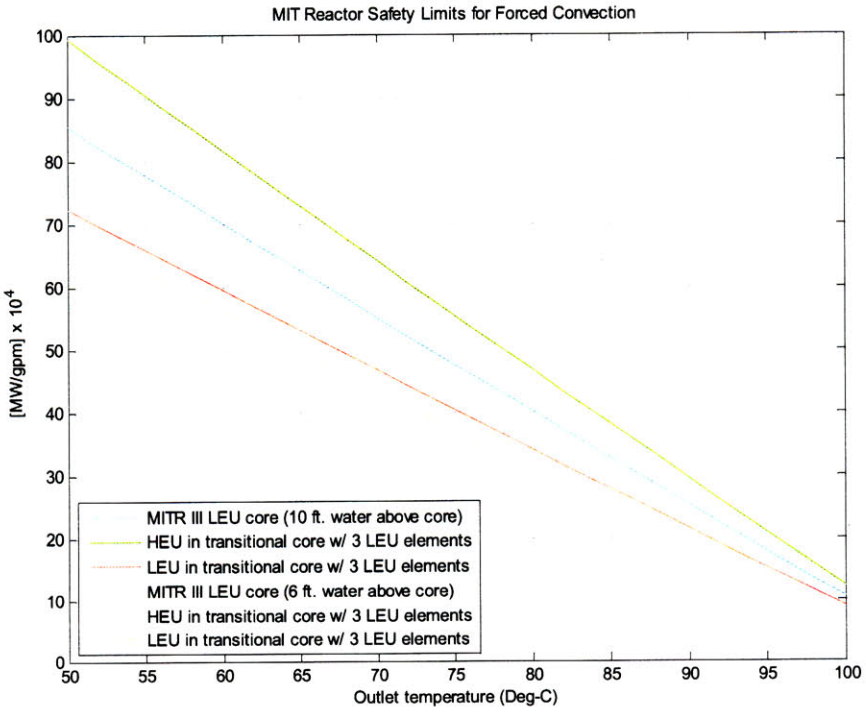

Figure 65: Figure 63 and Figure 64 combined.

6.2. Limiting Safety System Settings

6.2.1. Forced Convection Operation

In addition to the engineering hot channel factor for enthalpy rise F_h, similar factor for film temperature rise F_{dT} is also included in a rough estimation of the Limiting Safety System Settings before using the MULCH-II code.

	LSSS (two pumps)	LSSS (one pump)
Power (MW)	6.5	3.2
Flow rate of primary coolant (gpm)	1800	900
Temperature of core outlet (deg-C)	60	60
Core tank level	4" below overflow or 10' above core outlet	4" below overflow or 10' above core outlet

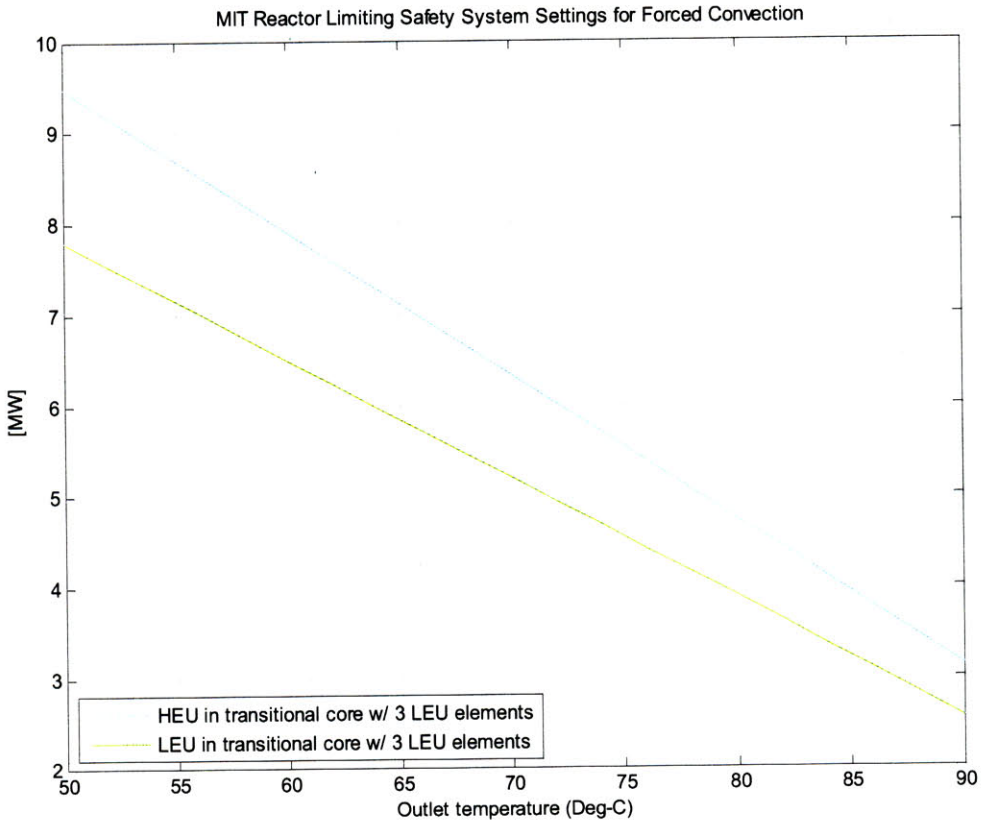

Figure 66: Limiting safety system settings for forced convection in transitional core with 3 LEU elements, at primary flow of 1800 gpm and core tank level at 4" below overflow.

6.2.2. Methods and Assumption

The Limiting Safety System Settings for transitional core operation of the MIT Reactor is calculated using the MIT Reactor in-house code for multi-channel thermal-hydraulic analysis, also known as MULCH.

The basic instructions for creating the necessary input files and running MULCH-II are given in [2].

6.2.3. MULCH for Transitional Core Analysis

In order to calculate the LSSS for transitional core operation using MULCH code, new parameters $\left(F_r^{heu'}, F_r^{leu'}, d_f^{heu'}, d_f^{leu'}\right)$ are introduced to describe the power and flow distribution in the transitional core.

Hot channel power:

$$P_{hc}^{heu} = F_r^{heu'} \cdot \left(\overline{P_{plate}}\right)_{HEU} \tag{65}$$

$$P_{hc}^{leu} = F_r^{leu'} \cdot \left(\overline{P_{plate}}\right)_{LEU} \tag{66}$$

Minimum primary flow:

$$w_{p,\min}^{heu} = d_f^{heu'} \cdot \left(\overline{w_p}\right)_{HEU} \tag{67}$$

$$w_{p,\min}^{leu} = d_f^{leu'} \cdot \left(\overline{w_p}\right)_{LEU} \tag{68}$$

and the variables are defined as follows.

$\left(\overline{P_{plate}}\right)_{HEU}$ is the average power per fuel plate in the homogenous HEU core, where

$$\left(\overline{P_{plate}}\right)_{HEU} = \frac{P_{rx}}{N_{plate}^{all,heu}} \tag{69}$$

$\left(\overline{P_{plate}}\right)_{LEU}$ is the average power per fuel plate in the homogenous LEU core, where

$$\left(\overline{P_{plate}}\right)_{LEU} = \frac{P_{rx}}{N_{plate}^{all,leu}} \tag{70}$$

$\left(\overline{w_p}\right)_{HEU}$ is the average primary flow per flow channel in the homogenous HEU core, where

$$\left(\overline{w_p}\right)_{HEU} = \frac{W_p}{N_{plate}^{all,heu}} \tag{71}$$

$\left(\overline{w_p}\right)_{LEU}$ is the average primary flow per flow channel in the homogenous LEU core, where

$$\left(\overline{w_p}\right)_{LEU} = \frac{W_p}{N_{plate}^{all,leu}} \tag{72}$$

$F_r^{heu'}$ is the modified hot channel factor in the HEU fuel for transitional core analysis, where

$$F_r^{heu'} = F_r^{heu} \cdot \frac{N_{plate}^{all,heu}}{N_{plate}^{all,tran}} \tag{73}$$

$F_r^{leu'}$ is the modified hot channel factor in the LEU fuel for transitional core analysis, where

$$F_r^{leu'} = F_r^{leu} \cdot \frac{N_{plate}^{all,leu}}{N_{plate}^{all,tran}} \tag{74}$$

$d_f^{heu'}$ is the modified flow disparity factor in HEU flow channels for transitional core analysis, where

$$d_f^{heu'} = \frac{d_f^{heu} \cdot \overline{w_p^{heu}}}{\overline{w_p}} = \frac{d_f^{heu} \cdot F_{mf}^{heu}}{N_{plate}^{all,trans} \Big/ N_{plate}^{all,heu}} \tag{75}$$

$d_f^{heu'}$ is the modified flow disparity factor in LEU flow channels for transitional core analysis, where

$$d_f^{leu'} = \frac{d_f^{leu} \cdot \overline{w_p^{leu}}}{\overline{w_p}} = \frac{d_f^{leu} \cdot F_{mf}^{leu}}{N_{plate}^{all,trans} \Big/ N_{plate}^{all,leu}} \tag{76}$$

$N_{plate}^{all,heu}$ is the total number of fuel plates in the HEU core, where

$$N_{plate}^{all,heu} = N_{fuel}^{all} \cdot N_{plate}^{heu} \tag{77}$$

$N_{plate}^{all,leu}$ is the total number of fuel plates in the LEU core, where

$$N_{plate}^{all,leu} = N_{fuel}^{all} \cdot N_{plate}^{leu} \tag{78}$$

$N_{plate}^{all,trans}$ is the total number of fuel plates in the transitional core, where

$$N_{plate}^{all,trans} = N_{plate}^{all} = N_{fuel}^{heu} \cdot N_{plate}^{heu} + N_{fuel}^{leu} \cdot N_{plate}^{leu} \tag{79}$$

6.2.4. Transitional core configuration

Table 7: Core configuration assumptions for transitional core with 24 fuel elements (incl. 3 LEU elements).

Transitional Core w/24 fuel elements (incl. 3 LEU elements)		
Number of fuel elements	24	
Number of HEU elements	21	
Number of LEU elements	3	
HEU element		
Number of plates per element	15	
Thickness of fuel	0.030	"
Thickness of clad	0.015	"
Thickness of plate, excl. fin	0.060	"
Flow channel area	1.320E-04	m^2
Flow channel volume	8.711E-05	m^3
Equivalent diameter of channel	2.236E-03	m
LEU element		
Number of plates per element	18	
Thickness of fuel	0.020	"
Thickness of clad	0.010	"
Thickness of plate, excl. fin	0.040	"
Flow channel area	1.223E-04	m^2
Flow channel volume	8.075E-05	m^3
Equivalent diameter of channel	2.081E-03	m
Total number of plates	369	

Table 8: Adjusted core configuration assumption for transitional core with 23 fuel elements (incl. 3 LEU elements).

Transitional Core w/23 fuel elements (incl. 3 LEU elements)	
Number of fuel elements	23
Number of HEU elements	20
Number of LEU elements	3
Total number of plates	354

6.2.5. Distribution of Primary Flow Assumption

Table 9: Adjusted core configuration assumption for transitional core with 23 fuel elements (incl. 3 LEU elements).

Number of LEU elements in Transitional Core	Distribution of primary flow in HEU and LEU fuel in the 23,24-element transitional core w/ 3 LEU elements			
	23-element mixed core		*24-element mixed core*	
	HEU	LEU	HEU	LEU
0	1	*N/A*	1	*N/A*
1	1.0062	0.8858	1.006	0.886
2	1.0124	0.8912	1.0119	0.8911
3	**1.0187**	**0.8961**	**1.0179**	**0.8956**
4	1.0246	0.9024	1.0236	0.9017
5	1.0309	0.9074	1.0296	0.9063
6	1.0369	0.913	1.0354	0.9116
7	1.0427	0.9187	1.041	0.917
8	1.0492	0.9231	1.0465	0.9225
9	1.0547	0.929	1.0528	0.9267
10	1.0603	0.9347	1.0578	0.9325
11	1.0662	0.9398	1.0641	0.9369
12	1.0727	0.9445	1.0691	0.9424
13	1.0779	0.9501	1.0758	0.9465
14	1.0836	0.9552	1.0811	0.9517
15	1.0897	0.9601	1.0857	0.9571
16	1.0957	0.9651	1.0912	0.962
17	1.102	0.97	1.0967	0.9668
18	1.1064	0.9754	1.1034	0.9713
19	1.1121	0.9803	1.1079	0.9763
20	1.1177	0.9853	1.113	0.9812
21	1.1233	0.9902	1.1184	0.9859
22	1.1289	0.9951	1.1238	0.9906
23	*N/A*	1	1.1291	0.9953
24			*N/A*	1

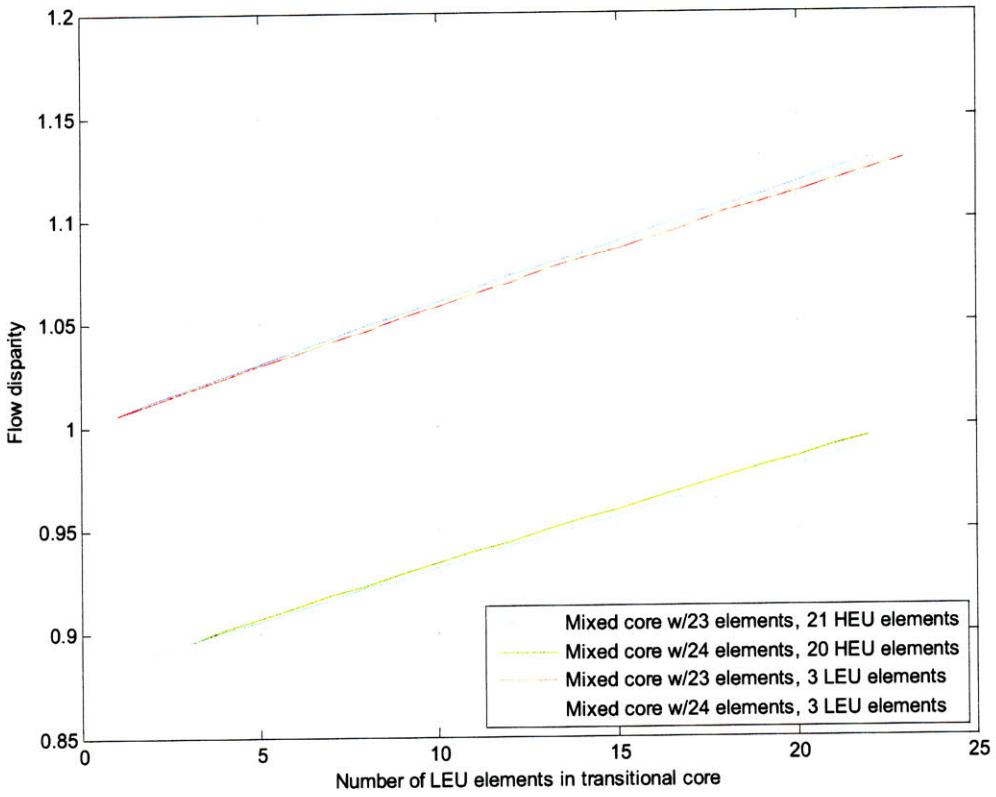

Figure 67: Distribution of primary flow in HEU and LEU fuel in the transitional core with 23 and 24 fuel elements.

6.2.6. Results

6.2.6.1. Case 1 – Transitional core with 24 fuel elements (21 HEU, 3 LEU)

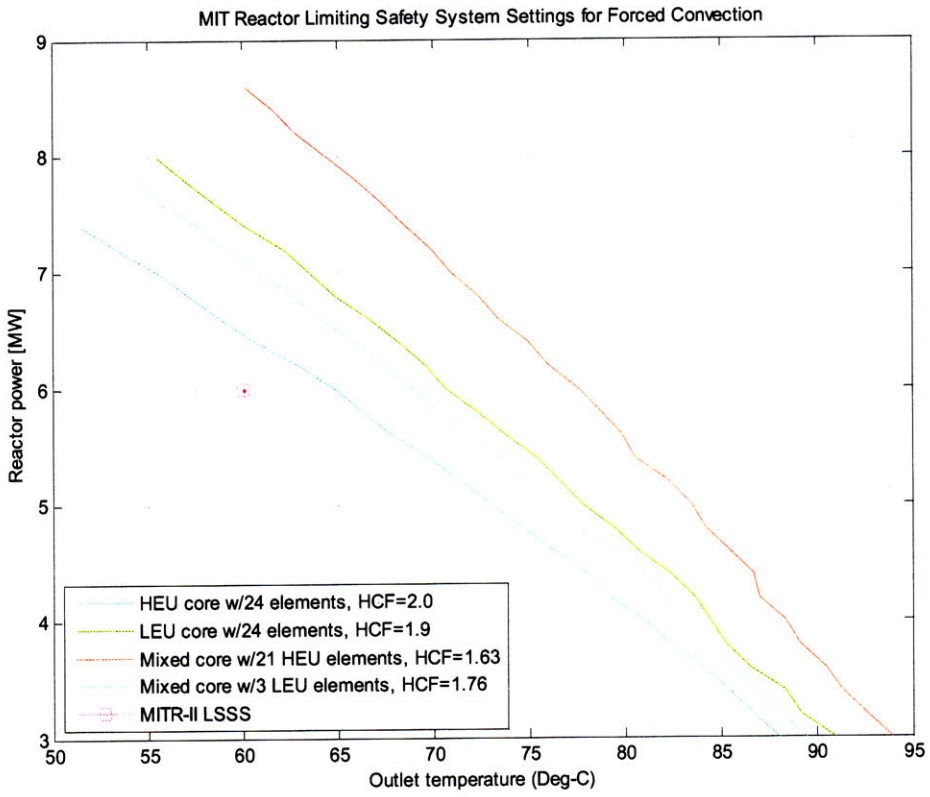

Figure 68: MIT Reactor limiting safety system settings for forced convection, assuming HCF=1.63 in HEU fuel and 1.76 in LEU fuel of the transitional core with 3 LEU elements.

Assumption of power and flow distributions		
Total primary flow	1800	gpm
Core tank level	2.968	m
Hot channel factors		
mHEU	1.63	
mLEU	1.76	
Average flow distribution		
mHEU	1.0179	
mLEU	0.8956	
Flow disparity factors		
mHEU	0.864	
mLEU	0.864	

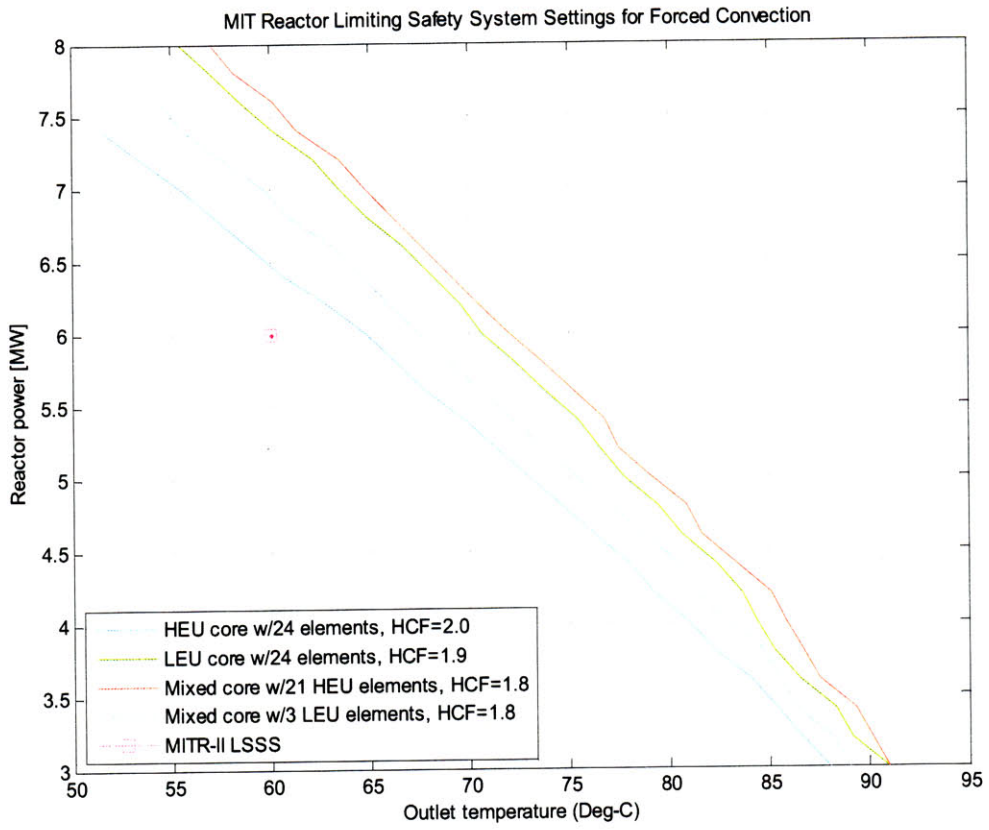

Figure 69: MIT Reactor limiting safety system settings for forced convection, assuming HCF=1.8 in HEU and LEU fuel of the transitional core with 3 LEU elements.

Power and Flow Distribution		
Total primary flow	1800	gpm
Core tank level	2.968	m
Hot channel factors		
mHEU	1.80	
mLEU	1.80	
Average flow distribution		
mHEU	1.0179	
mLEU	0.8956	
Flow disparity factors		
mHEU	0.864	
mLEU	0.864	

6.2.6.2. Case 2 – Transitional core with 23 fuel elements (20 HEU, 3 LEU)

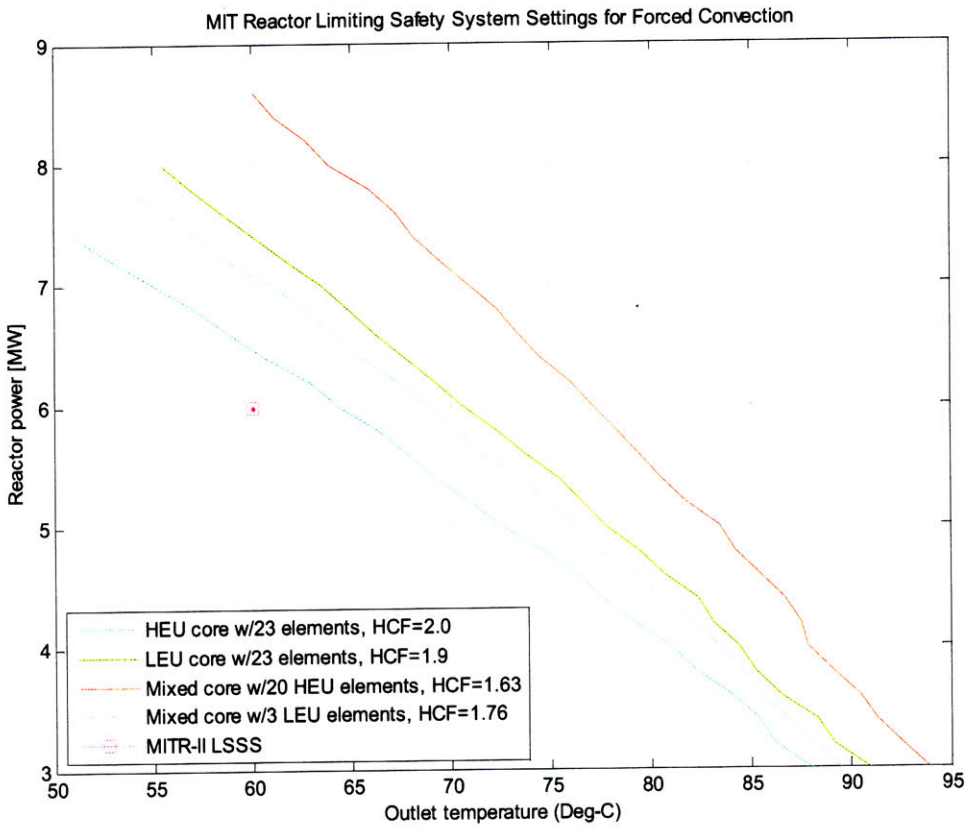

Figure 70: MIT Reactor limiting safety system settings for forced convection, assuming HCF=1.63 in HEU fuel and 1.76 in LEU fuel of the transitional core with 3 LEU elements.

Assumption of power and flow distributions		
Total primary flow	1800	Gpm
Core tank level	2.968	M
Hot channel factors		
mHEU	1.63	
mLEU	1.76	
Average flow distribution		
mHEU	1.0187	
mLEU	0.8961	
Flow disparity factors		
mHEU	0.864	
mLEU	0.864	

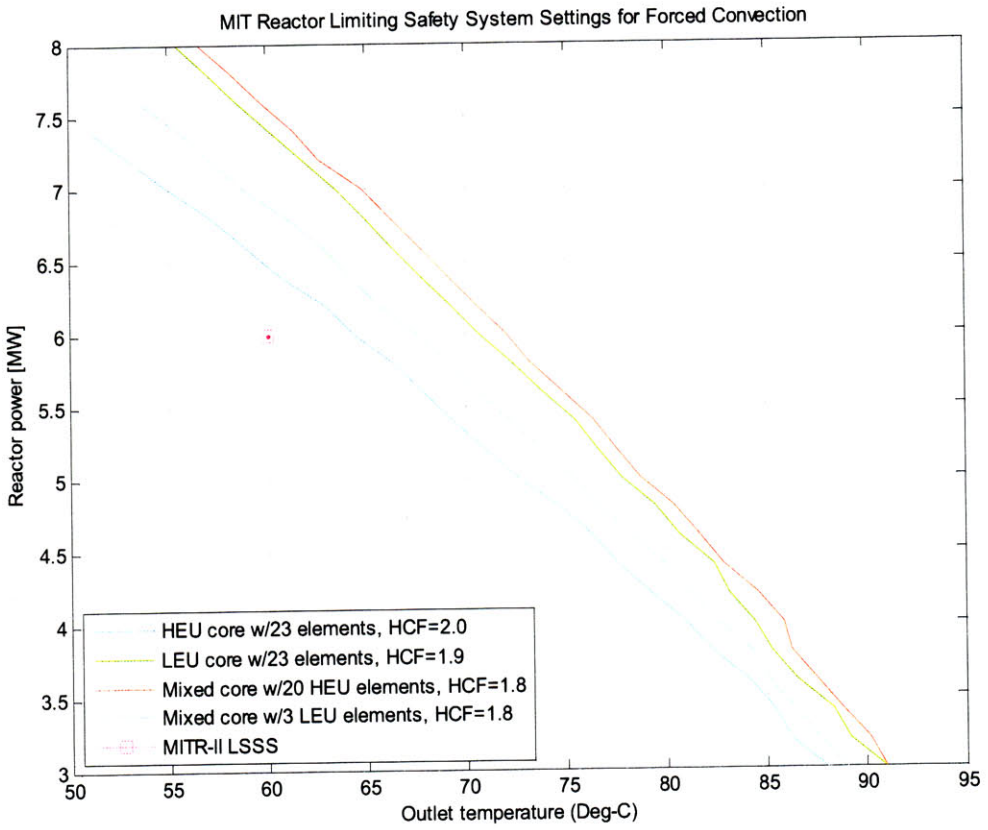

Figure 71: MIT Reactor limiting safety system settings for forced convection, assuming HCF=1.80 in HEU and LEU fuel of the transitional core with 3 LEU elements.

Power and Flow Distribution		
Total primary flow	1800	Gpm
Core tank level	2.968	M
Hot channel factors		
mHEU	1.80	
mLEU	1.80	
Average flow distribution		
mHEU	1.0187	
mLEU	0.8961	
Flow disparity factors		
mHEU	0.864	
mLEU	0.864	

7. Conclusion

7.1. Summary

7.1.1. Friction pressure drop in rectangular ducts with continuous longitudinal rectangular fins

It is concluded in Section 4.5 that for laminar flow in rectangular ducts with continuous, longitudinal and rectangular fins, the Darcy friction factors f_d in Eq.(10) should be considered, along with the pseudo equivalent hydraulic diameter D_s^{finned}, for good prediction of the friction pressure drop characteristics for MITR's finned fuel elements. Experiment data show that the laminar friction pressure drop is unaffected by the presence of the rectangular fins. This is consistent with the existing theory that friction factors are independent of surface roughness for laminar flow.

For turbulent flow, however, a new correlation for the Darcy friction factor f_d has been proposed. The new friction factor correlation uses the same exponent as the Blasius friction factor in Eq.(12), and is multiplied by a coefficient that are determined for the finned, rectangular coolant channels. The correlation is given as:

$$f_d = 0.575 \cdot \mathrm{Re}_s^{-0.25} \tag{46}$$

where $15{,}000 < \mathrm{Re}_s < 30{,}000$.

The significant levels of experimental data scattering in the transition flow region, as well as the difficulty in repeating the experiment data, cause tremendous challenge to drawing any meaningful conclusion to the friction pressure drop characteristics for transition flows in finned rectangular channels. Future work is needed to obtain reliable experimental data for transition flows.

7.1.2. Transitional core flow distribution analysis

In the transitional core flow distribution analysis in Section 5, methods are proposed to estimate the friction pressure drop and the flow distribution

of the primary coolant in the reactor core during the progressive conversion from HEU to LEU fuels, and to demonstrate the feasibility of the transitional core from a thermal hydraulic perspective.

Results of the flow distribution analysis for transitional core with 3, 6 and 9 LEU fuel elements are discussed in Section 5.2.2. The mean velocity of flow in an LEU full channel is generally 6% below that in a full channel of the HEU fuel element.

7.1.3. Transitional core thermal hydraulic limits analysis

In the study of the transitional core thermal hydraulic limits analysis, a method is proposed in Section 6.1.3 to re-calculate the safety limits for forced convection operation in the transitional core of the MIT Reactor. It is demonstrated that, with the recent update of hot channel and engineering factors from Ref.[1, 2], the transitional core shows reasonable feasibility from a thermal-hydraulic perspective.

7.2. Recommendations for Future Work

7.2.1. Friction pressure drop experiment for higher fluid temperature

The friction pressure drop experiment in Sections 3 and 4 is performed under room temperature conditions. The fluid temperature, measured by two K-type thermocouples at the inlet of the test assembly and the D.I. water storage tank, vary between $28-34^{\circ}C$, in the experiments.

For verification purposes, it is suggested that similar friction pressure drop tests can be performed under slightly heated conditions at $50-60^{\circ}C$ that correspond to the normal operating conditions at the MIT Reactor.

7.2.2. Transitional core flow distribution analysis

The transitional core flow distribution analysis in Section 5, while currently focusing on the momentum equation, can be coupled with the energy equation in order to fully account for the axial and radial power

distribution and, thus, the effect of the temperature and fluid properties of the primary coolant in the reactor core.

The coupling of the momentum and energy equations will give a better picture of the actual primary flow distribution in the reactor core due to both the friction and buoyancy effects of the flow.

7.2.3. Transitional core thermal hydraulic limits analysis

The basic assumptions of the transitional core thermal hydraulic limits analysis in Section 6, which include the reactor power distribution calculations by the on-going efforts of the low enrichment uranium conversion design study at the MIT Reactor, may be revised as more detailed analysis for different transition core configuration is performed. The objective is to establish new sets of Safety Limits and Limiting Safety System Settings that can be applied to the transitional core operations during the conversion phase of the MIT Reactor.

8. Appendix

8.1. Equivalent Hydraulic Diameter Calculation

Core Parameters					
# channels per element		15			
# elements		24		360	
Fuel Element Parameters					
Projection	theta	0.5236	radian	30	deg
Side-plate to side-plate width		6.033E-02	m	2.375	"
Distance b/w ends of SP		6.045E-02	m	2.380	"
Side-plate thickness		4.775E-03	m	0.188	"
Shoulder width		6.109E-02	m	2.405	"
Nozzle width		5.382E-02	m	2.119	"
Gap b/w shoulder and SP		3.810E-04	m	1.500E-02	"
Gap b/w shoulder and end of SP		3.175E-04	m	1.250E-02	"
Gap b/w shoulder and nozzle		3.632E-03	m	1.430E-01	"
Gap b/w element and edge of core		6.223E-03	m	0.245	"
Full Channel Parameters					
Channel width	w_channel	5.863E-02	m	2.308E+00	"
Channel height (base-base)	h_channel	2.489E-03	m	0.098	"
Flow area	A_flow	1.316E-04	m2	2.040E-01	"sq
Perimeter	P_w	2.350E-01	m	9.252E+00	"
Hydraulic diameter	D_h	2.240E-03	m	8.820E-02	"
Half Channel Parameters					
Channel width	w_channel	5.863E-02	m	2.308E+00	"
Channel height (base-base)	h_channel	1.372E-03	m	0.054	"
FP-FP Full Channel Parameters					
Channel width	w_channel2	5.863E-02	m	2.308E+00	"
Channel height (base-base)	h_channel2	3.378E-03	m	0.1330	"
Flow area	A_flow	1.837E-04	m2	2.848E-01	"sq
Perimeter	P_w	2.368E-01	m	9.322E+00	"
Hydraulic diameter	D_h	3.104E-03	m	1.222E-01	"
FP-SP Half Channel Parameters					
Channel width	w_half1	5.863E-02	m	2.308E+00	"
Channel height (all)	h_half1	2.070E-03	m	0.0815	"
Flow area	A_flow	1.142E-04	m2	1.770E-01	"sq
Perimeter	P_w	1.778E-01	m	6.999E+00	"
Hydraulic diameter	D_h	2.570E-03	m	1.012E-01	"
FP-EoC Half Channel Parameters					
Channel width	w_half2	5.863E-02	m	2.308E+00	"
Channel height (all)	h_half2	4.280E-03	m	0.1685	"
Flow area	A_flow	2.438E-04	m2	3.778E-01	"sq
Perimeter	P_w	1.822E-01	m	7.173E+00	"
Hydraulic diameter	D_h	5.351E-03	m	2.107E-01	"
Fin Parameters					
Width	a_fin	2.540E-04	m	0.01	"
Height	b_fin	2.540E-04	m	0.01	"
Pitch	d_fin	2.540E-04	m	0.01	"
# fins per plate		111			

8.2. Moody Diagram

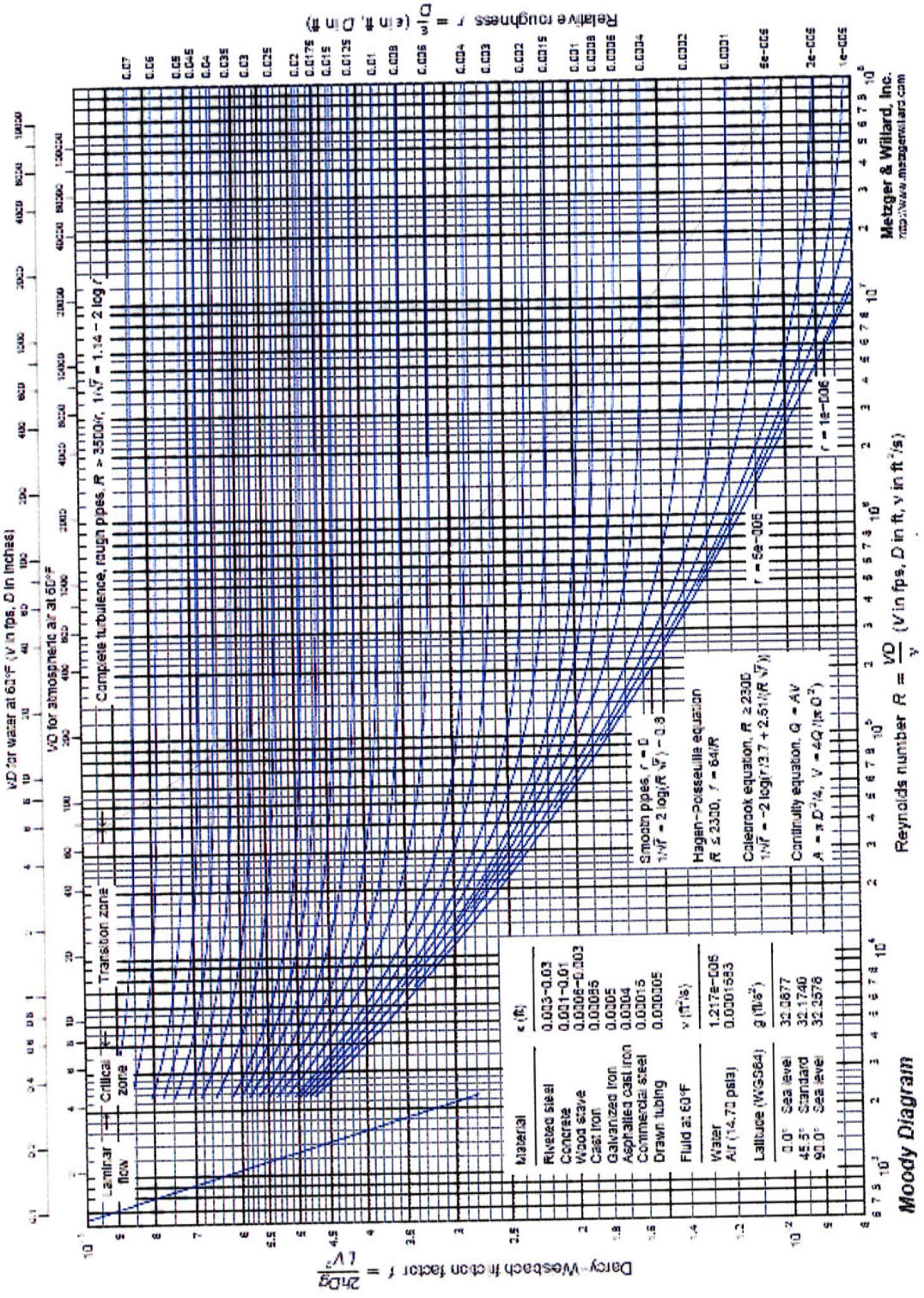

Figure 72: Moody diagram (adopted from [47]).

8.3. Experiment Drawing

The engineering drawings of the individual parts of the test assembly are compiled in this section.

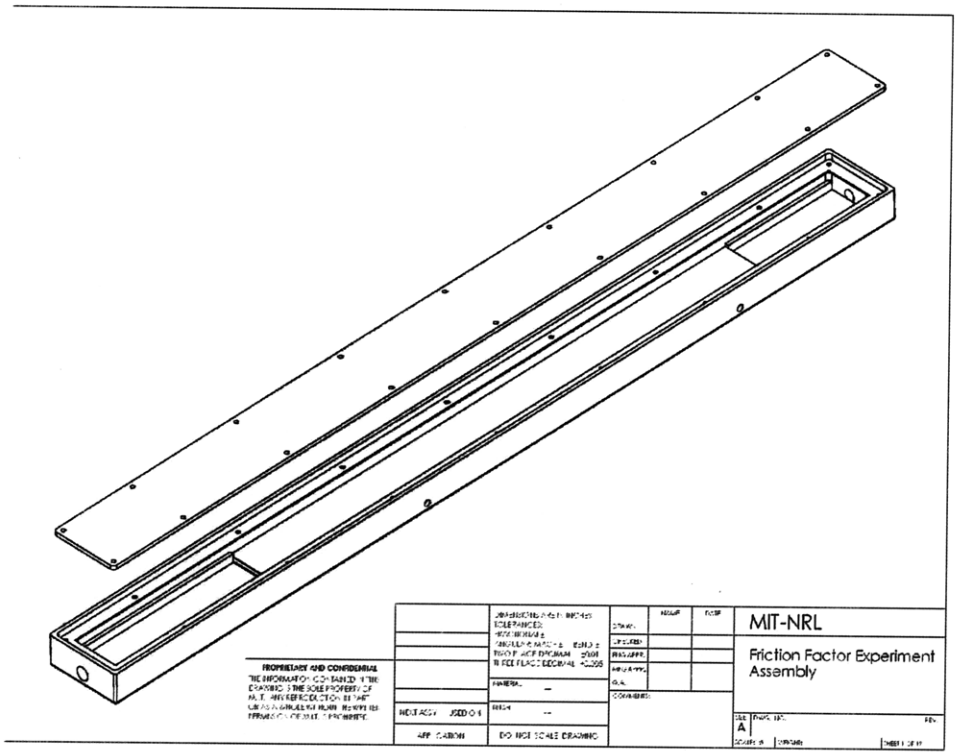

Figure 73: Friction pressure drop test assembly.

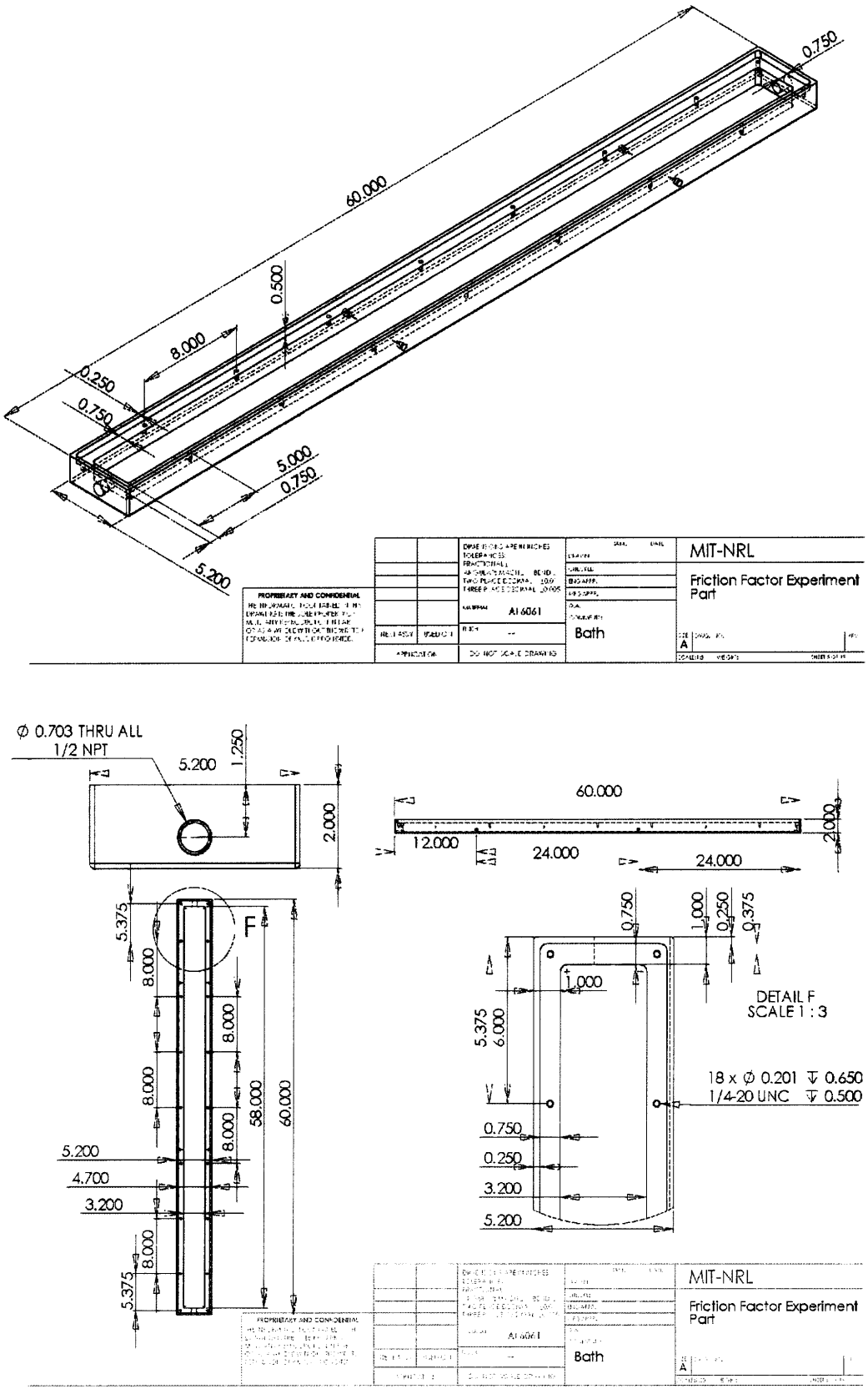

Figure 74: Test assembly part - bath.

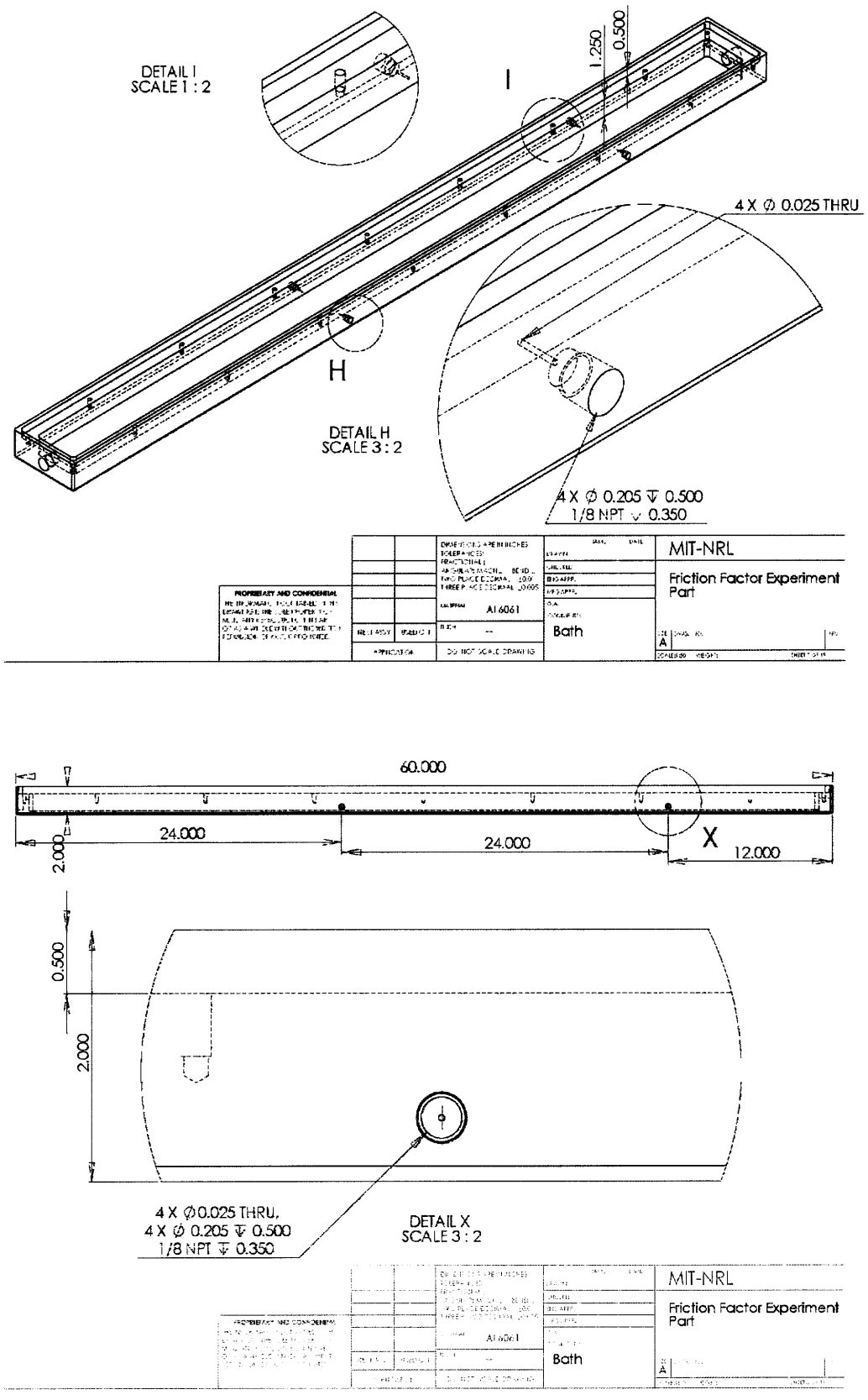

Figure 75: Test assembly part – 4 tap holes on two sides of the test section.

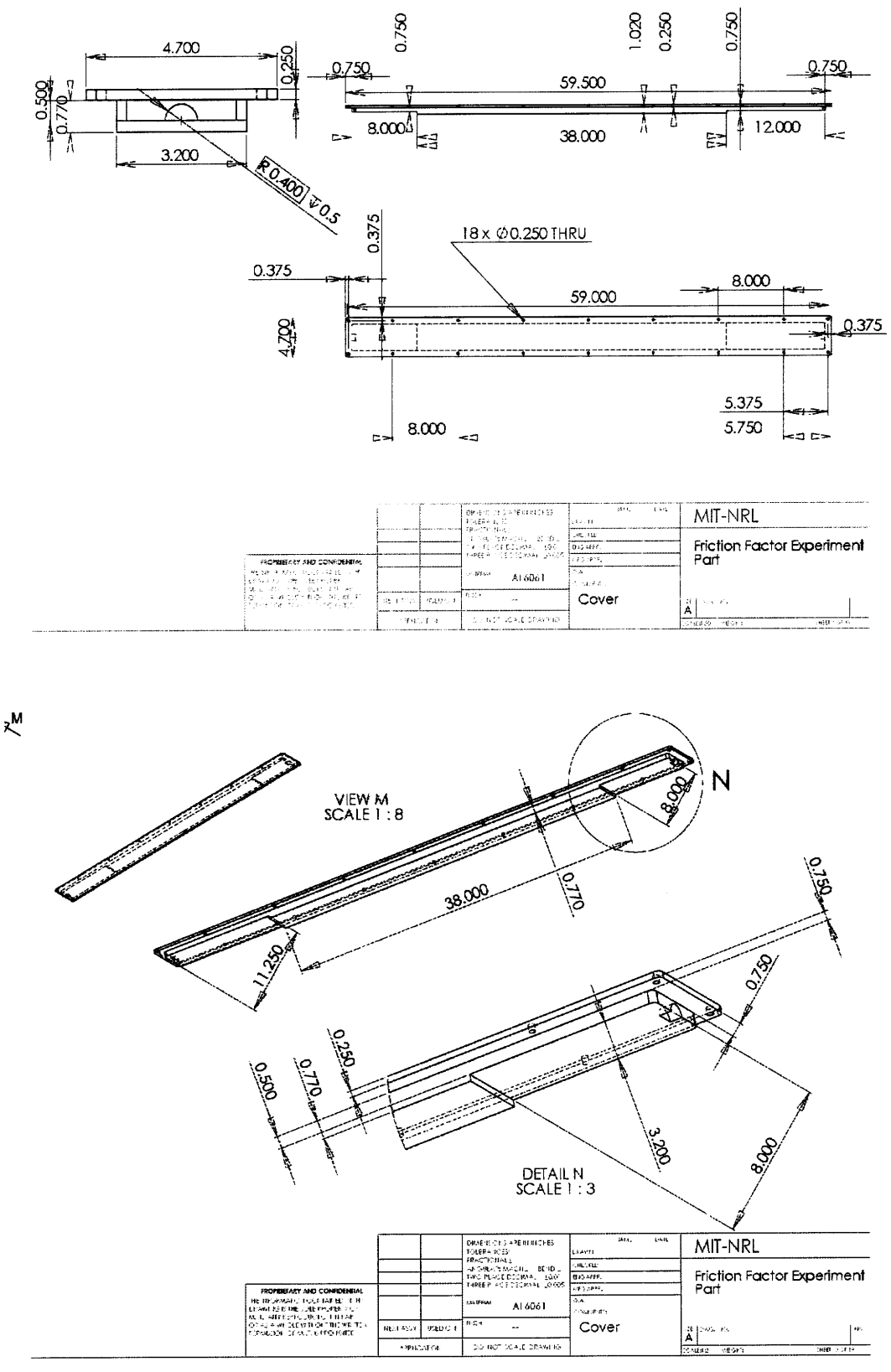

Figure 76: Test assembly part - cover.

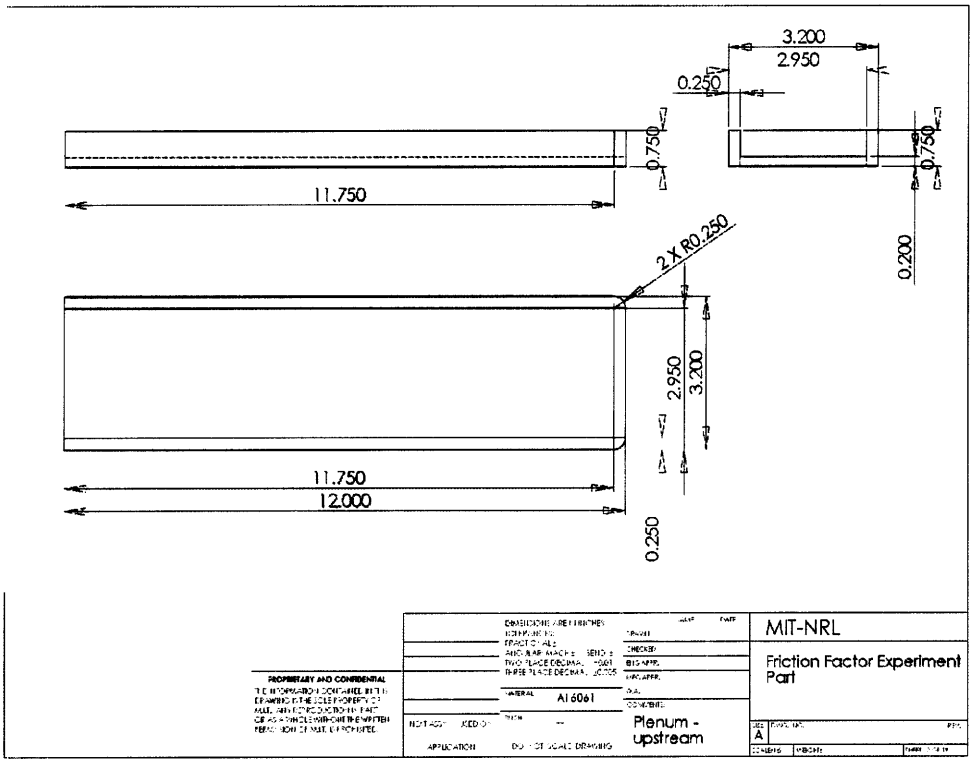

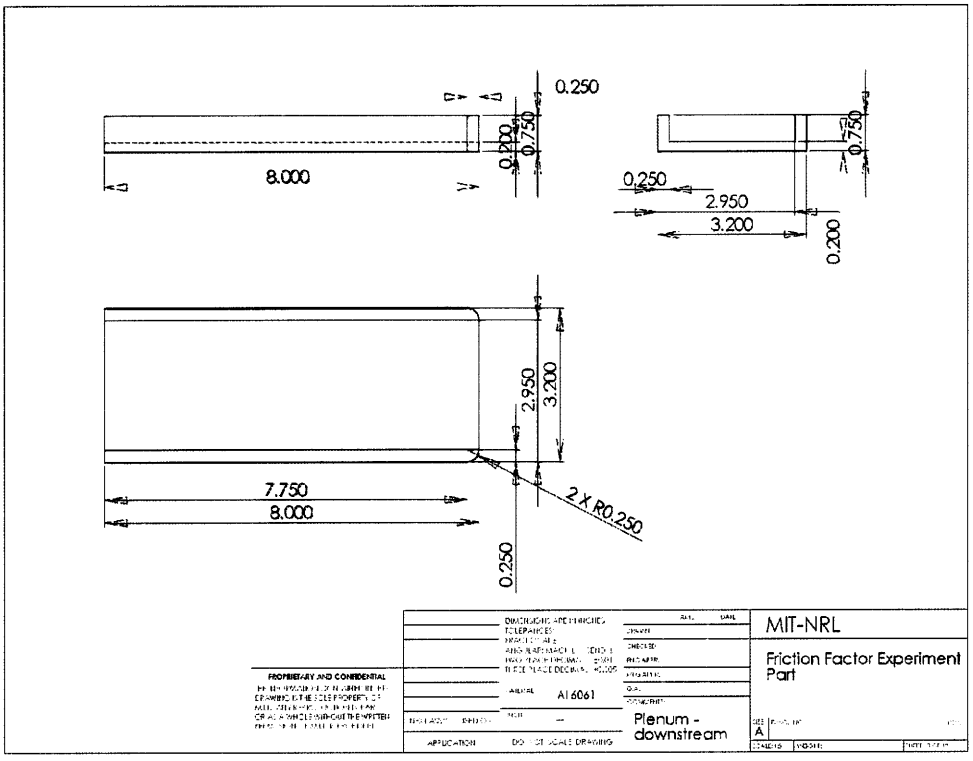

Figure 77: Test assembly parts – upstream and downstream plenums.

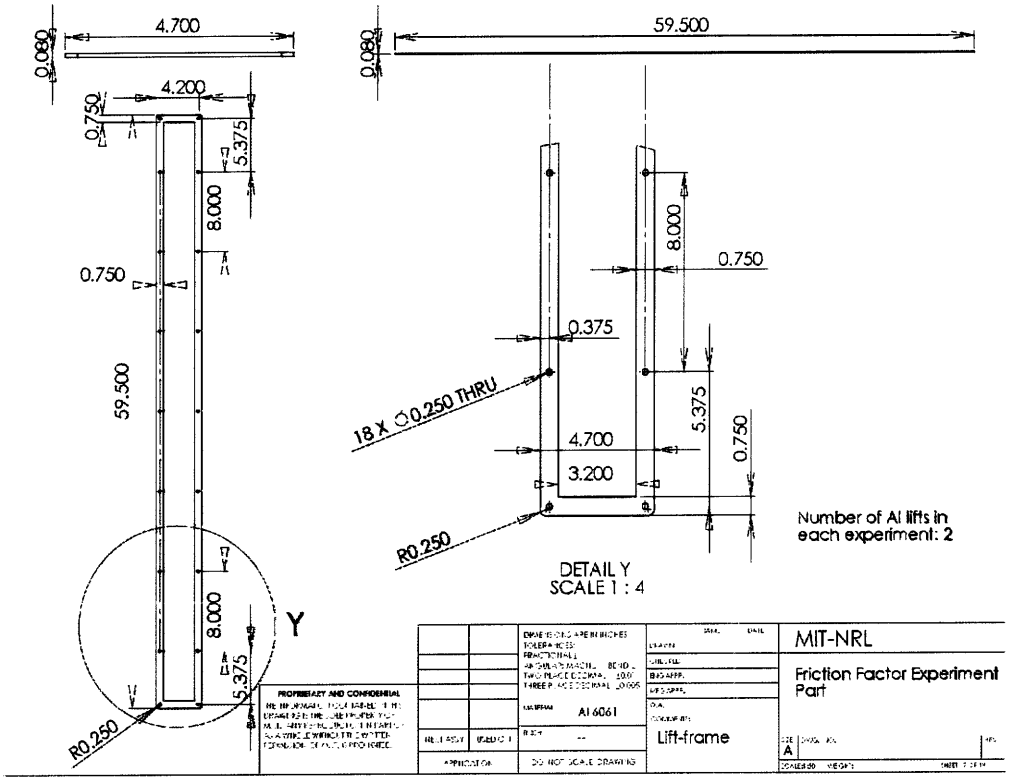

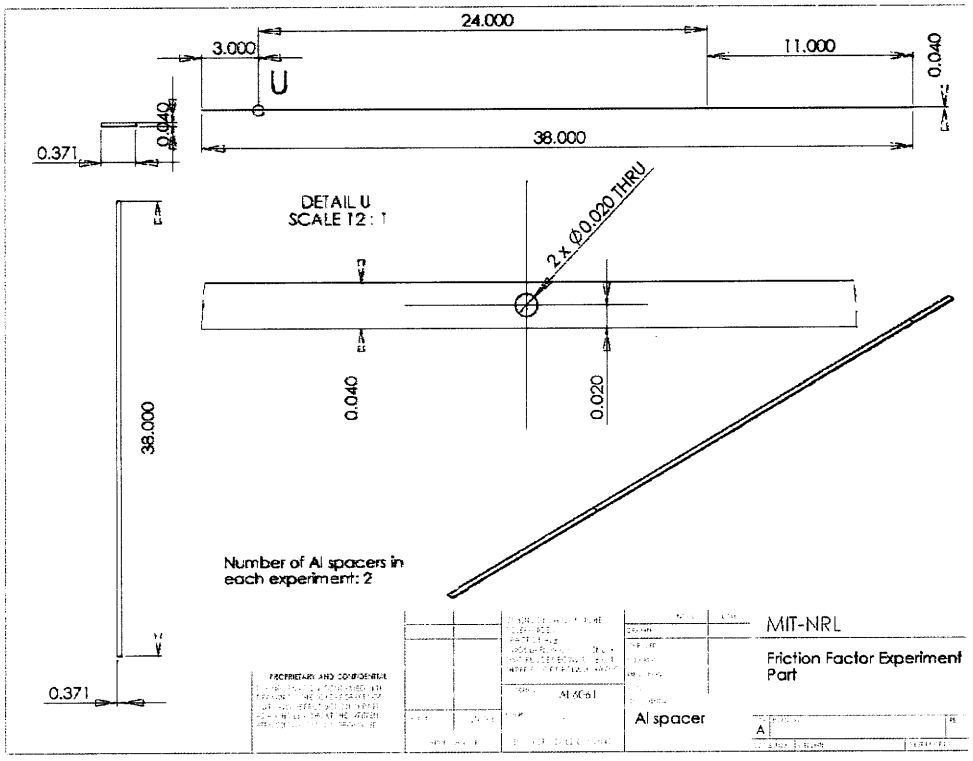

Figure 78: Test assembly parts – shims and spacers.

8.4. Parts Measurement

The assembly parts, except the rectangular plates with continuous longitudinal rectangular fins, are manufactured by the MIT Central Machine Shop. The dimensions of the assembly parts are measured and recorded below:

MIT Friction Pressure Drop Expt

Apr 9, 2008

Shim	Thickness (mils)		Measure1	Measure2	Measure3
40a		38.50	38.5	38.5	38.5
40b		38.50	38.5	38.5	38.5
80a		78.00	78	78	78
80b		78.00	78	78	78
100a		96.17	96.5	96	96
100b		96.17	96	96.5	96
125a		125.17	125	125.5	125
125b		125.00	125	125	125

Plate	Thickness (mils)		Measure1	Measure2	Measure3
Flat dummy plate a		256.00	256	256	256
Flat dummy plate b		256.17	256	256.5	256

8.5. Instrument Calibration

Friction Pressure Drop Loop Calibration

Summary

Instrument	Omega	Output (min)	Output (max)	Channel
Pressure Transducer (Signal in)	PX302-100GV	0	10V	SC1Mod1/a6
Pressure Transducer (Signal out)		0	10V	SC1Mod1/a2
Flow Meter and Voltage Output	FTB-904/FLSC-61	0	10V	SC1Mod1/a3
D/P Transmitter (Low Range)	PX154-025DI	.7704V	3.66V	SC1Mod1/a5
D/P Transmitter (High Range)	PD3000-200-52-11	4mA	20mA	SC1Mod/a4
Assembly Inlet Temperature	KQSS-304	-200 degC	1250 deg-C	SC1Mod1/a0
Storage Water Temperature	KQSS-304	-200 degC	1250 deg-C	SC1Mod1/a1
Pump Speed Ctrl				SC1Mod1/a6

FTB-904 (s/n: 264482) / FLSC-61 (s/n: 265367)

Point		Flow Rate (gpm)	Appox Freq (Hz)		Output (Volt)	Note
	1	19.037701	1243.5627	0.015309	24.871254	0.015305243
	2	15.057436	984.8152	0.015289606	19.696304	
	3	8.454662	552.1599	0.015311981	11.043198	
	4	5.685054	371.5378	0.015301415	7.430756	
	5	1.737647	113.4663	0.015314212	2.269326	
Omega			500		10	Adjust span (R8)
			375		7.503	
			250		5.002	
			125		2.5	
			0		0	
SW 05/20/2008		1.913155339	125	0.015305243	0.83	
		3.826310677	250		1.66	
		5.739466016	375		2.50	
		7.652621355	500		3.33	
		9.565776693	625		4.17	
		11.47893203	750		5.00	
		13.39208737	875		5.83	
		15.30524271	1000		6.72	
		18.36629125	1200		8.05	
		22.95786406	1500		10.03	
		24.48838834	1600		10.70	
		26.01891261	1700		11.36	
		27.54943688	1800		11.40	

FTB-9511 (s/n: 265963) / FLSC-61 (s/n: 265367)

Point		Flow Rate (gpm)	Appox Freq (Hz)		Output (Volt)	Note
	1	2.0980493	1155.0997	0.001816336	23.101994	0.001916856

	2	1.9788597	1081.2406	0.001830175	21.624812
	3	1.9229241	1054.5406	0.001823471	21.090812
	4	1.919362	1054.3059	0.001820498	21.086118
	5	1.773505	967.4087	0.001833253	19.348174
	6	1.5827443	859.6202	0.001841213	17.192404
	7	1.5160217	819.386	0.001850192	16.38772
	8	1.5130222	819.0116	0.001847376	16.380232
	9	1.3218875	707.8559	0.001867453	14.157118
	10	1.2581137	672.0468	0.001872063	13.440936
	11	1.1298777	601.2693	0.001879154	12.025386
	12	1.1298868	600.5641	0.001881376	12.011282
	13	0.8794755	461.182	0.001907003	9.22364
	14	0.7622034	398.3087	0.0019136	7.966174
	15	0.6754253	350.0539	0.001929489	7.001078
	16	0.5382774	274.4578	0.001961239	5.489156
	17	0.4065588	203.3492	0.001999313	4.066984
	18	0.2996244	146.5168	0.002044983	2.930336
	19	0.2195356	104.9915	0.002090985	2.09983
	20	0.093296	40.0766	0.002327942	0.801532
Omega			500		10 Adjust span (R8)
			375		7.503
			250		5.002
			125		2.5
			0		0
SW 05/28/2008		0.23960697	125	0.001916856	0.83
		0.47921394	250		1.66
		0.71882091	375		2.50
		0.95842788	500		3.33
		1.19803485	625		4.17
		1.437641821	750		5.00
		1.677248791	875		5.83
		1.916855761	1000		6.72
		2.300226913	1200		8.05

PX154-025DI (s/n: 37111-1W2)

183

Point	Range (in.H2O)	Output (mA)	Output (V)
1	0	4.21	0.7877
2	3	20	1.109
3	6		1.427
4	9		1.749
5	12		2.07
6	15		2.391
7	18		2.714
8	21		3.037
9	0		0.7943
10	25		3.465

PD3000-200-52-11 (s/n: I9537)

22

Point	Range (in.H2O)	Output (mA)	Output (mV)
1	0	4	84.23
2	200	20	536.1
3	5		95.52

4	10	106.8
5	15	118.2
6	20	129.5
7	25	140.8
8	30	152.1
9	35	163.5
10	40	174.9
11	50	197.5
12	60	220.1
13	70	242.8
14	80	265.4
15	90	288.1
16	100	310.6
17	110	333.2
18	120	355.7
19	130	378.2
20	140	400.8
21	150	423.3
22	160	445.9
23	170	468.3
24	180	490.8
25	190	513.4
26	200	536

8.6. Experiment Procedures

1. Turn on 12V/24V power supply, SCXI and VFD control
2. Open DatAcq06.vi
3. Turn on DatAcq06 and verify instrument readings on DatAcq06.vi

a. Thermocouples reading at room temperature

b. FTB-904 flow meter reading at zero

c. PX-154/PD-3000 D/P transmitters reading at zero

d. PX-302 pressure transducer indicating level in Storage Tank

4. Turn off DatAcq06
5. Set up test assembly
6. Apply vacuum grease and close cover
7. Open ball valve at pump outlet
8. Turn on DatAcq06
9. Adjust pump frequency on VFD control
10. Wait until flow rate stabilizes
11. Verify D/P within range of PX-154 (25in.H2O) / PD-3000 (200in.H2O)
12. Wait 2-3 minutes for data acquisition
13. Turn off DatAcq06
14. Repeat steps 8-13
15. Stop pump
16. Close ball valve at pump outlet
17. Open cover and verify that both plates remain in test assembly
18. Drain water from test assembly inlet
19. Cloth dry test assembly, shims and plates
20. Download output files
21. Refill Storage Tank with de-ionized water
22. Turn off 12V/24V power supply, SCXI and VFD control

8.7. Data Acquisition Methodology

The data acquisition (DAQ) system is set-up via LABVIEW 8.5 by National Instruments. The purpose of using data acquisition is to measure an electrical or physical phenomenon, such as, voltage, current, temperature, pressure, etc., by using a combination of modular hardware, application software and computer for data measurements.

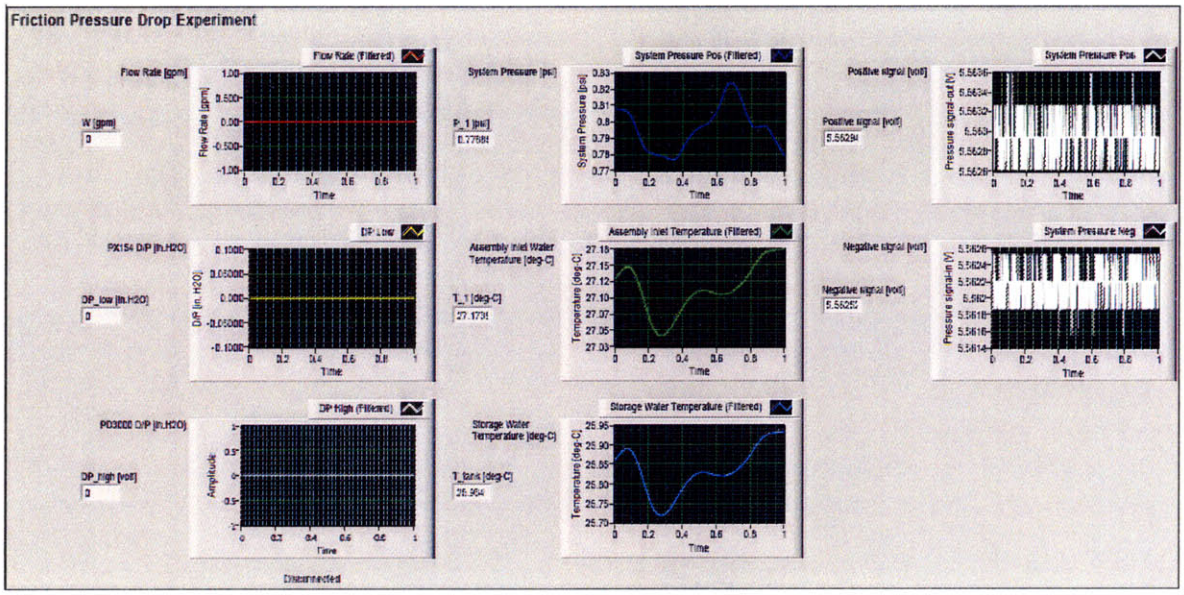

Figure 79: Front panel of the Friction Pressure Drop Experiment DAQ.

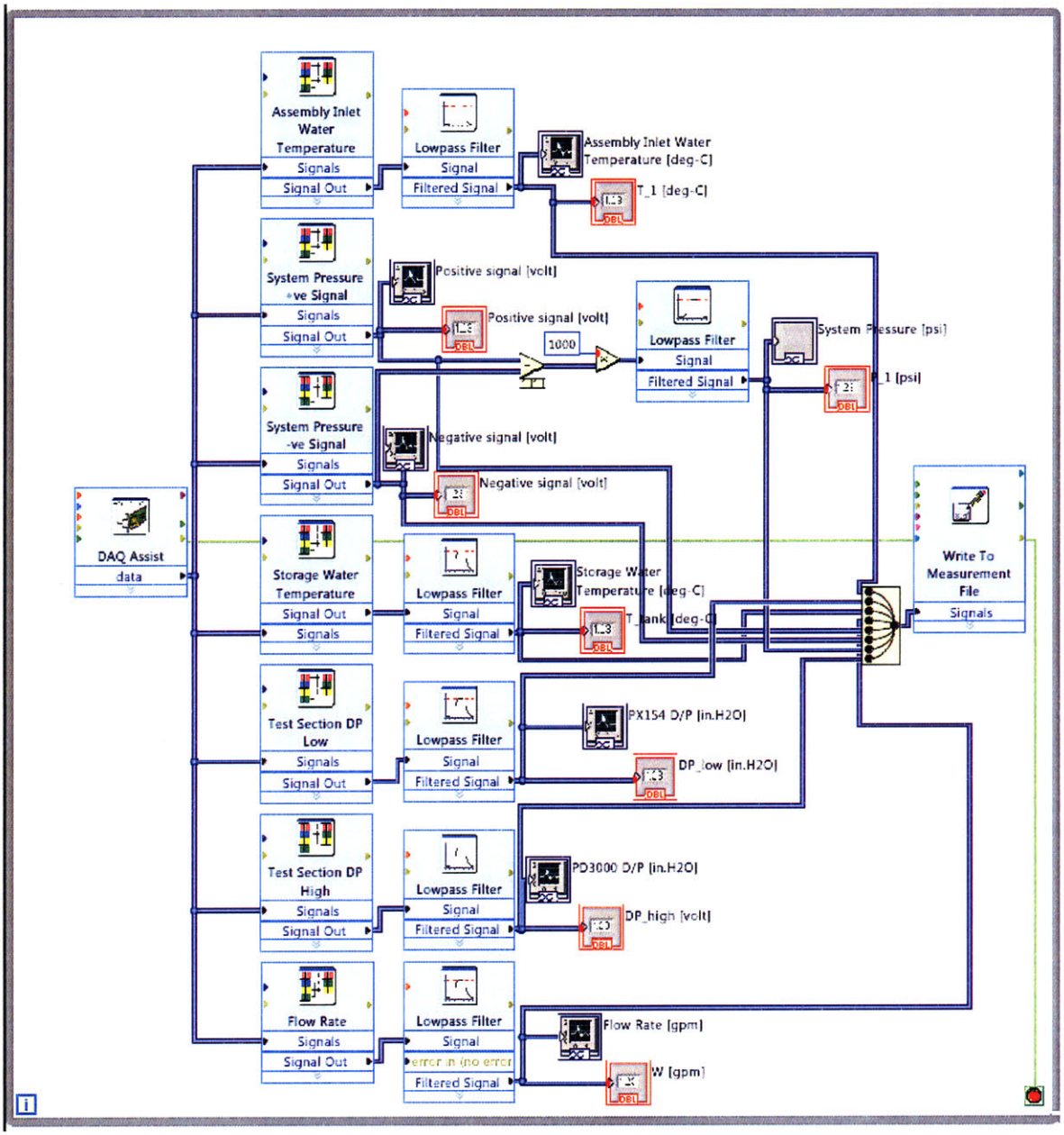

Figure 80: Block diagram of DAQ set-up.

Propagation of Errors

Instrument	Model	Accuracy	
System pressure transducer	PX-302	0.25%	9.00%
Differential pressure transmitter	PD 3000	0.25%	2.00%
Thermocouple 1	Std K 3"	1.67%	1.67%
Thermocouple 2	Std K 3"	1.67%	1.67%
Flow meter (high range)	FTB-904	0.50%	2.50%

dP	40000	2.00%		nf	111	
density	998	1.67%		A	1.462E-04	
viscosity	0.0008			w	3.19	0.31%
velocity	2.5	2.50%		h	0.078	12.82%
axial length	0.6096	0.04%		hf	0.01	20.00%
diameter (4A/P)	2.10E-03	2.05%		wf	0.01	20.00%
K	**1.283E+01**			dA	1.535E-05	10.50%
dK1	-2.565E-01	6.580E-02				
dK2	2.138E-01	4.569E-02		P_in	10.976	
dK3	6.413E-01	4.112E-01		P	2.788E-01	
dK	5.985E-01	**4.67%**		dP_in	0.928	
				dP	2.357E-02	8.45%
f	**4.413E-02**					
df1	2.060E-03	4.242E-06			6.516	
df2	9.036E-04	8.165E-07		P_pseu	1.655E-01	
df3	1.839E-05	3.382E-10			0.036	
df	2.982E-03	**6.76%**		dP_pseu	9.144E-04	0.55%
f_pseu	7.434E-02				6.536E+00	
df1	3.469E-03	1.204E-05		P_smooth	1.660E-01	
df2	7.397E-03	5.472E-05			0.04	
df3	3.098E-05	9.596E-10		dP_smooth	1.016E-03	0.61%
df_pseu	1.090E-02	**14.66%**				
				D	**2.098E-03**	
f_smooth	7.412E-02			**dD**	4.295E-05	**2.05%**
df1	3.459E-03	1.196E-05				
df2	7.353E-03	5.406E-05		**D_pseu**	**3.534E-03**	
df3	3.088E-05	9.537E-10		**dD_pseu**	3.516E-04	**9.95%**
df_smooth	1.084E-02	**14.63%**				
				D_smooth	**3.523E-03**	
				dD_pseu	3.495E-04	**9.92%**

8.8. Matlab Script for Flow Distribution Analysis for Transitional Core

```
% 22.ThG Friction pressure drop in transitional core with different number of LEU fuel
elements
% Susanna Wong
% Mar 29, 2008

% Output figure: Flow Disparity v4f23 Fig 1,2,3,4
% Output file: F_mf_1800 24.txt

% Constants
inch = 2.54E-02;          % inch to metre conversion
gpm = 6.309E-05;          % gpm to cubic metre conversion
D_h0 = 2.2363E-03;        % hydraulic diameter of HEU channel
A_0 = 1.3199E-004;        % flow area of HEU channel
V_0 = 3.8555E-004;        % volumetric flow rate w/24,15,0.098 HEU config at 2200 gpm
v_0 = 2.9211;             % flow velocity w/24,15,0.098 HEU config at 2200 gpm
v_1800 = 2.3900;          % flow velocity w/24,15,0.098 HEU config at 1800 gpm
dP_2200 = 3.2930E+004;    % friction pressure drop w/24,15,0.098 HEU config at 2200 gpm
dP_1800_24 = 2.3180E+004;   % friction pressure drop w/24,15,0.098 HEU config at 2200 gpm

% Core config
n_felement = 24;          % number of fuel element in core
N_plate = [15;18];        % number of plates in HEU and LEU fuel elements
n2 = size(N_plate,1);

% Channel heights with different number of plates per element
h_element = 2.380;
t_fmeat_in = [0.030;0.020];      % fuel thickness in HEU and LEU fuel plates
t_clad_in0 = 0.015;              % clad thickness in HEU fuel
t_clad_in = 0.010;  % clad thickness
n1 = size(t_clad_in,2);
D_channel = zeros(n1*n2,1);
for j = 1:n2
    for i = 1:n1
        if j == 1
            D_channel((j-1)*n1+i) = floor(h_element*1000/N_plate(j))/1000 - t_fmeat_in(j) -
2*t_clad_in0;
        else
            D_channel((j-1)*n1+i) = floor(h_element*1000/N_plate(j))/1000 - t_fmeat_in(j) -
2*t_clad_in(1,i);
        end
    end
end

% Fluid properties
    T = 50;

    % Density
    C0_den = 1000.1;
    C1_den = 0.0026863;
    C2_den = -0.0054424;
    C3_den = 1.2324 * 10 ^ -5;
    den_w = C0_den + C1_den * T + C2_den * T ^ 2 + C3_den * T ^ 3;

    % Viscosity
    C0_vis = 1726.9;
    C1_vis = -43.349;
    C2_vis = 0.47475;
    C3_vis = -0.0018307;
    vis_w = 1E-6 * (C0_vis + C1_vis * T + C2_vis * T ^ 2 + C3_vis * T ^ 3);

N_leu = 1:1:n_felement-1;
n3 = size(N_leu,2);
D_h = zeros(n1,n2);
A_flow = zeros(n1,n2);
V_ch = zeros(n1,n2,n3);
v_ch = zeros(n1,n2,n3);
V_ch_all = zeros(n1,n2,n3);
Re = zeros(n1,n2);
```

```
dP = zeros(n1,4,n3);
F_mf = zeros(n1,n2,n3);              % Ratio of average primary flow through HEU/LEU
element to average primary flow through the fuel
for k = 1:n3
    n_leu = N_leu(1,k);              % number of HEU fuel element in mixed core
    n_heu = n_felement - n_leu;
    n_all = n_heu*N_plate(1)+n_leu*N_plate(2);
    for i = 1:n1
        for j = 1:n2
            % Channel dimensions
            theta = pi()/6;
            d_fplate_in = 2.552;     % fuel plate width
            d_fplate = d_fplate_in*inch;
            if j == 1
                t_fplate_in = t_fmeat_in(j) + t_clad_in0*2;      % HEU fuel plate thickness
            else
                t_fplate_in = t_fmeat_in(j) + t_clad_in(i)*2;    % LEU fuel plate thickness
            end
            t_fplate = t_fplate_in*inch;
            l_fplate = 0.5842;       % fuel plate length in metre
            d_channel = D_channel((j-1)*n1+i)*inch;      % base to base channel gap in
metre
            d_splate_in = 0.118;     % side plate projected depth
            d_splate1 = d_splate_in*inch/cos(theta);
            d_splate2 = d_splate1 - t_fplate*tan(theta);
            w_channel = d_fplate-d_splate1-d_splate2;

            % Fin dimensions
            t_fin_in = 0.01;
            t_fin = t_fin_in*inch;
            d_fin_in = 0.01;
            d_fin = d_fin_in*inch;
            pitch_fin_in = 0.01;
            pitch_fin = pitch_fin_in*inch;
            n_fin = 110;             % number of fin spacing

            A_flow(i,j) = w_channel*d_channel - 2*(n_fin+1)*t_fin*d_fin;
            P_w = (w_channel + d_channel/cos(theta) + 2*(n_fin+1)*t_fin) * 2;
            D_h(i,j) = 4*A_flow(i,j)/P_w;      % hydraulic diameter

            % NOP conditions
            V_w_gpm = 1800;          % volumetric flow rate in core in gpm
            V_w = V_w_gpm*gpm;
            if j == 1
                v_ch(i,j,k) = v_0;
            else
                V_ch(i,j,k) = V_w/(n_leu*N_plate(j)); % volumetric flow rate per channel
                v_ch(i,j,k) = V_ch(i,j,k)/A_flow(i,j);
            end
        end

        dP_blasius = [dP_1800_24;0];
        V_ch_all(i,j,k) = n_heu * N_plate(1) * A_flow(i,1) * v_ch(i,1,k) + n_leu *
N_plate(2) * A_flow(i,2) * v_ch(i,2,k);
        while abs(V_ch_all(i,j,k) - V_w)/V_w > 0.005
            if V_ch_all(i,j,k) - V_w > 0.002
                v_ch(i,2,k) = v_ch(i,2,k)*0.998;
            else
                v_ch(i,2,k) = v_ch(i,2,k)*1.002;
            end
            while abs(dP_blasius(2) - dP_blasius(1))/dP_blasius(1) > 0.002
                if dP_blasius(2) - dP_blasius(1) > 0
                    v_ch(i,2,k) = v_ch(i,2,k)*0.998;
                else
                    v_ch(i,2,k) = v_ch(i,2,k)*1.002;
                end
                V_ch(i,2,k) = A_flow(i,2)*v_ch(i,2,k);
                Re(i,2) = den_w*v_ch(i,2,k)*D_h(i,2)/vis_w;

                % Recalculate flow in HEU channels
                V_ch(i,1,k) = (V_w - n_leu * N_plate(2) * V_ch(i,2,k)) / (n_heu *
N_plate(1));
                v_ch(i,1,k) = V_ch(i,1,k)/A_flow(i,1);
                Re(i,1) = den_w*v_ch(i,1,k)*D_h(i,1)/vis_w;
```

```
                % LOF conditions
                m_w = 1.45;             % kg/s

                for j = 1:n2
                    % Blasius correlation
                    f_blasius = .316*Re(i,j)^-.25;
                    dP_blasius(j) = .5*f_blasius*den_w*v_ch(i,j,k)^2*(l_fplate/D_h(i,j));
                    % Choi correlation
                    f_choi = Re(i,j)/24;
                    dP_choi(j) = .5*f_choi*den_w*v_ch(i,j,k)^2*(l_fplate/D_h(i,j));
                end
            end
            V_ch_all(i,j,k) = n_heu * N_plate(1) * A_flow(i,1) * v_ch(i,1,k) + n_leu *
N_plate(2) * A_flow(i,2) * v_ch(i,2,k);
        end
        dP(i,:,k) = [dP_blasius(2) dP_blasius(1) 0 0];

        % Flow disparity
        for j = 1:n2
            F_mf(i,j,k) = A_flow(i,j) * v_ch(i,j,k) / (V_w / n_all);
        end
    end
end

V_print = zeros(n2,n3);
V_print = reshape(V_ch(1,:,:),n2,n3);
v_print = zeros(n2,n3);
v_print = reshape(v_ch(1,:,:),n2,n3);
dP_print = zeros(size(dP,2),n3);
dP_print = reshape(dP(1,:,:),size(dP,2),n3);
F_mf_print = zeros(n2,n3);
F_mf_print = reshape(F_mf(1,:,:),n2,n3);

% Output plots
string_t1 = ('[illegible]
[illegible]');
string_t2 = ('[illegible]');
string_t3 = ('[illegible]
[illegible]');
string_t4 = ('[illegible]
[illegible]');
string_t5 = ('[illegible]');
string_t6 = ('[illegible]');
string_x1 = ('[illegible]');
string_x2 = ('[illegible]');
string_y1 = ('[illegible]');
string_y2 = ('[illegible]');
string_y3 = ('[illegible]
[illegible]');
string_y4 = ('[illegible]');
string_y5 = ('[illegible]
[illegible]');
string_y6 = ('[illegible]');
string_leg1 = ('[illegible]');
string_leg2 = ('[illegible]');
string_leg3 = ('[illegible]');
string_leg4 = ('[illegible]');
string_leg5 = ('[illegible]');
string_leg6 = ('[illegible]');
string_leg7 = ('[illegible]');

plot(N_leu,1E-5*dP_print(1,:),N_leu,1E-5*dP_print(2,:),...
    0,1E-5*dP_1800_24, [illegible]);
title(string_t1);
xlabel(string_x2);ylabel(string_y1); grid [illegible];
legend(string_leg1, string_leg4, string_leg7, [illegible], [illegible]);
print [illegible]

figure;
plot(N_leu,v_print(1,:),N_leu,v_print(2,:),...
    0,v_1800, [illegible]);
title(string_t3);
xlabel(string_x2);ylabel(string_y2); grid [illegible];
```

```
legend(string_leg1, string_leg4, string_leg7,                    );
print

figure;
plot(N_leu,V_print(1,:)/gpm,N_leu,V_print(2,:)/gpm,...
    0,V_w_gpm/(n_felement*N_plate(1)),    );
title(string_t4);
xlabel(string_x2);ylabel(string_y4); grid   ;
legend(string_leg1, string_leg4, string_leg7,                    );
print

figure;
plot(N_leu,F_mf_print(1,:),N_leu,F_mf_print(2,:));
title(string_t6);
xlabel(string_x2);ylabel(string_y6); grid   ;
legend(string_leg1, string_leg4,                    );
print

dlmwrite(                    ,F_mf_print');
```

8.9. Matlab Script for Flow Distribution Analysis for Half Channels

```
% MITR Flow Distribution Analysis with Half Channels
% Susanna Wong
% Jun 24, 2008

% HEU core w/4 types of channels (full: 2; half: 2)

clear;

% Constants
inch = 2.54E-02;          % inch to metre conversion
gpm = 6.309E-05;          % gpm to cubic metre conversion
V_0 = 3.8555E-004;        % volumetric flow in full channel w/24,15,0.098 HEU config
v_0 = 2.9211;             % velocity in full channel w/24,15,0.098 HEU config
dP_0 = 3.2930E+004;       % friction pressure drop w/24,15,0.098 HEU config
dP_lam0 = 85.4092;

% Fluid properties
T = 50;
% Density
C0_den = 1000.1;
C1_den = 0.0026863;
C2_den = -0.0054424;
C3_den = 1.2324 * 10 ^ -5;
den_w = C0_den + C1_den * T + C2_den * T ^ 2 + C3_den * T ^ 3;
% Viscosity
C0_vis = 1726.9;
C1_vis = -43.349;
C2_vis = 0.47475;
C3_vis = -0.0018307;
vis_w = 1E-6 * (C0_vis + C1_vis * T + C2_vis * T ^ 2 + C3_vis * T ^ 3);

% Channel Parameters
theta = pi()/6;
d_fplate_in = 2.552;      % fuel plate width
d_fplate = d_fplate_in*inch;
l_fplate = 0.5842;        % fuel plate length in metre
t_fplate = 0.06*inch;     % fuel plate thickness in metre
d_splate_in = 0.118;      % side plate projected depth
d_splate1 = d_splate_in*inch/cos(theta);
d_splate2 = d_splate1 - t_fplate*tan(theta);
% w_channel = d_fplate-d_splate1-d_splate2;
w_channel = 2.3082*inch;

% Fin Parameters
d_fin = 0.01*inch;
t_fin = 0.01*inch;
p_fin = 0.01*inch;
n_fin = 110;              % number of fin spacings

% Full/Half Channel Distribution
n_felement = 24;          % number of fuel elements in core
n_plate = 15;             % number of plates per element

% % number of type A, B & C half channels in core
% n_fpsp = input('Number of "fuel-plate to side-plate" half channels in reactor core: ');
% n_fpce = input('Number of "fuel-plate to edge of core" half channels in reactor core: ');
n_fpsp = 3;
n_fpce = 2;
n_half = [n_fpsp n_fpce];

% % number of type A, B & C full channels in core
% n_fpfp = input('Number of "fuel-plate to fuel-plate (non-spider)" combined channels in
reactor core: ');
% n_spid = input('Number of "fuel-plate to fuel-plate (spider)" combined
% channels in reactor core: ');
n_fpfp = 8;
n_spid = 0;
n_reg = n_felement*n_plate - sum(n_half)/2 - n_fpfp - n_spid;
```

```
n_full = [n_reg n_fpfp];     % ignore spider gaps

n_ch = horzcat(n_full,n_half);
n3 = size(n_full,2);         % number of types of full channel
n4 = size(n_half,2);         % number of types of half channel
n2 = n3 + n4;                % number of types of channel in core

d_channel = zeros(n2,1);
for i = 1:n2
    if i == 1
        d_channel(i) = 0.098*inch;  % base to base full channel gap in metre
    elseif i == 2
        % 0.0665" + 0.0665"
        d_channel(i) = 0.133*inch;  % base to base combined half channel gap in metre
  elseif i == 3
        % 0.0665" + 0.0150"
        d_channel(i) = 0.0815*inch; % base to base type B half channel gap in metre
    elseif i == 4
        d_channel(i) = 0.1685*inch; % base to base type B half channel gap in metre
    end
end

% Full/Half Channel
A_flow = zeros(n2,1);
P_w = zeros(n2,1);
D_h = zeros(n2,1);
for j = 1:n2
    if j<=2              % full channel
        A_flow(j) = w_channel*d_channel(j) - 2*(n_fin+1)*t_fin*d_fin;
        P_w(j) = (w_channel + d_channel(j)/cos(theta) + 2*(n_fin+1)*t_fin) * 2;
        D_h(j) = 4*A_flow(j)/P_w(j);
    else                 % half channel
        A_flow(j) = w_channel*d_channel(j) - (n_fin+1)*t_fin*d_fin;
        P_w(j) = (w_channel + d_channel(j)/cos(theta) + (n_fin+1)*t_fin) * 2;
        D_h(j) = 4*A_flow(j)/P_w(j);
    end
end

n1 = 9;                  % volumetric flow rate in core in gpm
V_w_gpm = zeros(1,n1);
for i = 1:n1
    if i == 1
        V_w_gpm(i) = 23.26;
    elseif i == 2
        V_w_gpm(i) = 900;
    else
        V_w_gpm(i) = 1000+200*(i-2);
    end
end
% V_w_gpm = [23.5 900 1800 2000 2200 2300]
V_w = V_w_gpm*gpm;

n1 = size(V_w,2);
v_ch = ones(n1,n2) * v_0;
V_ch = zeros(n1,n2);
V_ch_all = zeros(n1,n2);
Re = zeros(n1,n2);
dP_blasius = zeros(n1,n2);
dP_lam = zeros(n1,n2);
dP_temp = zeros(n1,n2);
for i = 1:n1
    dP_blasius(i,:) = dP_0 * eye(1,n2);
    dP_lam(i,:) = dP_lam0 * eye(1,n2);
    dP_temp(i,:) = dP_blasius(i,:);
    for j = 1:n2
        % Calculate total flow rate in core
        V_ch_all(i,j) = 0;
        k = 1;
        while k <= n2
            V_ch_all(i,j) = V_ch_all(i,j) + n_ch(k) * A_flow(k) * v_ch(i,k);
            k = k+1;
        end

        p = 1;
```

```
        repeat_V = false;
        if or(abs(V_ch_all(i,j) - V_w(i))/V_w(i) > 0.002, p==1)
            repeat_V = true;
        end

        while repeat_V
            if V_ch_all(i,j) - V_w(i) > 0
                v_ch(i,:) = v_ch(i,:)*0.999;
            else
                v_ch(i,:) = v_ch(i,:)*1.001;
            end

            for h = 1:n2
                m = h;
                while m >= 1
                    repeat_dP = false;
                    for m_check = 1:m
                        if or(abs(dP_temp(i,m_check)-dP_temp(i,1))/dP_temp(i,1)>0.002,m==1)
                            repeat_dP = true;
                        end
                    end

                    while repeat_dP
                        if dP_temp(i,m) - dP_temp(i,1) > 0
                            v_ch(i,m) = v_ch(i,m)*0.999;
                        elseif dP_temp(i,m) - dP_temp(i,1) < 0
                            v_ch(i,m) = v_ch(i,m)*1.001;
                        end
                        V_ch(i,m) = A_flow(m) * v_ch(i,m);
                        Re(i,m) = den_w * v_ch(i,m) * D_h(m) / vis_w;

                        % Recalculate flow in full channels
                        for m_recalc = 1:m
                            if m_recalc ~= m
                                V_ch(i,m_recalc) = (V_w(i) - n_ch * V_ch(i,:)' +
n_ch(m_recalc) * V_ch(i,m_recalc)) / n_ch(m_recalc);
                                v_ch(i,m_recalc) = V_ch(i,m_recalc)/A_flow(m_recalc);
                                Re(i,m_recalc) = den_w * v_ch(i,m_recalc) * D_h(m_recalc) /
vis_w;
                            end
                        end

                        % Calculate dP
                        for k = 1:n2
                            % Blasius correlation
                            f_blasius(i,k) = .316*Re(i,k)^-.25;
                            dP_blasius(i,k)
= .5*f_blasius(i,k)*den_w*v_ch(i,k)^2*(l_fplate/D_h(k));
                            % Laminar correlation
                            f_lam(i,k) = 91.5/Re(i,k);
                            dP_lam(i,k) = .5*f_lam(i,k)*den_w*v_ch(i,k)^2*(l_fplate/D_h(k));
                        end

                        if Re(i,m)>3000     % Define range of Re for turbulent flows
                            dP_temp(i,:) = dP_blasius(i,:);
                        else
                            dP_temp(i,:) = dP_lam(i,:);
                        end

                        repeat_dP = false;
%                         for m_check = 1:m
                            if abs(dP_temp(i,m)- dP_temp(i,1))/dP_temp(i,1) > 0.002
                                repeat_dP = true;
                            end
%                         end
                    end
                    m = m - 1;
                    % Calculate total flow rate in core
                    V_ch_all(i,h) = 0;
                    k = 1;
                    while k <= n2
                        V_ch_all(i,h) = V_ch_all(i,h) + n_ch(k) * A_flow(k) * v_ch(i,k);
                        k = k+1;
                    end
```

```
            end

            % Calculate total flow rate in core
            V_ch_all(i,h) = 0;
            k = 1;
            while k <= n2
                V_ch_all(i,h) = V_ch_all(i,h) + n_ch(k) * A_flow(k) * v_ch(i,k);
                k = k+1;
            end
        end

        % Re-calculate total flow rate in core
        V_ch_all(i,h) = 0;
        k = 1;
        while k <= n2
            V_ch_all(i,h) = V_ch_all(i,h) + n_ch(k) * A_flow(k) * v_ch(i,k);
            k = k+1;
        end

        p = p+1;
        repeat_V = false;
        if or(abs(V_ch_all(i,j) - V_w(i))/V_w(i) > 0.002, p==1)
            repeat_V = true;
        end
    end
end
dP(i,:) = horzcat(dP_blasius(i,:),dP_lam(i,:));
V_ratio(i,:) = V_ch(i,:)/V_ch(i,1);
end

% Output plots
string_t1 = ('
ed');
string_t2 = ('
string_x1 = ('
string_y1 = ('
string_y2 = ('
string_leg1 = ('
string_leg2a = ('
string_leg2b = ('
string_leg2c = ('
string_leg3a = ('
string_leg3b = ('

plot(V_w_gpm,V_ratio*100,'
title(string_t1);
xlabel(string_x1);ylabel(string_y1); grid   ;
legend(string_leg2a, string_leg2b, string_leg3a, string_leg3b,
print

figure;
plot(V_w_gpm,V_ch/gpm);
title(string_t2);
xlabel(string_x1);ylabel(string_y2); grid   ;
legend(string_leg2a, string_leg2b, string_leg3a, string_leg3b,
print
```

9. Reference

1. Newton, T., M.S. Kazimi, and E. Pilat, *Development of a Low Enrichment Uranium Core for the MIT Reactor*. 2006, Massachusetts Institute of Technology: Cambridge.
2. Ko, Y.C., *Thermal Hydraulics Analysis of the MIT Research Reactor in support of a Low Enrichment Uranium (LEU) Core Conversion*, in *Department of Nuclear Science and Engineering*. 2008, Massachusetts Institute of Technology: Cambridge, MA.
3. Travelli, A., *The U.S. RERTR Program Status and Progress*. 1997, Argonne National Laboratory: Argonne, Illinois.
4. *Reduced Enrichment for Research and Test Reactors*. [cited; Available from: http://www.rertr.anl.gov/.
5. [cited Aug 14, 2008]; Available from: http://www.stimson.org/cnp/?SN=CT200705211264.
6. *U.S. Code of Federal Regulations*.
7. Gehret, J., *Thermal-hydraulic Aspects of the Use of Low Enriched Uranium in the MIT Research Reactor*. 1984, Massachusetts Institute of Technology.
8. Ko, Y.C., L.W. Hu, and M.S. Kazimi. *Thermalhydraulic Analysis of the MIT Research Reactor Low Enrichment Uranium (LEU) Core*. in *International Congress on Advances in Nuclear Power Plants*. 2008. Anaheim, CA, USA.
9. Ko, Y.C., L.W. Hu, and M.S. Kazimi, *Thermal Hydraulic Analysis of a Low Enrichment Uranium Core for the MIT Research Reactor*. 2008, Massachusetts Institute of Technology: Cambridge.
10. Ko, Y.C., L.W. Hu, and M.S. Kazimi, *Thermal Hydraulic Analysis of a Low Enrichment Uranium Core for the MIT Research Reactor*. 2008, Massachusetts Institute of Technology: Cambridge. p. 55.

11. Taborda-Romero, J.A., *Design of MITR II Fuel Plates. Heat Transfer in Longitudinal Finned Narrow Channel*, in *Department of Nuclear Engineering*. 1971, MIT: Cambridge.
12. Spurgeon, *Preliminary Design Studies for High Flux Reactor*, in *Department of Nuclear Engineering*, MIT: Cambridge.
13. Todreas, N.E. and M.S. Kazimi, *Nuclear Systems I: Thermal Hydraulics Fundamentals*. Vol. 1. 1993: Taylor and Francis.
14. Hesselgreaves, J.E., *Selection, design, and operation*, in *Compact heat exchangers*. 2001, Pergamon: Amsterdam, New York. p. 174-193.
15. Kays, W.M., *Convective Heat and Mass Transfer*. 1966, New York: McGraw-Hill.
16. Papautsky, I., et al., *Effects of rectangular microchannel aspect ratio on laminar friction constant*. Proceedings of SPIE, 1999. **3877**: p. 147-158.
17. Wang, C.C., et al., *Frictional performance of highly viscous fluid in minichannels*. Applied Thermal Engineering, 2004. **24**: p. 2243-2250.
18. Streeter, V.L., *Fluid Mechanics*. 4 ed. 1966: McGraw-Hill, Inc.
19. Moody, L.F., *Friction factors for pipe flow*. Trans. ASME, 1944. **66**(671).
20. Sieder, E.N. and G.E. Tate, *Heat Transfer and Pressure Drop of Liquids in Tubes*. Industrial and Engineering Chemistry, 1936. **28**: p. 1429-1435.
21. Keevil. 1930, Massachusetts Institute of Technology: Cambridge.
22. Drew, Hogan, and McAdams, *Ind. Eng. Chem.* 1931. **23**: p. 936.
23. Clapp and Fitzsimmons. 1928, Massachusetts Institute of Technology: Cambridge.
24. De Lorenzo, B. and E.D. Anderson, *Heat Transfer and Pressure Drop of Liquids in Double-Pipe Fin-Tube Exchangers*. ASME Trans., 1945. **67**: p. 697-702.
25. Taborek, J., *Double-Pipe and Multitube Heat Exchangers with Plain and Longitudinal Finned Tubes*. Heat Transfer Engineering, 1997. **18**(2): p. 34-45.

26. Braga, C.V.M. and F.E.M. Saboya, *Turbulent heat transfer, pressure drop and fin efficiency in annular regions with continuous longitudinal rectangular fins.* Experimental Thermal and Fluid Science, 1999. **20**(2): p. 55-65.

27. Kostic, M. and J.P. Hartnett, *Predicting Turbulent Friction Factor of non-Newtonian Fluids in Non-Circular Ducts.* Int. Comm. Heat Mass Transfer, 1984. **1984**(11): p. 345-352.

28. Gunter, A.Y. and W.A. Shaw, *Heat Transfer, Pressure Drop and Fouling Rates of Liquids for Continuous and Non-continuous Longitudinal Fins.* ASME Trans., 1942. **64**: p. 795-802.

29. Davies, S.J. and C.M. White, *A Review of Flow in Pipes and Channels.* Engineering, 1929.

30. Peng, X.F. and B.X. Wang, *Experimental investigation of heat transfer in flat plates with rectangular microchannels.* Int. J. Heat Mass Transfer, 1995. **38**: p. 127-137.

31. Wang, B.X. and X.F. Peng, *Experimental investigation of liquid forced convection heat transfer through microchannels.* Int. J. Heat Mass Transfer, 1994. **37**: p. 73-82.

32. Warrier, G.R., V.K. Dhir, and L.A. Momoda, *Heat transfer and pressure drop in narrow rectangular channels.* Experimental Thermal and Fluid Science, 2002. **26**(1): p. 53-64.

33. Naik, S., S.D. Probert, and C.I. Wood, *Thermal-Hydraulic Characteristics of a Heat Exchanger: The Certical Rectangular Fins Being Aligned Parallel to the Mean Air Fow in the Duct.* Applied Energy, 1988. **29**: p. 217-252.

34. Thombre, S.B. and S.P. Sukhatme, *Turbulent flow heat transfer and friction factor characteristics of shrouded fin arrays with uninterrupted fins.* Experimental Thermal and Fluid Science, 1995. **10**(3): p. 388-396.

35. Yang, C.Y. and R.L. Webb, *Friction pressure drop of R-12 in small hydraulic diameter extruded aluminum tubes with and without micro-fins.* Int. J. Heat Mass Transfer, 1996. **39**(4): p. 801-809.

36. Hartnett, J.P. and M. Kostic, *Turbulent Friction Factor Correlation For Power-law Fluids in Circular and Non-Circular Channels.* Int. Comm. Heat Mass Transfer, 1990. **17**: p. 59-69.

37. Tam, K.C. and C. Tiu, *A general correlation for purely ciscous non-Newtonian fluids flowing in ducts of arbitrary cross section.* Can. J. Chem. Eng, 1988. **66**: p. 542-549.

38. Akgun, F. and R. Jawad, *Determination of Friction Factor of Fluids Flowing Turbulently through an Eccentric Annulus.* International Journal of Petroleum Science and Technology, 2007. **1**(1): p. 37-49.

39. Langhaar, H.L. and P.H. No, *Steady flow in the transition length of a straight tube.* J. Appl. Mech. Sect. 3, 1942. **9**.

40. Shah, R.K. and A.L. London, *Laminar Flow Forced Convection in Ducts: A Source Book for Compact Heat Exchanger Analytical Data.* 1978: Academic Pr.

41. Hesselgreaves, J.E., *Selection, design, and operation*, in *Compact heat exchangers*. 2001, Pergamon: Amsterdam, New York. p. 157-174.

42. Qu, W., et al., *Experimental and Computational Investigation of Flow Development and Pressure Drop in a Rectangular Micro-channel.* Journal of Electronic Packaging, 2006. **128**(1): p. 1-9.

43. Kays, W.M. and A.L. London, *Compact Heat Exchangers*. 1984, McGraw-Hill Book Company. p. 120-121.

44. Kern, D.Q., *Process Heat Transfer*. 1950.

45. Bevington, P.R. and D.K. Robinson, *Data Reduction and Analysis for Physical Sciences.* 2003.

46. Roglans, J., *Research and Test Reactor Conversion*, A.N. Laboratory, Editor. p. 1.

47. Davis, T. [cited Aug 7, 2008]; Available from: http://www.mathworks.com/matlabcentral/fileexchange/loadFile.do?objectId=7747&objectType=File.